Molecular Vision 2016; 22:847-885 <http://www.molvis.org/molvis/v22/847>
Received 27 March 2016 | Accepted 21 July 2016 | Published 23 July 2016

The cellular and compartmental profile of mouse retinal glycolysis, tricarboxylic acid cycle, oxidative phosphorylation, and ~P transferring kinases

Elda M. Rueda,[1] Jerry E. Johnson Jr.,[2,3] Anand Giddabasappa,[3] Anand Swaroop,[4] Matthew J. Brooks,[4] Irena Sigel,[1] Shawnta Y. Chaney,[3] Donald A. Fox[1,3,5]

[1]College of Optometry, University of Houston, Houston TX; [2]Department of Natural Sciences, University of Houston-Downtown, Houston TX; [3]Department of Biology and Biochemistry, University of Houston, Houston TX; [4]National Eye Institute, Bethesda, MD; [5]Department of Pharmacology and Pharmaceutical Sciences, University of Houston, Houston TX

Purpose: The homeostatic regulation of cellular ATP is achieved by the coordinated activity of ATP utilization, synthesis, and buffering. Glucose is the major substrate for ATP synthesis through glycolysis and oxidative phosphorylation (OXPHOS), whereas intermediary metabolism through the tricarboxylic acid (TCA) cycle utilizes non-glucose-derived monocarboxylates, amino acids, and alpha ketoacids to support mitochondrial ATP and GTP synthesis. Cellular ATP is buffered by specialized equilibrium-driven high-energy phosphate (~P) transferring kinases. Our goals were twofold: 1) to characterize the gene expression, protein expression, and activity of key synthesizing and regulating enzymes of energy metabolism in the whole mouse retina, retinal compartments, and/or cells and 2) to provide an integrative analysis of the results related to function.

Methods: mRNA expression data of energy-related genes were extracted from our whole retinal Affymetrix microarray data. Fixed-frozen retinas from adult C57BL/6N mice were used for immunohistochemistry, laser scanning confocal microscopy, and enzymatic histochemistry. The immunoreactivity levels of well-characterized antibodies, for all major retinal cells and their compartments, were obtained using our established semiquantitative confocal and imaging techniques. Quantitative cytochrome oxidase (COX) and lactate dehydrogenase (LDH) activity was determined histochemically.

Results: The Affymetrix data revealed varied gene expression patterns of the ATP synthesizing and regulating enzymes found in the muscle, liver, and brain. Confocal studies showed differential cellular and compartmental distribution of isozymes involved in glucose, glutamate, glutamine, lactate, and creatine metabolism. The pattern and intensity of the antibodies and of the COX and LDH activity showed the high capacity of photoreceptors for aerobic glycolysis and OXPHOS. Competition assays with pyruvate revealed that LDH-5 was localized in the photoreceptor inner segments. The combined results indicate that glycolysis is regulated by the compartmental expression of hexokinase 2, pyruvate kinase M1, and pyruvate kinase M2 in photoreceptors, whereas the inner retinal neurons exhibit a lower capacity for glycolysis and aerobic glycolysis. Expression of nucleoside diphosphate kinase, mitochondria-associated adenylate kinase, and several mitochondria-associated creatine kinase isozymes was highest in the outer retina, whereas expression of cytosolic adenylate kinase and brain creatine kinase was higher in the cones, horizontal cells, and amacrine cells indicating the diversity of ATP-buffering strategies among retinal neurons. Based on the antibody intensities and the COX and LDH activity, Müller glial cells (MGCs) had the lowest capacity for glycolysis, aerobic glycolysis, and OXPHOS. However, they showed high expression of glutamate dehydrogenase, alpha-ketoglutarate dehydrogenase, succinate thiokinase, GABA transaminase, and ~P transferring kinases. This suggests that MGCs utilize TCA cycle anaplerosis and cataplerosis to generate GTP and ~P transferring kinases to produce ATP that supports MGC energy requirements.

Conclusions: Our comprehensive and integrated results reveal that the adult mouse retina expresses numerous isoforms of ATP synthesizing, regulating, and buffering genes; expresses differential cellular and compartmental levels of glycolytic, OXPHOS, TCA cycle, and ~P transferring kinase proteins; and exhibits differential layer-by-layer LDH and COX activity. New insights into cell-specific and compartmental ATP and GTP production, as well as utilization and buffering strategies and their relationship with known retinal and cellular functions, are discussed. Developing therapeutic strategies for neuroprotection and treating retinal deficits and degeneration in a cell-specific manner will require such knowledge. This work provides a platform for future research directed at identifying the molecular targets and proteins that regulate these processes.

Correspondence to: Dr. Donald A. Fox, University of Houston, College of Optometry, 4901 Calhoun Road, Houston TX 77204-2020; Phone: (713) 743-1694; FAX: (713) 743-2053; email:dafox@uh.edu

The mature retina is a multilaminated structure that contains structurally and functionally diverse neurons with highly specialized-cellular and compartmental sub-cellular organization. In addition, Müller glial cells (MGCs), whose processes extend through most of the retinal layers, provide

structural, functional, and metabolic support for retinal neurons. These features, as well as the graded and sustained firing rates of most retinal neurons, necessitate cellular and compartmentalized intercellular and intracellular regulation of bioenergetic metabolism to regenerate the local high-energy phosphate (~P) pool at the rate of utilization. Glycolysis and oxidative phosphorylation (OXPHOS) are the major metabolic pathways that synthesize ATP. Classical studies of bioenergetic metabolism in perfused cat, rabbit, and rat retinas revealed the retina's capacity for aerobic glycolysis (the Warburg effect) and the Pasteur effect [1-3]. Previous studies also measured whole retinal lactate production and oxygen consumption to estimate photoreceptor glycolysis and OXPHOS, respectively [1-3]. Studies of layer-by-layer retinal oxygen tension [4,5], oxygen consumption [6,7], cytochrome c oxidase (COX) activity [8], COX subunit IV (COX IV) expression [9], mitochondrial number, distribution, and ultrastructure [9,10], and the specific activity and expression of glycolytic enzymes, lactate dehydrogenase (LDH) and succinate dehydrogenase [11-16], established that glycolysis and OXPHOS were differentially distributed in the adult mammalian retina. Together, these studies demonstrated the interdependent relationship between energy metabolism and retinal function.

The metabolic heterogeneity in the retina likely plays a role in cell-selective vulnerability. For example, inhibition of glycolysis by iodoacetate produces rod cell death before cone cell death [17-19], rod- and cone-driven electroretinograms (ERGs) exhibit differential sensitivity to experimentally-induced variations of glucose concentrations [20-22]. Oxygen deprivation decreases the ERG b-wave/PII response of bipolar cells (BCs) before affecting the photoreceptor a-wave/PIII response [23]. Retinal BCs die first in a model of chronic hypoglycemia [24], and retinal ganglion cells die faster than photoreceptors after experimental ischemia [25-27]. The major characteristics of photoreceptor glycolysis and OXPHOS have been reported [4,8-10,12,16,28]. However, tricarboxylic acid (TCA) cycle metabolism and the ~P transferring kinase systems in photoreceptors are relatively unexplored. Moreover, little is known about the cellular and/or compartmental bioenergetic metabolism and profile of horizontal cells (HCs), BCs, amacrine cells (ACs), and retinal ganglion cells. New evidence suggests that mouse MGCs do not significantly metabolize glucose to produce ATP, but instead play a role in intercellular metabolite shuttling that helps maintain energy and neurotransmitter homeostasis [29,30]. In contrast, cultured human MGCs undergo the Pasteur effect [31], and MGCs isolated from avascular retinas show high lactate production [32]. Thus, the cellular and compartmental profiles of glycolysis, OXPHOS, the TCA cycle, and ~P transferring kinases in the mouse retina are not completely characterized or well understood.

Our overall goals were to characterize the gene expression, protein expression, and activity of the synthesizing and regulating enzymes of ATP energy metabolism in the whole mouse retina, retinal compartments, and/or cells and to provide an integrative analysis of the results related to function. Therefore, we provide a brief, but comprehensive, review of the characteristics of the enzymes involved in these processes so that our immunohistochemistry (IHC), laser scanning confocal microscopy, and enzyme histochemistry findings can be fit into this framework.

LDH reversibly catalyzes the reduction of pyruvate to lactate, which is coupled to the oxidation of NADH to NAD^+. Five LDH isozymes have tissue-specific distribution, subunit composition, and different affinities for and inhibition by pyruvate [33-35]. LDH isozymes are homo- and heterotetramers composed of M (muscle) and H (heart) subunits. LDH-5 (the *Ldha* gene) is composed of four M-subunits and is predominantly found in highly glycolytic cells such as skeletal muscle and the liver [33]. LDH-5-mediated activity is the least inhibited by physiologic concentrations of pyruvate [33,34], which enables LDH-5 to support a high rate of aerobic glycolysis under physiologic glucose concentrations. LDH-1 (the *Ldhb* gene) is composed of four H-subunits, is predominantly found in the heart, and is inhibited by physiologic concentrations of pyruvate, and the Michaelis constant of LDH-1 is significantly lower than that of LDH-5 [33-36]. COX is the terminal oxidase of the electron transport chain, which catalyzes the transfer of electrons for the complete reduction of oxygen to support ATP synthesis. To accurately determine glycolysis and OXPHOS at the cellular and compartmental levels in the retina, as has been done with the brain [37,38], histochemical analysis of LDH and COX activity is needed, respectively. Thus, in the present study, we examined the relative mRNA and protein expression levels of LDH and COX IV isoforms, as well as the LDH and COX activity, in the adult mouse retina.

As there is a paucity of information about bioenergetic metabolism in the neurons of the inner retina, we characterized further glycolysis in all layers of the mouse retina. Glycolysis is regulated by three irreversible kinase reactions catalyzed by hexokinase (HK), phosphofructokinase (PFK), and pyruvate kinase (PK). HK catalyzes the phosphorylation of glucose to glucose-6-phosphate (G6P) using ATP as a phosphoryl donor and producing ADP and inorganic phosphate (Pi). Four homologous HK isoforms are expressed in mammalian tissues: HK-1 (the *Hk1* gene), HK-2 (the *Hk2* gene), HK-3 (the *Hk3* gene), and glucokinase (GK/HK-4; the

Gck gene) [39-41]. Soluble, insoluble-active, and insoluble-latent HKs were detected in calf retinas [42]. Reidel et al.'s proteomic study showed that peptide fragments of HK-1 and HK-2 are abundant in rat outer retinal layer homogenates and are differentially distributed in the rat retina [16]. The distribution of HK-1 and HK-2 in the mouse retina is uncharacterized.

PFK catalyzes the ATP-dependent phosphorylation of fructose-6-phosphate (F6P) to fructose-1,6-bisphosphate (F-1,6-BP). Three PFK isoforms encoded by different genes exist in mammalian tissues: the liver type (the *Pfkl* gene), muscle type (the *Pfkm* gene), and fibroblast type (the *Pfkp* gene) [43,44]. Brain tissue expresses PFK-L and PFK-M [45]. Fructose 2,6-biphosphate similarly increases the affinity of F6P in PFK-L and PFK-M isozymes, and the amino acids that compose the active sites of PFK-L and PFK-M are highly similar [45,46]. In situ studies of permeabilized yeast cells showed that of all the glycolytic enzymes, only PFK exhibits enzyme concentration-dependent activity [47]. Small changes in ATP induce large changes in AMP/ATP, which leads to a significant increase in PFK activity [48]. The layer-by-layer activity profile of PFK in the monkey retina showed that PFK activity is lower in the inner segments (ISs) compared to the photoreceptor synaptic terminals [12], indicating compartment-selective activity. The distribution of PFK in the mouse retina is uncharacterized.

PK catalyzes the last step of glycolysis: the transfer of a phosphate from phosphoenolpyruvate to ADP generating two ATP molecules per glucose used by glycolysis. Four isoforms of PK exist: PK-L is the major isozyme in the liver; PK-R is the major isozyme of erythrocytes; PK-M1 is present in skeletal muscle, the heart, and the brain; and PK-M2 is present in the liver, spleen, and fetal and neoplastic tissues. L and R are common products of the *Pklr* gene, whereas PK-M1 and PK-M2 are common products of the *Pkm* gene [49]. The major isozyme of PK in the brain is PK-M1, which has the lowest Michaelis constant of all PK isozymes for its substrate and is less allosterically regulated by F-1,6-BP, the product of PFK [50-52]. In primary cell cultures, PK-M1 promotes metabolic activity, whereas PK-M2 supports macromolecular biosynthesis during cellular proliferation [53]. Evidence also suggests that PK-M2 activity stimulates antioxidant responses [54]. In the mouse retina, PK-M1 is expressed in most retinal neurons, although not in MGCs, whereas PK-M2 expression is observed in photoreceptors [30,55] and at saturating laser intensity in the MGCs [30,55]. In the present study, we examined adult mouse retinal mRNA expression and the cellular and compartmental protein expression of HK, PFK, and PK isozymes.

Glucose is the major substrate for glycolysis and OXPHOS in the brain. Additionally, intermediary metabolism acting through the TCA cycle utilizes ketoacids, monocarboxylic acids, or amino acids as substrates for mitochondrial metabolism and metabolite homeostasis in neurons. For example, the glutamate-glutamine shuttle and a lactate shuttle between glial cells and neurons support energy and neurotransmitter homeostasis in the brain [56-59]. In the glutamate-glutamine shuttle, glutamate is preferentially taken up by the glial cells, through glial-specific excitatory amino acid transporters (EAATs), and is then used by glial cells to produce glutamine via glutamine synthetase (GS). Glutamine is then transported into the neurons through sodium-coupled neural amino acid transporters (SNT1/SNT2) that facilitate uptake of glutamine. MGCs abundantly express EAAT1 (glutamate-aspartate transporter, GLAST), but the expression of SNT1/SNT2 mostly occurs in the inner retina, and no significant expression is observed in the photoreceptors [60]. Accordingly, inhibition of glutamine production in MGCs affects the b-wave, but not the a-wave [61]. To date, the characterization of the cellular and compartmental presence of the glutamine-glutamate shuttle in the retina is not complete. Initial studies of cultured MGCs and photoreceptors suggested a lactate shuttle in the retina [32]. In the lactate shuttle, glial cells uptake glucose and mainly produce lactate, which is then transported into the neurons through monocarboxylate transporters (MCTs). Lactate, in neurons, is reoxidized to pyruvate which moves directly into the mitochondria and fuels OXPHOS. The presence of a lactate shuttle presumes a Warburg effect in the MGCs and a low glycolytic flux in neurons. However, the absence of PK expression or pyruvate metabolism in MGCs [30] indicates a minimal capacity for a Warburg effect in MGCs and challenges the existence of a lactate shuttle in the mouse retina. The rat retina exhibits expression of MCT1, MCT2, and MCT4 [62,63], isoforms with different affinities for lactate, pyruvate, and ketone bodies [64]. A cell-by-cell assessment of the enzymes related to glutamine and lactate production and uptake is required to determine the existence and significance of these shuttles to retinal function. In the present study, we examined the cellular and compartmental expression of the enzymes and transporters involved in glutamine, glutamate, and lactate metabolism.

The homeostatic regulation of cellular ATP is regulated by the competing rates of ATP utilization and synthesis and is buffered by specialized equilibrium-driven ~P transferring kinases. In tissues with high energy fluctuations, steady-state levels of ATP are supported by the ~P transferring kinases: nucleoside diphosphate kinase (NDPK), adenylate kinase (AK), and creatine kinase (CK) [65]. NDPK is a

multifunctional ubiquitous enzyme localized in the cytosol, mitochondria, and nucleus and is associated with protein and nucleic acid synthesis, as well as GTP-dependent mechanisms [66,67]. NDPK reversibly catalyzes the phosphorylation of nucleoside-diphosphates to nucleoside-triphosphates (e.g., ADP to ATP or GDP to GTP) to support phosphotransfer between cellular compartments. Similarly, AK reversibly catalyzes nucleotide phosphoryl exchanges between AMP, ADP, and ATP. This helps maintain the energy charge and contributes to the regulation of the major energy-sensing modulator AMP-activated protein kinase: AMPK [68,69]. Overall, the levels of ATP and GTP, as well as NDPK-specific activity, are higher in the inner, compared to the outer, monkey retina [70]. However, and unexplained, the levels of GTP are similar in the inner segments and the outer plexiform layer (OPL) [70]. Although little is known about the cellular and compartmental distribution of NDPK and AK in the retina, studies in isolated bovine outer segments (OSs) demonstrated the expression and activity of NDPK and AK [71-74]. The cellular expression profile of NDPK and AK in the mouse retina is unknown.

CK reversibly catalyzes the exchange of ~P between creatine (Cr) and ATP to create a phosphocreatine pool. The resulting phosphocreatine pool enables ~P transfer between cellular compartments without significantly altering the magnitude of the adenine nucleotide pool [75-77]. In whole brain and brain homogenates, GTP, AMP, ADP, and phosphocreatine are depleted faster than ATP after experimental ischemia [70,78]. This indicates that ~P transferring kinases rapidly respond to maintain steady-states of ATP in neurons, but that mitochondrial GTP production via succinate thiokinase (STK) activity in the TCA cycle is sensitive to ischemia. Four isoforms of CK based on tissue, cellular, and compartmental localization have been characterized. Cytosolic CKs (brain type CK [CK-B, the *Ckb* gene] and muscle type [CK-M, the *Ckm* gene]) exist as three isoenzymes: CK-MM, CK-MB, and CK-BB and the mitochondrial CKs exist as ubiquitous mitochondrial CK (hereafter referred to as mi-CK, the *Ck-mt1* and *Ck-mt2* genes]) and sarcomeric CK (S-MtCK). The compartmental localization of each isozyme supports the CK phosphotransfer capacity to regenerate local ATP levels [65,79-81]. CK-B and mi-CK are expressed in the cone-dominated chicken retina [77] and in the rod-dominated bovine [82] and mouse [83,84] retinas. CK-B is selectively expressed in the outer retina of the mouse [83]. The expression pattern of the different isoforms of CK in the mouse retina is not completely characterized. In the present study, we examined the mRNA and protein expression of several NDPK, AK, and CK isozymes in the adult mouse retina.

The results of this comprehensive and integrated study reveal cellular and compartmental differential regulation of glucose, glutamine, glutamate, lactate, and creatine metabolism, as well as distinct cellular and compartmental capacities of the ~P transfer. The findings reveal several previously uncharacterized bioenergetic differences between the outer and inner retina, rod and cone photoreceptors, inhibitory and excitatory neurons, and neurons and MGCs. The compartmentalization of ATP and GTP synthesis, maintenance, and regulation in relation to function in retinal neurons and MGCs are also discussed. A summary figure showing the relative antibody intensity levels across 22 major retinal neuronal and MGC compartments for glycolysis, aerobic glycolysis, OXPHOS, the TCA cycle, and ~P transferring kinases is presented.

METHODS

Experimental animals: Experimental and animal care procedures complied with the NIH Guide for the Care and Use of Laboratory Animals and Maintenance, were approved by the Institutional Animal Care and Use Committee of the University of Houston, and adhered to the ARVO Statement for Use of Animals in Research. Wild-type C57BL/6N mice (Harlan Sprague Dawley, Indianapolis, IN; Taconic Farms Inc., Hudson NY) and *neural retina leucine zipper*–enhanced green fluorescent protein (*Nrl*-EGFP) transgenic mice, of C57BL/6N background [85], from litters bred at our facility, were maintained on a 14 h:10 h light-dark cycle (100 lux: maximum cage luminance) with food and water available ad libitum. For these experiments, C57BL/6N mice were used, instead of the C57BL/6J substrain that lacks exons 7–11 of the nicotinamide nucleotide transhydrogenase (*Nnt*) gene that is important for glucose homeostasis and insulin secretion [86]. Although the C57BL/6N mice have the *rd8* mutation, we did not observe any patchy dysplasia, irregular variations in the thickness of any retinal layer, or the displacement of photoreceptor nuclei into the inner nuclear layer in the inferior or superior retina of any mouse eye during development or at the time of our experiments as noted [7]. Adult 60- to 90-day-old mice were decapitated between 1 and 2 h after light onset, and their eyes were rapidly removed and immersed in ice-cold PBS (1X; 140 mM NaCl, 7.7 mM Na_2HPO_4, 2.7 mM NaH_2PO_4, 305 mOsm, pH 7.40). The corneas were gently slit, and the eyes were fixed in 4% paraformaldehyde in 0.2 M cacodylate buffer for 30 min at 23 °C. In total, we used 325 adult mice: 200 males and 125 females. There were no age- or sex-dependent differences in any analysis. Thus, all data were combined for presentation.

Affymetrix of bioenergetic metabolism enzymes from the mouse genome array: Gene expression profiling experiments and data analysis were performed at the Microarray Core Facility at Kellogg Eye Center, University of Michigan (Ann Arbor, MI) essentially as previously described [87]. Briefly, labeling and hybridization were performed using the reagents, kits, and protocol provided by Affymetrix, Inc. (Santa Clara, CA). Two to three microns of total RNA were used to generate biotin-labeled complementary RNA (cRNA) using the Affymetrix target labeling kit. Total RNA was reverse-transcribed using the T7-oligo (dT) promoter primer for the first-strand cDNA synthesis, followed by the second-strand cDNA synthesis to make double-stranded cDNA. The double-stranded cDNA was cleaned using a sample cleanup module provided with the kit. The cleaned double-stranded cDNA was used as a template for the in vitro transcription (IVT) reaction to generate biotin-labeled cRNA. The cRNA was cleaned using the sample cleanup module, and the cRNA was quantified. Further, 15 µg of cRNA was fragmented using fragmentation buffer and stored at −80 °C until further use. The fragmented cRNA was hybridized onto the Affymetrix, Inc. Mouse Genome 430 2.0 Arrays for 16 h at 45 °C. After hybridization, the arrays were washed, stained, and processed using an Affymetrix Fluidic Station F450 according to the manufacturer's instructions and processed for scanning. The raw probe-level data obtained from the Affymetrix CEL files were normalized using robust multichip average (RMA) normalization. The differential mRNA expression (in log2) levels of isozymes involved in bioenergetic metabolism from three to four independent biologic replicates was used to determine the mean ± standard error of the mean (SEM) for each isoenzyme. For each gene, we compared the expression level of different isozymes. Doubling of the mRNA amount was considered a twofold change.

Antibodies: Table 1 presents the list of commercially available and validated primary antibodies that were selected for their ability to selectively label single or multiple isozymes involved in glycolysis, aerobic glycolysis, the TCA cycle, OXPHOS, and the ~P transferring kinases. Polyclonal rabbit antibodies used to characterize the expression of the different isozymes involved in glycolysis and aerobic glycolysis included anti-HK-1 and HK-2 antibodies (Cell Signaling Technology, Inc.; Danvers, MA) that detected a band of 102 kDa in retinal homogenates (data not shown) and are used to selectively label HK isoforms in cancer cells [88-90], an anti-PFK-L antibody that detects a single 85 kDa band (Abgent, San Diego, CA; data not shown) that detects a single 85 kDa band (Sigma, St. Louis, MO; Abcam, Cambridge MA; and Cell Signaling Technology, Inc.), anti-PK-M1 and PK-M2 antibodies (Sigma, Abcam, and Cell Signaling) that detects a 60 kDa band in retinal homogenates (data not shown) and are used to selectively detect PK-M isoforms in cancer cells [91,92], and anti-LDH-A (LDH-5) and pan-LDH antibodies (Abgent) that detect a band at 30–35 kDa (manufacturer technical information). Antibodies used to characterize the expression of different enzymes involved in the mitochondria-mediated TCA cycle included anti-oxoglutarate/alpha-ketoglutarate dehydrogenase (OGDH) antibody that detects a single 125 kDa band in retinal homogenates (data not shown), the anti-glutaminase (GLS) antibody (Abcam) that detects a single 78 kDa band in Hela cell extracts (manufacturer technical information) and is used to detect GLS in proliferating cells [93-95], an anti-glutamate dehydrogenase (GDH) antibody (Novus Biologicals, Littleton, CO) that detects a single 55 kDa band (manufacturer information), and an anti-GABA transaminase (GABA-T) antibody that was a gift from Jang-Yen (John) Wu. Antibodies used to characterize the expression of the different isozymes involved in ~P transferring kinases included an anti-NDPK rabbit polyclonal antibody (Abbiotec, San Diego, CA), an anti-AK1 mouse monoclonal antibody (Abnova, Walnut, CA) that detects a single 20–25 kDa band in the Hela cell lysate (manufacturer technical information), an anti-AK2 rabbit polyclonal antibody (Abcam) that detects a 26 kDa band in the human T cell lymphoblast-like cell lysate and is detected in an ovarian cancer cell line [96], an anti-CK-B rabbit polyclonal antibody (Abcam) that detects a 43 kDa band, a rabbit polyclonal antibody that targets the human CK-M (Bioss, Woburn, MA), and a goat polyclonal anti-mitochondrial (mi)-CK antibody (UMtCK: Santa Cruz) that detects a 47 kDa band. An extensive panel of well-characterized primary antibodies directed against cell- and organelle-specific markers in the retina was used in the double- and triple-labeling experiments. These were antibodies for S-and M-opsins, and M-cone arrestin (M-Car) [97,98]: gifts from Cheryl Craft; vesicular glutamate transporter 1 (VGLUT1) [99], protein kinase C α (PKCα), glutamine synthetase (GS), calbindin, choline acetyltransferase (ChAT), GABA [100], disabled 1 (DAB1) [101], CHX10 [102], and GLAST. Primary antibodies previously characterized in our studies [9] include anti-COX subunit IV, anti-pan-plasma membrane calcium ATPase (PMCA), and sarco/endoplasmic reticulum calcium-ATPase isoform 3 (SERCA 3). We conducted extensive preliminary antibody titration experiments through a broad range of dilutions (three orders of magnitude) to determine the optimal working dilution and to ensure that every antibody used had the appropriate specificity and penetration. Negative control experiments included running experiments in the absence of the primary antibody or secondary antibody.

Table 1. Cell and compartmental specific primary antibodies.

Primary antigen	Abbreviation	Immunogen	Host	Source	Dilution	References
Glycolysis						
Hexokinase 1	HK1	Human HK1	Rabbit	Cell Signaling	1:500	89
Hexokinase 2	HK2	Human AA 341 size16-20 AA	Rabbit	Cell Signaling	1:200	88-90
Phosphofructokinase L1	PFK-L1	Human Synthetic Pep AA 669-699 C-terminus	Rabbit	Abgent	1:200	
Pyruvate kinase M1	PK-M1	Human Synthetic Peptide AA 398-416	Rabbit	Sigma	1:500	91
Pyruvate kinase M2	PK-M2	Human AA 380-440	Rabbit	Abcam	1:500	92
Pyruvate kinase M2	PK-M2	Human PK-M2 full length	Rabbit	Cell Signaling	1:500	30, 55
Pan-lactate dehydrogenase	pan-LDH	Human LDH	Rabbit	Santa Cruz	1:500	
Lactate dehydrogenase 5	LDH5	Human LDH AA 203-232 C-terminus	Rabbit	Abgent	1:500	
TCA cycle and OXPHOS						
Oxoglutarate (α-ketoglutarate) dehydrogenase	OGDH	Human OGDH AA 705-1000	Rabbit	Thermo Scientific	1:500	
Glutaminase	GLS	Human GLS AA 580-670	Mouse	Abcam	1:500	93-95
Glutamate dehydrogenase 1	GDH 1	Recombinant GDH1 AA 1-265	Mouse	Novus Biologicals	1:500	
GABA transaminase	GABAT	Mouse brain GABA-T full length	Rabbit	Jang-Yen Wu gift	1:1000	
Cytochrome oxidase subunit IV	COX IV	Human full length subunit IV	Mouse	Invitrogen	1:500	9
High-energy phosphate transferring kinases						
Nucleoside diphosphate kinase A	NDPK-A	Human Synthetic Peptide region on N-terminus	Rabbit	Abbiotec	1:500	
Adenylate kinase 1	AK1	Recombinant AK1 AA 1-194	Mouse	Abnova	1:500	
Adenylate kinase 2	AK2	Human Synthetic Peptide AA 1-100	Rabbit	Abcam	1:500	96
Creatine kinase - BB-brain type	CK-B	Human full length-brain cells	Rabbit	Abcam	1:500	
Creatine kinase - MM-Muscle type	CK-M	Human synthetic peptide	Rabbit	Bioss	1:500	
Mitochondrial creatine kinase	CK-mi	Human peptide of CK-mi (uMtCK)	Goat	Santa Cruz	1:500	
Cell and organelle specific markers						
Cone M-Opsin	M-opsin	Mouse M-opsin peptide (residues 3-16)	Rabbit	Cheryl Craft gift	1:1000	98
Cone S-Opsin	S-opsin	Recombinant human blue opsin	Rabbit	Chemicon	1:1000	97, 98

Cell and organelle specific markers

Middle wavelength-sensitive cone arrestin	M-Car	AA 369-381 of C-terminus	Rabbit	Cheryl Craft gift	1:500	99
Pan-plasma membrane calcium ATPase	pan-PMCA	Human erythrocyte calcium ATPase	Mouse	Affinity Bioreagents	1:400	9
Sarcoplasmic-endoplasmic reticulum calcium ATPase 3	SERCA3	Synthetic Peptide: V(29) T D A R E R Y G P N(39)	Rabbit	Affinity Bioreagents	1:500	9
CHX10	CHX10	Human CHX10 AA 1 to 131 of N terminus	Sheep	Exalpha	1:500	102
Protein kinase C-α	PKCα	Rat PKCα AA 659-672	Mouse	Serotec	1:1000	9
Calbindin	Calb	Chicken gut D28-K	Mouse	Swant	1:1000	
Choline acetyltransferase	ChAT	Porcine CHAT N-terminus	Sheep	Chemicon	1:500	
Disabled-1	DAB1	Mouse DAB1 AA 400-555	Rabbit	Chemicon	1:500	101
GABA	GABA	GABA Glutaraldehyde-BSA	Rabbit	Chemicon	1:1000	100
Vesicular glutamate transporter 1	VGLUT1	Synthetic peptide from rat VGLUT1	Guinea pig	Chemicon	1:1000	9
Glutamate/Aspartate transporter	GLAST	Synthetic peptide from Rat GLAST C-terminus	Guinea pig	Chemicon	1:1000	
Glutamine synthetase	GS	Sheep brain GS	Mouse	Sigma	1:1000	

IHC and confocal microscopy: Frozen sections of retinas from four to seven mice from different litters were immunolabeled in parallel to ensure identical processing as described [9,103]. Briefly, sections obtained 200–400 µm from the optic nerve head were thawed and post-fixed by immersion in 4% paraformaldehyde for 15 min to improve tissue adherence to Superfrost slides. Sections were rinsed in nanopure water (npH_2O) and briefly immersed in 1% sodium borohydrate to reduce autofluorescence. Sections were rinsed with PBS and incubated for 2 h at 4 °C with a blocking solution containing 10% normal goat serum, 5% bovine serum albumin, 1% fish gelatin, and 0.3% Triton X-100 in PBS (pH 7.4). Slides were incubated for 48 h in primary antibodies. Sections were rinsed three times in PBS and blocked for 30 min at 23 °C. Dilutions of Alexa Fluor 488-, 555-, and 647-conjugated secondary antibodies (Life Technologies, Carlsbad CA) were applied and incubated for 1 h in the dark at 23 °C. For the double- and triple-labeling experiments, primary or secondary antibodies from different hosts were applied simultaneously. After incubation with secondary antibodies, the sections were rinsed in PBS and npH_2O. Slides were dried and coverslipped with Vectashield antifade mounting medium (Vector Laboratories, Burlingame, CA).

Confocal images were acquired using a Leica TCS SP2 (Leica Microsystems, Exton, PA) as described [9,103]. Stacks of images from different Z-planes were obtained using identical exposure (non-saturating conditions) and scanning parameters. Confocal images were imported into Adobe Photoshop CS software (Adobe Systems, Inc., Mountain View, CA) for identical and minimal processing. The results shown are representative images from three to six separate immunolabeling experiments from three to five different mouse retinas, each from a different litter. “Colabeled” was assigned to images that showed significant fluorescent pixel overlapping, and “adjacent labeling” was assigned to images when close proximity in labels was seen, but significant pixel overlapping was not detected with 63X and 100X objectives. Immunolabeling intensity was assessed by three blinded viewers who examined a minimum of five coded confocal images per retina and ranked the immunolabeling intensity on a relative 5-point scale as previously described [9]: intense (++++), strong (+++), moderate (++), weak (+), or absent (0). The combined results had 90–95% concordance between the viewers and are presented in Appendix 1.

Histochemical analysis of LDH and COX activity: Eyes from 60-day-old mice were enucleated and fixed for 1 h in ice-cold 4% paraformaldehyde containing 4% sucrose in 0.1 M cacodylate buffer (pH 7.4). Fixed eyes were washed three times with a PBS/4% sucrose buffer for 10 min at 4 °C and then successively incubated in 10% and 20% sucrose solutions for 2 h at 4 °C. Eyes were cryoprotected in 30% sucrose overnight, embedded in ocular freezing media, and frozen in liquid nitrogen. The localization of LDH staining was determined using a modified brain or kidney histochemistry assays that previously used a super-saturating concentration of 100 mM lactate [37,104]. Adjacent frozen vertical sections (20 µm) were incubated for 5 min at 37 °C in a reaction medium containing 0.3 mg phenazine methosulfate (Sigma), 10% w/v polyvinyl alcohol (PVA-50; Sigma), 0.3 mg nicotinamide adenine dinucleotide (NAD^+ sodium salt; Sigma), 0.818 mg/ml nitroblue tetrazolium chloride (Sigma), and 10 mM potassium cyanide in 10 ml of 50 mM Tris buffer (pH 7.4) with 1 mM (the physiologic level in the blood and brain [105]), 5 mM or 10 mM sodium DL-lactate (Sigma). Negative control slides, which were processed simultaneously, were performed by the removal of lactate and/or NAD^+ or the inclusion of oxalate (10 mM): a non-competitive inhibitor of LDH [106]. Competitive inhibition of LDH activity was conducted using pyruvate [107] at 5, 10, or 20 mM. Sections were rinsed in PBS, dried, counterstained with cresyl violet to assess the tissue as well as cellular and layer localization, and coverslipped with Permount. The localization of the COX staining was determined using a histochemistry assay, essentially as described [38]. Frozen vertical sections (20 µm) from four to seven mice from different litters were incubated for 1 h at 37 °C in a reaction medium containing 5 mg diaminobenzidine (Sigma), 3 mg of cytochrome C type III (Sigma), 200 µg/ml catalase (Sigma), and 4% sucrose in 10 ml 0.1 M PBS (pH 7.4). To enhance the DAB staining, 1% nickel ammonium sulfate and 1% cobalt chloride were included in the reaction medium. Negative control slides, which were processed simultaneously, were performed by the removal of cytochrome C or inhibition of COX by buffered 5 mM potassium cyanide.

Quantitative densitometry: For LDH and COX densitometry, four sections per retina from non-adjacent central retinal sections from four to seven mice were obtained, imaged, and quantified. Images were acquired with a Leica DM2500 microscope under identical exposure and magnification conditions. For optical densitometry (OD) analysis, the images were saved as uncompressed TIFF files and imported into NIH Image-J. Six readings from a region of interest (ROI), obtained with an elliptical marquee, were acquired from each retinal section. The ROI OD values were acquired using the uncalibrated OD function. A mean OD value from the ROI readings from each retinal layer was obtained, and a combined mean ± SEM value was calculated for each layer. For LDH, a two-way ANOVA (layer and concentration) and the least significant difference post-hoc test determined

layer and concentration-dependent differences. For COX, a one-way ANOVA compared the photoreceptor layer to all other retinal layers. A p value of less than 0.05 was considered statistically significant.

RESULTS

Analysis of differential mRNA expression of isozymes of bioenergetic metabolism: The Affymetrix microarray data analyses revealed the differential gene expression of the muscle, liver, and brain isozymes for three glycolytic enzymes (HK, PFK, and PK), LDH, COX IV, NDPK, AK, and CK in adult light-adapted mouse retinas (Figure 1). Figure 1A shows that the gene expression of *Hk1* and *Hk2* was more than twofold higher compared to *Hk3* and *Gck*. Gene expression of the *Pfk* isoforms *l*, *m*, and *p* was detected at similar levels. *Pkm* was expressed approximately threefold higher than *Pklr*. *Ldha* and *Ldhb* were expressed approximately threefold higher than *Ldhc* and *Ldhd*. The gene expression of *Cox4i1* was approximately threefold higher than that of *COX4i2*. There were seven *Nme* genes (NDPK), five genes of different isoforms of *Ak*, and four *Ck* genes expressed in the retina (Figure 1B). The gene expression of isozymes *Nme1* and *Nme2* was higher than that for *Nme3–7*. The gene expression of the *Ak* isoforms was similar. The gene expression of *Ckb* was at least twofold higher than that of *Ckm*, whereas the *Ck-mt1* gene expression was at least twofold higher than that of *CK-mt2*. These Affymetrix results are consistent with our differential gene expression results using RNA sequencing (Rueda et al., manuscript in preparation). The Affymetrix gene profiles revealed that the whole retina has metabolic characteristics of the muscle, liver, and brain. Most importantly, these results provided baseline information that enabled us to choose relevant antibodies for the cellular and compartmental IHC and confocal microscopy studies.

Immunolabeling of rod and cone photoreceptor compartments: One of our central goals was to determine the protein expression and activity of key synthesizing and regulating enzymes of energy metabolism in retinal compartments and cells. Lowry et al.'s rat retinal enzymology studies [12], as well as Reidel et al.'s proteomic studies [16], used anatomic layer-by-layer sectioning techniques to identify selected energy-related enzymes. Although highly informative, these studies were confounded due to the overlap of the cone outer segments (COSs) in the rod inner segment (RIS) layer as well as the neuronal-MGC overlap. Figure 2 was constructed to address this important and relevant issue. As shown in the electron micrograph adapted from Johnson et al. [9] (Figure 2A), the longer and thicker rod outer segments (ROSs) make up most of the outer segment (OS) layer of the mouse retina, whereas the shorter COSs are located in the distal region of the inner segment (IS) layer adjacent to the rod inner segments (RISs; Figure 2A: white arrows). The *Nrl*-GFP retinas were used to distinguish the distribution of the immunolabels in rod and cone photoreceptors. In the *Nrl*-GFP mice retinas [85], the ROSs, RISs, rod somas, and spherules are fluorescent (Figure 2B). COX IV immunoreactivity (IR) in the *Nrl*-GFP retinas (Figure 2C) illustrates the location of mitochondria in the IS ellipsoid region and the distal perinuclear region of the cone somas (Figure 2C: white arrowheads) as we described [9]. The COSs were labeled with an antibody against M- and S-opsins that revealed the location of the COSs in close proximity to the RISs (Figure 2D). Double-labeling retinas with COX IV and M-CAr confirmed the close proximity of the COSs to the RISs and showed the COX-IV-IR perinuclear mitochondria (Figure 2E: white arrows) we previously described [9].

HK-1 and HK-2 have differential compartmental and laminar expression: As the relative gene expression of *Hk1* and *Hk2* was two- to threefold higher compared to that of *Hk3* and *Gck* (Figure 1A), we determined the distribution and relative intensity of HK-1-IR and HK-2-IR (Figure 3; Appendix 1). HK-1-IR was moderate to strong in the ISs and the distal parts of the inner nuclear layer (INL; Figure 3A), whereas HK-2-IR was intense in the ISs and the OPL and moderate to strong in the inner plexiform layer (IPL; Figure 3E). HK-1-IR and HK-2-IR were weak in the ganglion cell layer (GCL; Figure 3A,E). Double-labeling of HK-1 (Figure 3B) or HK-2 with VGLUT1 (Figure 3F) showed higher expression of HK-2 in the spherules and pedicles compared to HK-1. These results are consistent with those from the rat retina proteomic study [16]. We characterized HK-1 and HK-2 further in all retinal layers. The colabeling of HK-1 with PKCα (Figure 3C) and HK-2 with PKCα (Figure 3G) indicate strong expression of HK-1 in the rod BC dendrites and somas but only weak or no HK-2 expression in the rod BC dendrites and somas. There was weak or no HK-2-IR in the calbindin-IR HC somas and weak to moderate colabeling in the HC processes (Figure 3H: white arrows). HK-1-IR and HK-2-IR were not detected in MGCs (Figure 3D,E). The HK isozyme distribution revealed that retinal neurons phosphorylate significantly greater amounts of glucose than MGCs. The distribution of HK-2 in the photoreceptor compartments was characterized, at higher resolution, in the *Nrl*-GFP retinas (Figure 3I–K). HK-2-IR was distributed in the ellipsoid, myoid, and synaptic terminals of the rods (Figure 3I) and cones (Figure 3I: black arrows on the ISs). A closer examination showed HK-2-IR in selective regions of the cone photoreceptor somas (Figure 3K: white arrowheads on the location of the mitochondria [9]).

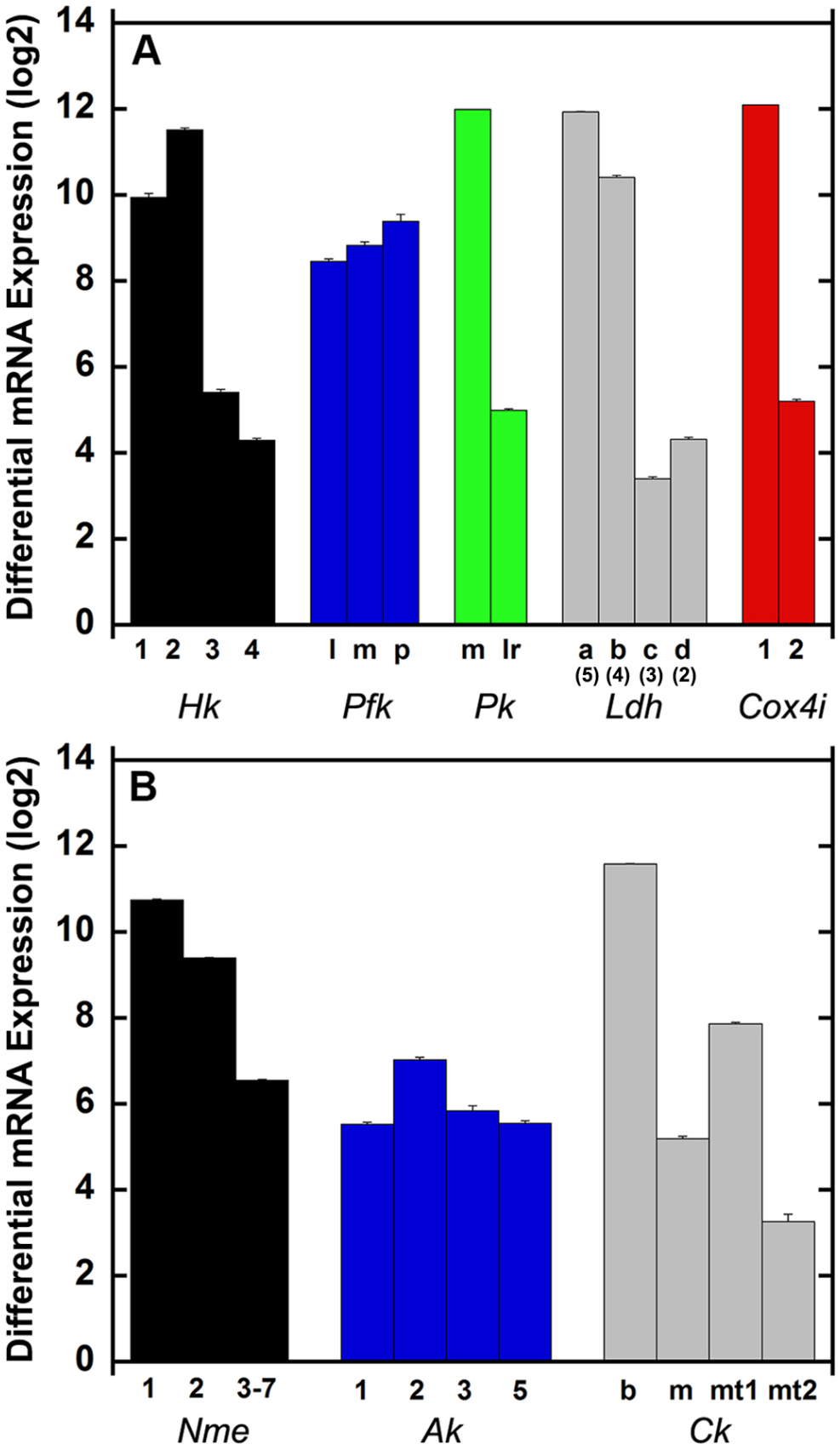

Figure 1. Differential mean ± SEM mRNA expression of metabolism-related genes in mature mouse retina. A doubling of the amount of mRNA is considered a twofold change. **A**: *Hk1* and *Hk2* showed greater than twofold higher expression when compared to *Hk3* and glucokinase (*Gk*). Isoforms *l*, *m* and *p* of *Pfk* showed similar levels of expression. *Pkm* showed greater than twofold higher expression compared to isoforms *Pklr*. To enhance readability, the protein isoform number appears under the gene name of each *Ldh* isoform. *Ldh* isoforms *a* (LDH-5, skeletal muscle) and *b* (LDH-1, heart) showed greater than twofold higher expression compared to the isoforms *c* (LDH-3) and *d* (LDH-4). *Cox4i* isoform *1* is expressed greater than twofold higher than *Cox4i2*. **B**: Several *Nme* isoforms are expressed in the retina, with *Nme1* and *Nme2* showing the highest relative expression. Genes of isoforms *1–3* and *5* of *Ak* showed similar expression. *Ckb* showed greater than twofold higher expression compared to *Ckm*, and *CK-mt1* showed greater than twofold higher expression compared to *Ck-mt2*.

To determine the association of HK-2 with mitochondria, we double-labeled retinas with HK-2 and COX IV (Figure 4). The distribution of HK-2 in the mitochondria-rich regions of the ONL, OPL, and IPL has not been reported. In the photoreceptor somas and the perinuclear mitochondria of cones, HK-2-IR and COX IV-IR were in close proximity (Figure 4A–C). HK-2-IR also was in close proximity to COX IV-IR in the photoreceptor synaptic terminals (Figure 4E). Using anti-pan PMCA, we detected HK-2-IR in the spherules and pedicles (Figure 4F), as PMCA is differentially expressed in both photoreceptor terminals [108,109], albeit more predominantly in spherules [9]. Strong COX IV-IR also was observed in the postsynaptic region of the OPL (Figure 4G). Glutamine/glutamate can serve as an accessory substrate for OXPHOS [110]. To determine the glutamine metabolism of BC dendrites, we examined the distribution of glutaminase (GLS). GLS-IR was weak in the photoreceptor terminals (Figure 4H) and intense in the rod BC dendrites and somas (Figure 4I). The retinal HK-2 expression pattern we observed is similar to the HK activity profile found in the monkey retina [12].

PFK-L1-IR is differentially expressed in the retina: Pfkl: Pfkm, and *Pfkp* are expressed at similar levels in the adult mouse retina (Figure 1A). As the liver isozyme, PFK-L1, is a key regulatory enzyme in glycolysis and is allosterically inhibited by ATP [111], we determined the relative retinal distribution and expression of PFK-L1 (Figure 5; Appendix 1). Although PFK-L1-IR was ubiquitous, different levels of PFK-L1-IR were detected in all retinal layers (Figure 5A). The ROSs and the COSs exhibited weak and moderate PFK-L1-IR, respectively. The weak to moderate PFK-L1-IR observed in the OSs and the intense PFK-L1-IR in the OPL and the inner retina (Figure 5A) is consistent with the PFK activity profile in the monkey retina: lowest in the OSs and highest in the OPL [12]. This suggests that the expression level of PFK may control PFK activity. Double-labeling experiments with PFK-L1 and VGLUT1 showed intense PFK-L1-IR in the OPL and the IPL (Figure 5B). PFK-L1-IR was most intense in the presynaptic region of the OPL compared to the postsynaptic region (Figure 5B,C). The PFK-L1-IR in the inner retina was intense in the GCL (Figure 5A). Double-labeling experiments with PFK-L1 and COX IV showed that PFK-L1-IR was similarly strong in the RIS and CIS myoid and ellipsoid regions (Figure 5C).

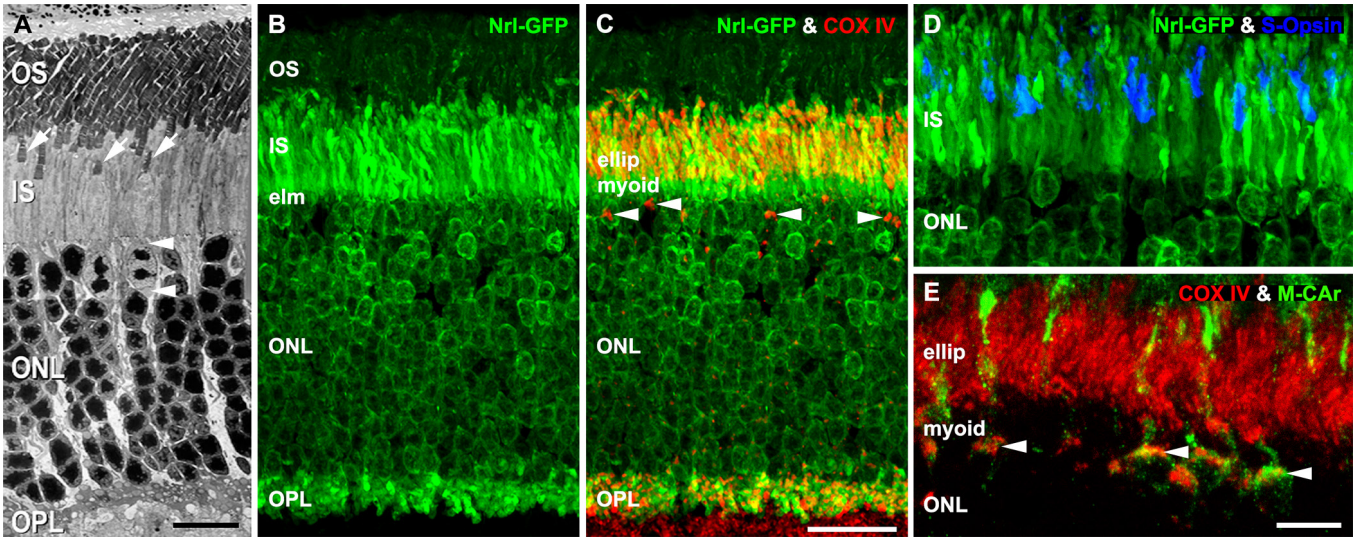

Figure 2. The relative location of the rod and cone outer segments, and myoid and ellipsoid regions of inner segments in the adult mouse retina are presented: electron and confocal microscopy images. Note that the cone OSs are located in the same layer as the rod inner segments (RISs). **A**: Low-magnification electron micrograph of a longitudinal section of the entire photoreceptor layer. Note the presence of cone OSs in the rod IS layer (white arrows) and the perinuclear mitochondria of the cones (white arrowheads). **B**: All compartments of the rods in the *neural retina leucine zipper*–green fluorescent protein (*Nrl*-GFP) transgenic mouse are fluorescent for GFP. **C**: Cytochrome oxidase subunit IV (COX IV) immunoreactivity (IR) colocalizes in the mitochondria-rich rod IS ellipsoid region and the OPL of *Nrl*-GFP transgenic mice (yellow-orange pixels). White arrowheads identify the cone perinuclear mitochondria. **D**: High-magnification image of *Nrl*-GFP transgenic mouse retina shows cone S-opsin-IR in the rod IS layer. **E**: High magnification of a retina double-labeled with COX IV and cone arrestin (M-CAr) shows cones (green pixels) in the rod IS ellipsoid region. White arrowheads identify the colabeled cone perinuclear mitochondria. **A**, scale bar = 10 µm. **B** and **C**, scale bar = 40 µm. **D** and **E**, scale bar = 20 µm. ELM = external limiting membrane, ellip = ellipsoid, ISs = inner segments, myo = myoid, ONL = outer nuclear layer, OPL = outer plexiform layer, OSs = outer segments.

PK-M1 and PK-M2 have differential compartmental and laminar expression: Pkm is expressed approximately three-fold higher than *Pklr* (Figure 1A). The distribution and relative intensity of PK-M1-IR and PK-M2-IR were determined (Figure 6; Appendix 1). Differential laminar intensity of PK-M1-IR was observed in all retinal layers (Figure 6A) consistent with previous studies [30,55]. We further characterized PK-M1 and PK-M2 in each retinal layer. The *Nrl*-GFP retinas double-labeled with COX IV and PK-M1 showed weak and moderate ROSs and COSs, respectively. Intense PK-M1-IR was observed in the rod ellipsoids and myoids (Figure 6B–E) and the photoreceptor synaptic terminals (Figure 6A,F). Double-labeling experiments with PK-M1 and PKCα (Figure 6G) and triple-labeling with PK-M1, CHX10, and calbindin (Figure 6H) indicated weak expression of PK-M1 in the BC dendrites and somas and the HC processes (Figure 6H: arrowheads) and no expression in the HC somas. PK-M1-IR was intense in the proximal INL and the IPL and strong in the GCL (Figure 6A,F–H). Our double-labeling experiments with PK-M1 and GS showed no PK-M1 expression in the MGCs (data not shown), consistent with Lindsay et al.'s experiments [30].

We used an Abcam anti-PK-M2 that recognizes a longer epitope region in the amino acid sequence of PK-M2 than the Novus or Cell Signaling antibodies, used by other investigators [30,55] and us (Appendix 2), and thus produces greater specificity. PK-M2-IR was observed in the photoreceptors

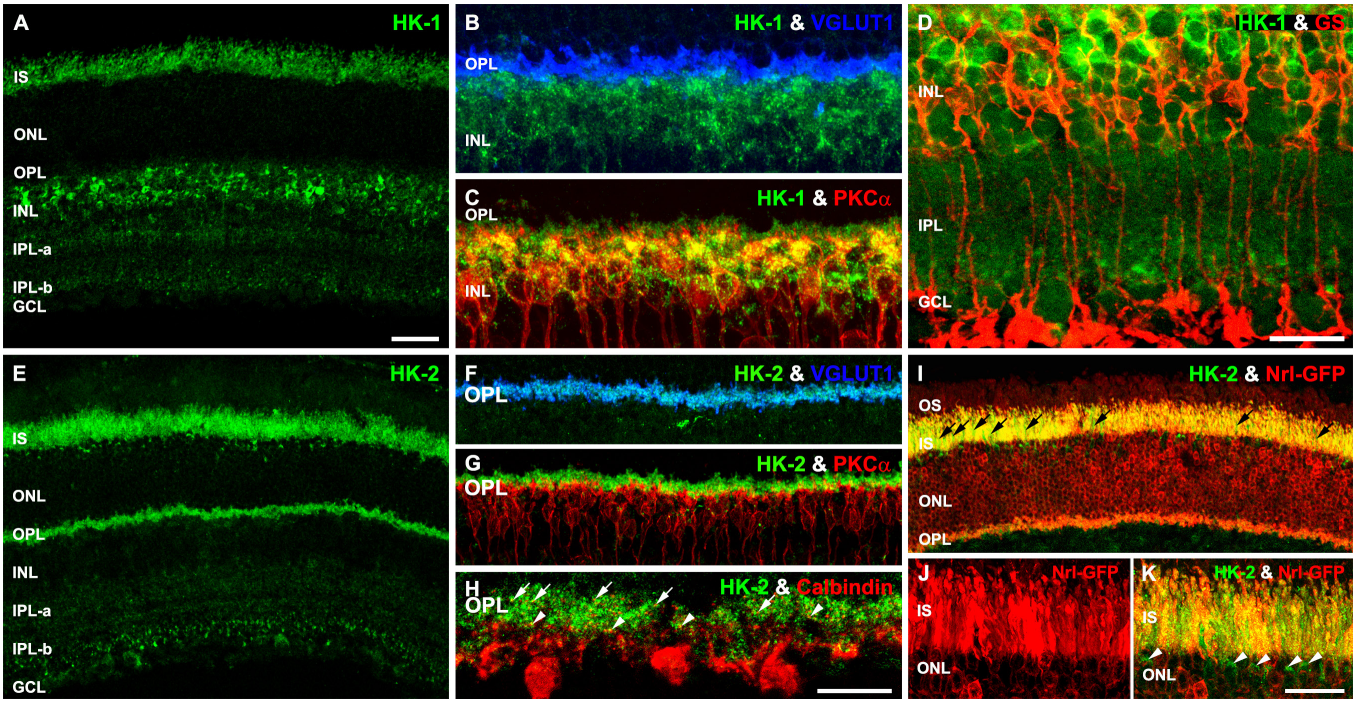

Figure 3. Confocal images reveal that two different isozymes of hexokinase, HK-1 and HK-2, have distinct compartmental and laminar distribution in the adult mouse retina. **A**: The anti-HK-1 antibody selectively and strongly labels the INL. **B**: High magnification of the OPL from retinas double-labeled for HK-1 and vesicular glutamate transporter 1 (VGLUT1) show no colocalization. **C**: A high-magnification image of the OPL from retinas double-labeled for HK-1 and protein kinase C alpha (PKCα) shows strong colocalization. **D**: Retinas double-labeled for HK-1 and glutamine synthetase (GS) show weak colocalization in the MGC somas. **E**: The anti-HK-2 antibody differentially labels the outer and inner retina. The anti-HK-2 antibody intensely labels the ISs and the OPL. **F**: A high-magnification image of the OPL double-labeled for HK-2 and VGLUT1 shows colocalization. **G**: HK-2 and PKCα do not colocalize. **H**: HK-2 and calbindin colocalize in horizontal cell axonal processes with rod terminals (white arrows) and in dendritic processes with cone terminals (white arrowheads). **I**: The outer retina of the neural retina leucine zipper–green fluorescent protein (*Nrl*-GFP) transgenic mice (pseudocolored in red) labeled for HK-2 shows colocalization in the rod IS and spherules (yellow-orange pixels) and HK-2 expression in the cone OSs and ISs (green pixels: black arrows) and pedicles (green pixels). **J**: High-magnification image of the OS-IS from *Nrl*-GFP transgenic mice (pseudocolored in red). **K**: High-magnification image of *Nrl*-GFP retina colabeled for HK-2 shows colocalization in the rod ISs and spherules (yellow-orange pixels) and localization of HK-2 in the cone OSs and ISs (green pixels) and somas in the ONL (green pixels: white arrowheads). GCL = ganglion cell layer, INL = inner nuclear layer, IPL = inner plexiform layer, IPL-a = IPL sublamina-a, IPL-b = sublamina-b, ISs = inner segments, ONL = outer nuclear layer, OPL = outer plexiform layer, OSs = outer segments. A, D, E, and I, scale bar = 40 µm. B–C and F–H, scale bar = 20 µm. J and K, the scale bar = 10 µm.

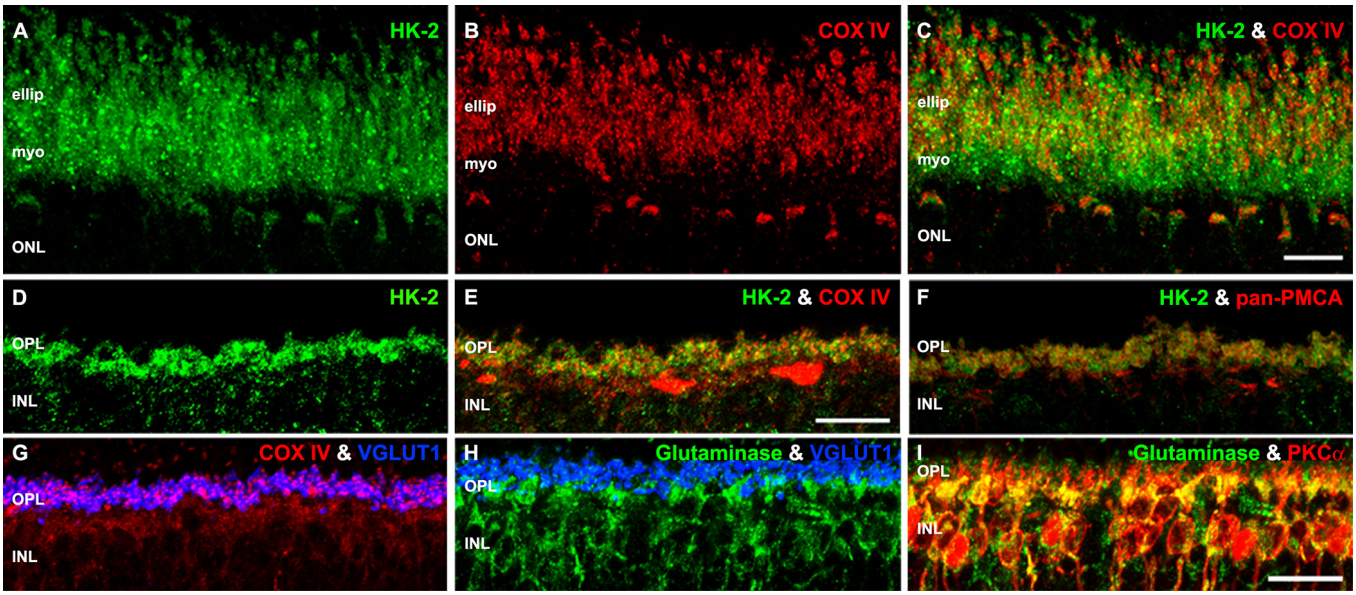

Figure 4. Confocal images reveal that photoreceptors intensely express HK-2 in the IS and the ONL compartments with mitochondria. **A**–**C**: High magnification images of the IS ellipsoid and myoid regions and the distal ONL immunolabeled for (**A**) HK-2, (**B**) COX IV, and (**C**) HK-2 and COX IV. Colocalization in the ellipsoids of the rods and cones and in the cone perinuclear mitochondria (white arrowheads) is visible (yellow-orange pixels). **D**–**F**: High-magnification images of the OPL immunolabeled for (**D**) HK-2, (**E**) HK-2 and COX IV, and (**F**) HK-2 and pan-plasma membrane Ca^{2+} ATPase (pan-PMCA). Colocalization is visible in the rod spherules (yellow-orange pixels) and the larger cone pedicles (green pixels: white arrows). High-magnification images of the OPL immunolabeled for (**G**) COX IV and VGLUT1, (**H**) GLS and VGLUT1, (**I**) and GLS and PKCα. Colocalization of GLS and PKCα is visible in the dendrites and somas of the rod bipolar cells (yellow-orange pixels). COX IV = cytochrome c oxidase subunit IV, ellip = ellipsoid, INL = inner nuclear layer, ISs = inner segments, myo = myoid, ONL = outer nuclear layer , OPL = outer plexiform layer, GLS = glutaminase, PKCα = protein kinase C α , VGLUT1 = vesicular glutamate transporter 1. A–C, scale bar = 10 µm. D–G, scale bar = 20 µm. H and I, scale bar = 40 µm.

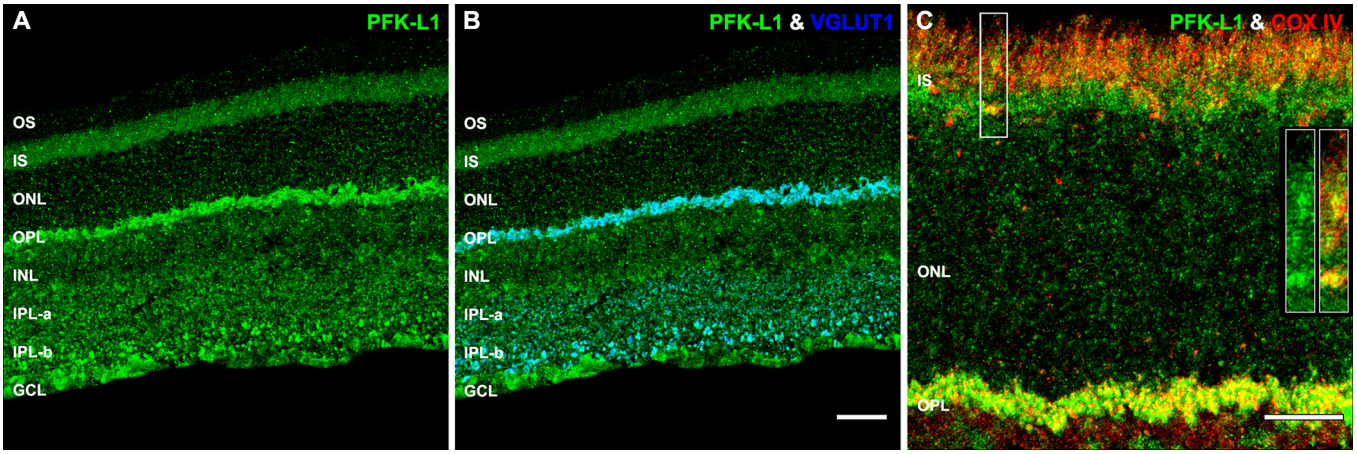

Figure 5. Confocal images reveal that PFK-L1 is expressed in all retinal cells and synapses. **A**: Retina immunolabeled for phosphofructokinase isoform L1 (PFK-L1). **B**: Retinas double-labeled for PFK-L1 and VGLUT1 show colocalization in the OPL and the IPL (aquamarine pixels). **C**: Retinas double-labeled for PFK-L1 and COX IV show intense colocalization in the IS and the OPL regions. High-magnification insets of highlighted cone shows single- and double-labeled colocalization in the OS, IS, and ONL of the perinuclear mitochondrion. COX IV = cytochrome c oxidase subunit IV, ISs = inner segments, IPL = inner plexiform layer, IPL-a = IPL sublamina-a, IPL-b = sublamina-b, ONL = outer nuclear layer, OPL = outer plexiform layer, OSs = outer segments, VGLUT1 = vesicular glutamate transporter 1. A and B, scale bar = 40 µm. C, scale bar = 20 µm.

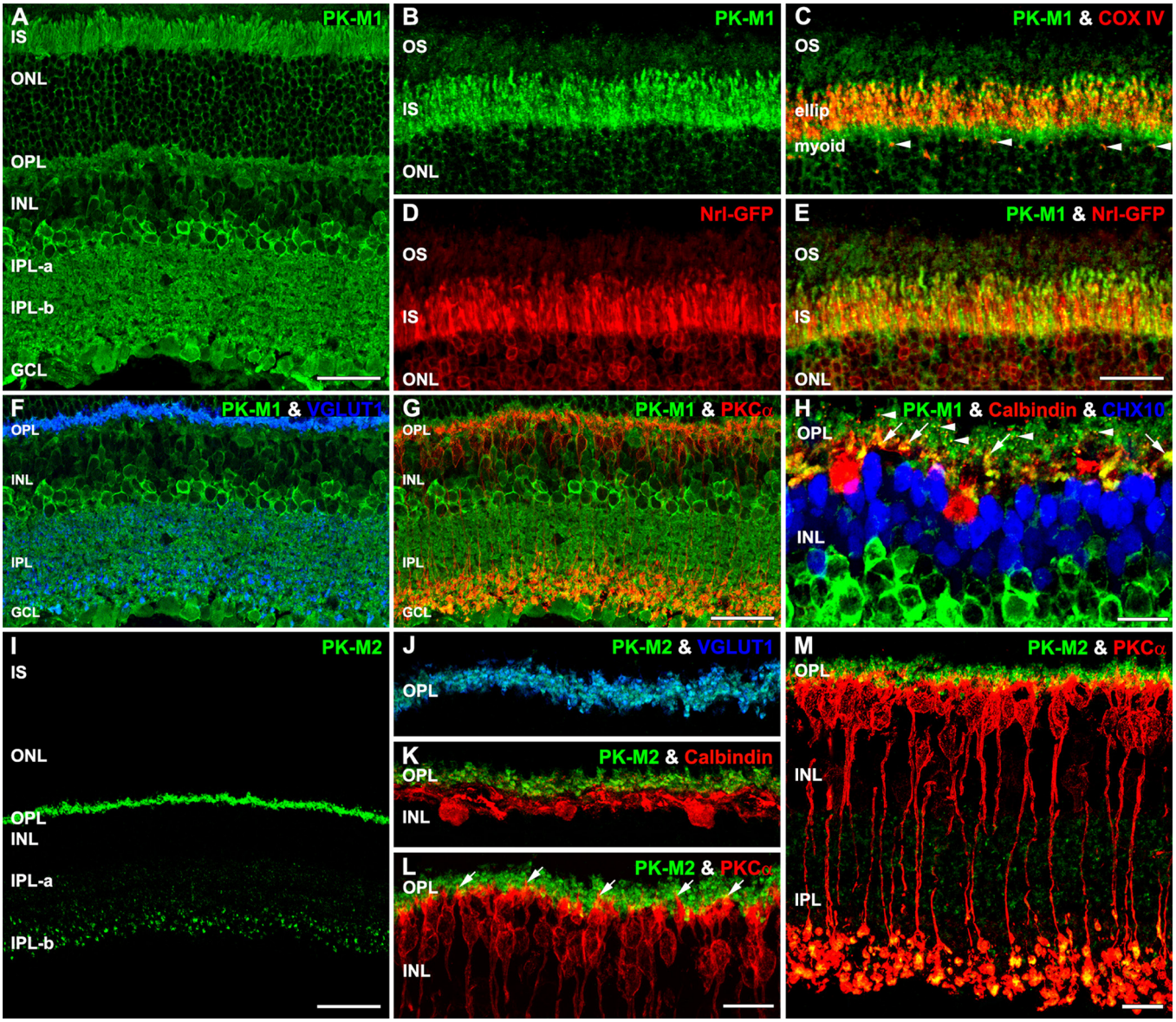

Figure 6. Confocal images show that two functionally distinct isozymes of pyruvate kinase M (PK-M1 and PK-M2) are differentially expressed throughout the adult retina. **A**: PK-M1 is expressed in all retinal neurons and synapses. **B**: High-magnification image of the outer retina immunolabeled for PK-M1. **C**: PK-M1 and COX IV colocalize (yellow-orange pixels) in the rod and cone IS and in cone perinuclear mitochondria (white arrowheads). **D**: High-magnification image of the outer retina from *neural retina leucine zipper*–green fluorescent protein (*Nrl*-GFP) transgenic mice (pseudocolored in red). **E**: PK-M1 is expressed in the rods (yellow-orange pixels: colabeled with *Nrl*-GFP) and cones (green only pixels). **F**: PK-M1 and VGLUT1 colocalized in the OPL and the IPL (aquamarine pixels). **G**: PK-M1 weakly colocalized in PKCα-IR rod bipolar cell dendrites and somas but colocalized in the rod bipolar cell axon terminals in the IPL-b (yellow-orange pixels). **H**: Retina triple-labeled for PK-M1, calbindin, and CHX10. PK-M1 and calbindin colocalize in horizontal cell axons in the rods (white arrowheads) and in dendrites in the cones (white arrows) but minimally in the somas. CHX10-IR bipolar cells weakly express PK-M1. **I**: PK-M2 is expressed in the OPL and the IPL. **J**: High-magnification image shows colocalization of PK-M2 and VGLUT1 throughout the OPL. **K**: High-magnification image only shows weak colocalization of PK-M2 and calbindin in horizontal cell processes. **L**: High-magnification image shows colocalization of PK-M2 and PKCα in the rod bipolar cell dendrites (yellow pixels: white arrows). **L**: High magnification of the OPL of a retina double-labeled for PK-M2 and VGLUT1. **M**: PK-M2 colocalized in the PKCα-IR rod bipolar cell dendrites and axon terminals (yellow-orange pixels) but not in the somas. COX IV = cytochrome c oxidase subunit IV, IPL = inner plexiform layer, IPL-a = IPL sublamina-a, IPL-b = sublamina-b, ISs = inner segments, ONL = outer nuclear layer, OPL = outer plexiform layer, OSs = outer segments, PKCα-IR = protein kinase C α immunoreactivity, VGLUT1 = vesicular glutamate transporter 1. A, F–G, and I, scale bars = 40 µm. B–E, H, and J–M, scale bars = 20 µm.

and the IPL (Figure 6I). PK-M2-IR was intense in the OPL and moderate to strong in the IPL (Figure 6I). To explore OPL labeling further, we double-labeled with VGLUT1 (Figure 6J), calbindin (Figure 6K), or PKCα (Figure 6L). Retinas double-labeled with PK-M2 and VGLUT1 (Figure 6J) showed colocalization. The HC somas and processes exhibited no or weak PK-M2-IR, respectively (Figure 6K). Double-labeling of PK-M2 with PKCα (Figure 6L,M) showed weak PK-M2-IR in the BC dendrites but strong PK-M2-IR in the BC synaptic terminals in the proximal IPL-b. The selective and moderate to intense expression of PK-M2 in the OPL and the IPL-b suggests differential regulation of glycolysis in these glutamatergic synaptic terminals.

LDH isoforms are differentially expressed in photoreceptor compartments and the inner retina: The microarray data indicate that the retina expresses high levels of *Ldha* and *Ldhb* and lower levels of *Ldhc* and *Ldhd* mRNA (Figure 1A). To determine the laminar and compartment distribution and expression levels of LDH, we immunolabeled retinas with a pan-antibody for LDH or an antibody selective for LDH-5 (*Ldha*). The antibodies for LDH-pan and LDH-5 used in this study recognized all isoforms that contain the M-subunit. Although LDH-5 is the most abundant LDH isozyme found in adult mouse retinal homogenates (~75% of LDH), LDH isozymes 2–4 also contain M subunits and were detected in much lower amounts [112,113]. The pan-LDH-IR (Figure 7A) and LDH-5-IR (Figure 7D) patterns of labeling and intensity were similar (Appendix 1). Strong to intense pan-LDH-IR and LDH-5-IR were observed in the photoreceptor compartments, except in the OSs where LDH-IR and LDH-5-IR were weak (Figure 7A,D). Double-labeling experiments with pan-LDH or LDH-5 and VGLUT1 showed colocalization in the OPL, but only weak colocalization in the IPL (Figure 7B,E). This finding suggests a low capacity for lactate metabolism in the IPL although the IPL expresses several MCT isoforms (Appendix 3). The MGCs exhibited no significant LDH-IR, except the external limiting membrane (ELM; Figure 7C). Double-labeling with LDH-5 and COX IV showed colocalization in the RISs, CISs (inset), OPL, and IPL (Figure 7F). The double-labeling experiments with LDH-5 and calbindin (Figure 7G), CHX10 (Figure 7H), and PKCα (Figure 7I) revealed no expression of LDH-5 in the HCs or in the BC dendrites and only weak to moderate LDH-5 expression in the rod BC somas. The GCL showed strong to intense pan-LDH-IR and moderate to strong LDH-5-IR (Figure 7A,D). The whole retinal mRNA amount and cellular distribution of LDH-5 we found are consistent with recent findings in the adult rat [55] and support the well-described capacity of photoreceptors for aerobic glycolysis [3,19,114-116].

LDH and COX activities vary in different layers of the mouse retina: To examine layer-by-layer LDH activity, we modified existing LDH histochemistry procedures and determined LDH activity in light-adapted mouse retinas (Figure 8). The level of LDH activity per layer, reflected by staining intensity, was dependent on the lactate substrate concentration, which has not previously been published for any tissue. We observed intense LDH activity in the ISs and the ELM at a physiologically relevant concentration of 1 mM lactate (Figure 8B). With 5 and 10 mM lactate, the ONL, OPL, and INL exhibited increased LDH activity (Figure 8C–D). As the Michaelis constant values of the substrate for LDH-5 are greater than those for the LDH isozymes 2–4 [33,34,36,117], these results indicate that the ONL, OPL, and INL express less LDH-5 and therefore have less LDH activity than the photoreceptors, which is consistent with the IHC data (Figure 7; Appendix 1). Interestingly, it appears that the cone ISs have lower LDH activity than the rod ISs as the LDH intensity noticeably increased in the cone ISs with increased lactate concentrations. Moreover, LDH-5 is more resistant to competitive inhibition by pyruvate compared to other LDH isoforms [36]. Therefore, we determined LDH-5 activity following the addition of pyruvate to the incubation media (Figure 8E–G). We observed persistent LDH activity in the ISs and decreased LDH in the other retinal layers after 1 or 5 mM pyruvate was added and therefore concluded that LDH-5 was the predominant isoform expressed in the ISs. Retinas incubated with 5 mM lactate and 5 mM pyruvate (Figure 8D,G) or 10 mM lactate and 5 mM pyruvate (Figure 8D,H) exhibited similar patterns of competitive inhibition, further validating our conclusion.

To determine the retinal layers with high COX activity, we quantified the COX histochemical reactivity in the light-adapted mouse retina (Figure 9). Similar to COX activity in the monkey retina [8], the mouse photoreceptor ISs exhibited the highest COX activity. Several perinuclear cone and rod mitochondria located in the distal and proximal regions of the ONL also showed strong COX activity. The proximal OPL and the distal INL were highly reactive for COX. Weak COX activity was observed throughout the middle and proximal INL. The IPL sublamina-a (IPL-a) and sublamina-b (IPL-b) showed similar high COX activity. The GCL showed high COX activity in the perinuclear mitochondria. The MGC external limiting membrane (elm) exhibited minimal COX activity, whereas the end-feet exhibited weak to moderate activity. The COX histochemical activity pattern (Figure 9) is consistent with our current IHC results (Figure 5; Appendix 1) and our previous COX IV-IR study [9] and supports the well-described retinal oxygen consumption [6,7] and oxygen tension [4,5] patterns in the rat, mouse, and monkey.

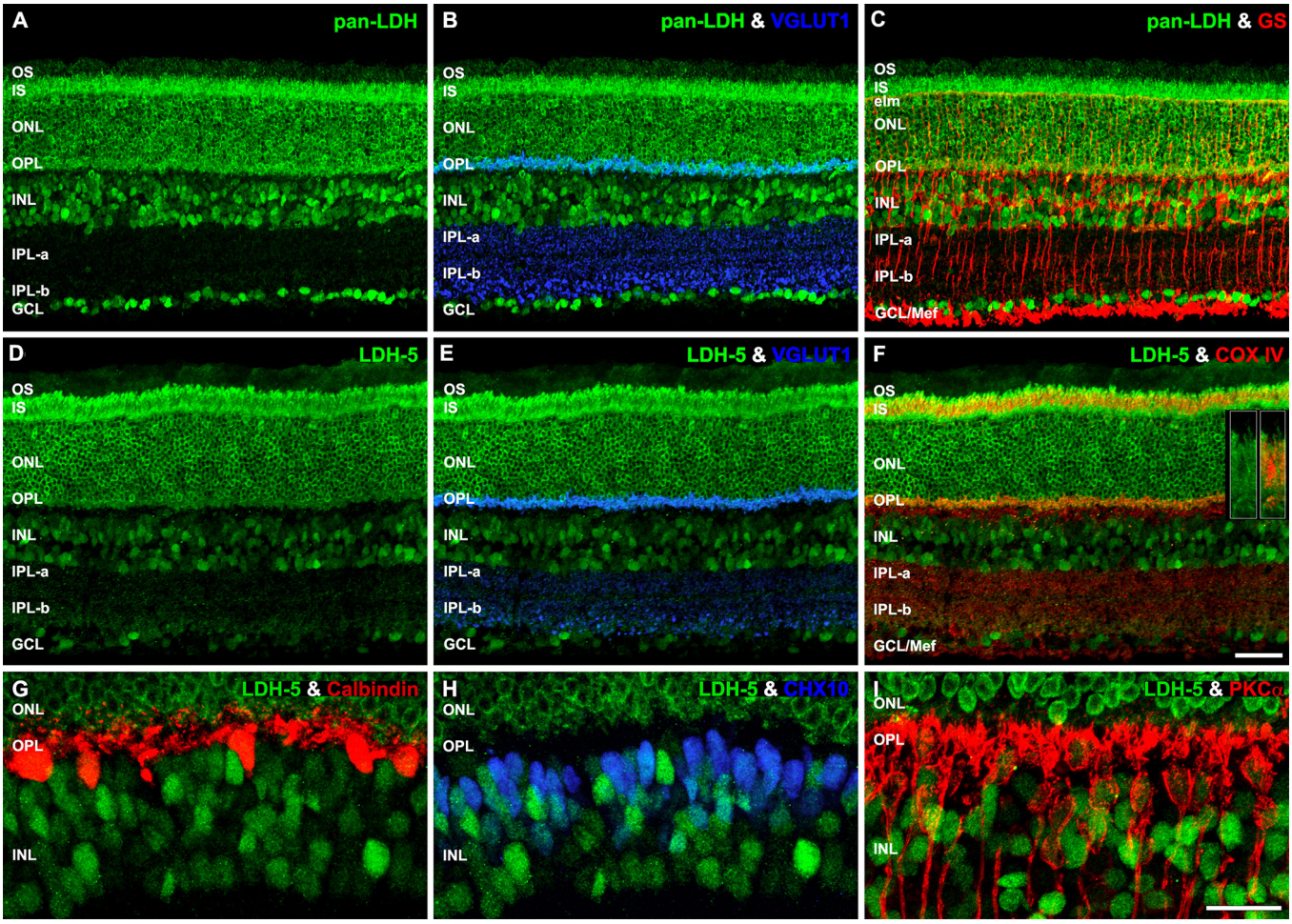

Figure 7. Confocal images show that pan-LDH and LDH isozyme 5 (LDH-5: liver and muscle type) are expressed in almost all retinal cells and synapses. **A**: Retina immunolabeled for pan-LDH. **B**: Retinas double-labeled for pan-LDH and VGLUT1 show colocalization in the OPL and the IPL (aquamarine pixels). **C**: Retinas double-labeled for pan-LDH and glutamine synthetase (GS) show weak colocalization in the MGC somas and ELM. **D**: Retina immunolabeled for LDH-5. **E**: Retinas double-labeled for LDH-5 and VGLUT1 show colocalization in the OPL and the IPL (aquamarine pixels). **F**: Retinas double-labeled for LDH-5 and COX IV show collocation in the ISs, OPL, and IPL. Inset: Single and double-labeled cone ISs from a high-magnification image revealing colocalization in the ISs. **G**: High-magnification image of a retina double-labeled for LDH-5 and calbindin shows no colocalization. **H**: High-magnification image of a retina double-labeled for LDH-5 and CHX10 reveals differential colocalization. **I**: High-magnification image of a retina double-labeled for LDH-5 and PKCα shows colocalization in the somas but not in the dendrites. COX IV = cytochrome c oxidase subunit IV, ELM = external limiting membrane, IPL = inner plexiform layer, IPL-a = IPL sublamina-a, IPL-b = IPL sublamina-b, ISs = inner segments, LDH = lactate dehydrogenase, MGC = Müller glial cell, ONL = outer nuclear layer, OPL = outer plexiform layer, OSs = outer segments, PKCα-IR = protein kinase C α immunoreactivity, VGLUT1 = vesicular glutamate transporter 1. A–F, scale bar = 40 µm. G–I, scale bar = 20 µm.

The mitochondrial enzymes GDH1, GABA-T, OGDH, and STK are differentially and highly expressed in photoreceptor mitochondria and the inner retina: Our previous work [9] characterized the distribution of retinal mitochondria using an antibody to COX IV, the well-accepted marker of mitochondria [8-10]. To further examine this question, we employed a panel of different mitochondrial enzyme markers. We immunolabeled the retina with anti-GDH1, -GABA-T, -OGDH, or -STK. The first two enzymes are involved in amino acid metabolism, and the latter two are part of the TCA cycle (Figure 10; Appendix 1). The expression of all four enzymes was intense in the rod and cone ISs and synaptic terminals and strong to intense in the ELM, IPL, GCL, and MGC end-feet. In the ONL, COX IV-IR (Figure 4C, Figure 5C, and Figure 7F [9]) and COX activity (Figure 9) were seen only in the cone somas and the proximal rod somas, and oxygen consumption was low [4,5]. The absence of COX labeling and activity in the ONL suggests that mitochondria

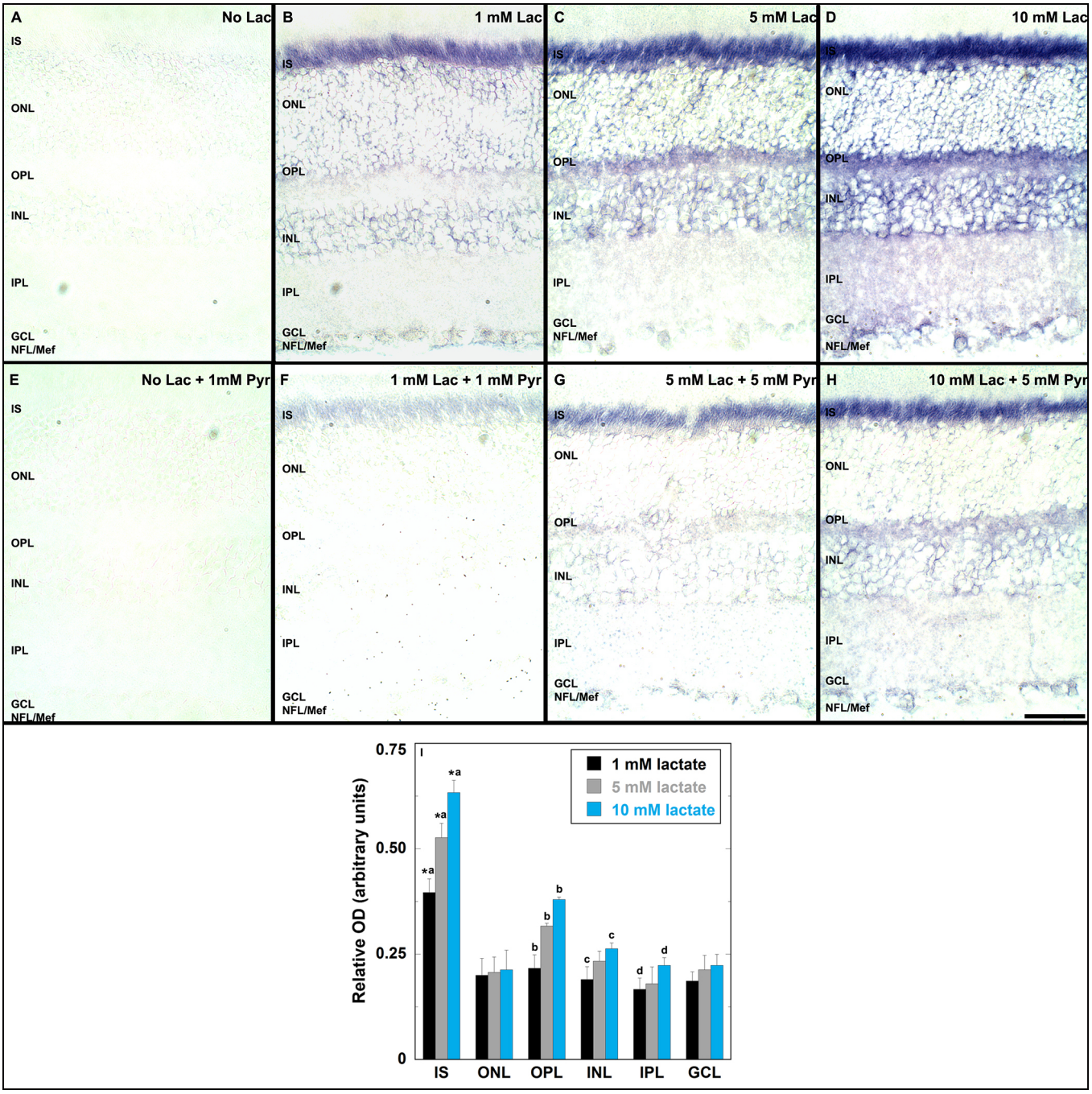

Figure 8. LDH histochemistry of the light-adapted mouse retina. Different concentrations of sodium DL-lactate showed selective activity of lactate dehydrogenase (LDH) in the ISs. **A**: Retinas incubated in the absence of the sodium DL-lactate. No LDH reactivity is observed. **B**: Retinas incubated with 1 mM sodium DL-lactate show LDH activity in the IS. **C**: Retinas incubated in 5 mM sodium DL-lactate show high LDH activity in the ISs and low LDH activity in the OPL. **D**: Retinas incubated in 10 mM sodium DL-lactate show intense LDH activity in the IS and strong LDH activity in the OPL, INL, and GCL. **E**: Retinas incubated in the absence of sodium DL-lactate and 1 mM sodium pyruvate. **F** and **G**: Retinas incubated with equimolar concentrations of sodium DL-lactate and sodium pyruvate show selective LDH activity in the ISs. **H**: Retinas incubated with 10 mM sodium DL-lactate and 5 mM sodium pyruvate show reduced activity of LDH in most retinal layers except the ISs. **I**: LDH activity in different retinal layers presented as mean ± SEM of relative optical density. The LDH activity in ISs was significantly greater at each concentration of lactate relative to the other retinal layers as indicated by asterisks ($p<0.05$). Bars for each retinal layer that share the same letter (a, b, c, or d) exhibit significant concentration-dependent increases in LDH activity with increasing concentration of lactate ($p<0.05$). GCL = ganglion cell layer, INL = inner nuclear layer, IPL = inner plexiform layer, ISs = inner segments, NFL = nerve fiber layer, ONL = outer nuclear layer, OPL = outer plexiform layer. Scale bar = 20 µm.

are not present there. However, we found the expression of GABA-T (Figure 10A), GDH1 (Figure 10C), and OGDH (Figure 10E) in the ONL is punctate and strong to intense, whereas the expression of STK (Figure 10F) is moderate and more like that of COX IV-IR (Figure 4 and Figure 5) [9]). This is consistent with IHC results in the adult rat ONL, which showed sparse GABA-T staining in the ONL [118].

The mitochondrial enzymes GDH1-, GABA-T-, OGDH, and STK are differentially expressed in MGCs: Mitochondria in MGCs exhibit relatively weak COX IV-IR (Figure 4, Figure 5, and Figure 7) and minimal COX activity (Figure 9). The low COX expression and activity in MGCs suggest that their mitochondria maintain minimal OXPHOS capacity. Cultured MGCs showed significant metabolism of amino acids and recycling of metabolic intermediates [30]. To examine further the expression of mitochondrial markers in MGCs, we colabeled with anti-GDH1, -GABA-T, -OGDH or -STK, and GLAST (Figure 10; Appendix 1). The double-labeling experiments with GDH1 or GABA-T and GLAST showed strong to intense GDH1-IR or GABA-T-IR throughout the MGCs (Figure 10B,D, respectively). Strong to intense GDH1-IR and GABA-T-IR were observed in the MGC ELM, distal and proximal processes, OPL, somas, and end-feet (Appendix 1). The pattern of OGDH-IR (Figure 10F) and STK-IR in the MGCs (Figure 10H) was different from that of GDH1 or GABA-T. OGDH-IR and STK-IR were strong in the MGC ELM and moderate to strong in the distal and proximal processes, OPL, somas, and end-feet (Appendix 1). Together, the low expression of COX IV, low COX activity, and higher expression of GDH1, GABA-T, OGDH, and STK in the MGCs indicate that low OXPHOS flux and higher glutamate metabolism occur in MGC mitochondria compared to neuronal mitochondria. Moreover, the presence of GLAST, GDH1, OGDH, and STK in the MGCs indicates that they utilize glutamine and glutamate to generate GTP via the TCA cycle under normal physiologic conditions: discussed in detail below. It is also possible that the MGCs use these and other amino acids under pathophysiological conditions [119].

NDPK is ubiquitously expressed in the mouse retina: Gene expression for *Nme1* (NDPK-A) and *Nem2* (NDPK-B)

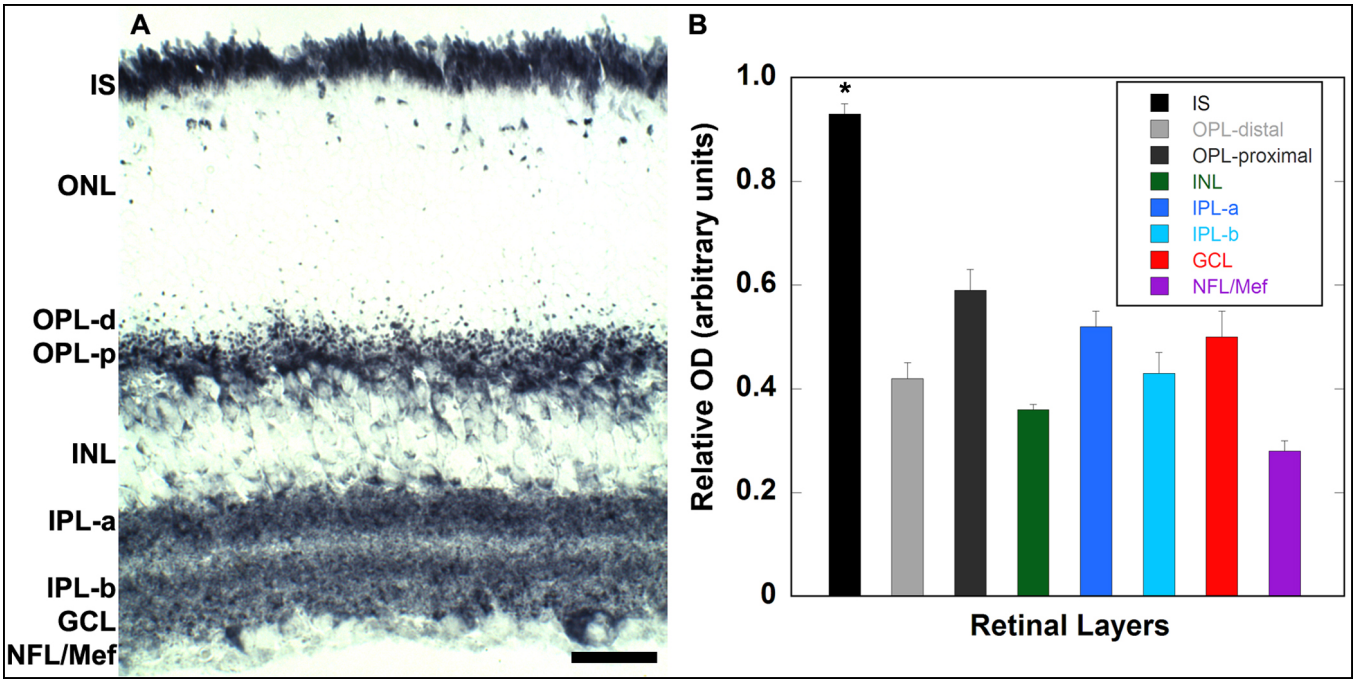

Figure 9. COX activity in the light-adapted mouse retina is compartmentalized. **A**: The y-axis shows the retinal layers. There was no detectable cytochrome oxidase (COX) activity in the photoreceptor OSs. COX activity was strongest in the photoreceptor ISs, OPL, and outermost region of the INL. Moderate reactivity is localized in the proximal INL. The IPL-a is more reactive compared to the IPL-b. The GCL shows strong COX reactivity localized to the mitochondria near the somas and is more reactive in some retinal ganglion cells than others. The NFL/MGC end-feet was less reactive compared to the rest of the reactive layers. **B**: COX activity in different retinal layers presented as mean ± SEM of relative optical density. The COX activity in ISs is significantly greater than that in all other retinal layers as indicated by asterisk ($p<0.05$). GCL = ganglion cell layer, INL = inner nuclear layer, IPL-a = IPL sublamina-a, IPL-b = IPL sublamina-b, ISs = inner segments, MGC = Müller glial cell, NFL = nerve fiber layer, ONL = outer nuclear layer, OPL = outer plexiform layer, OSs = outer segments. A, scale bar = 20 μM.

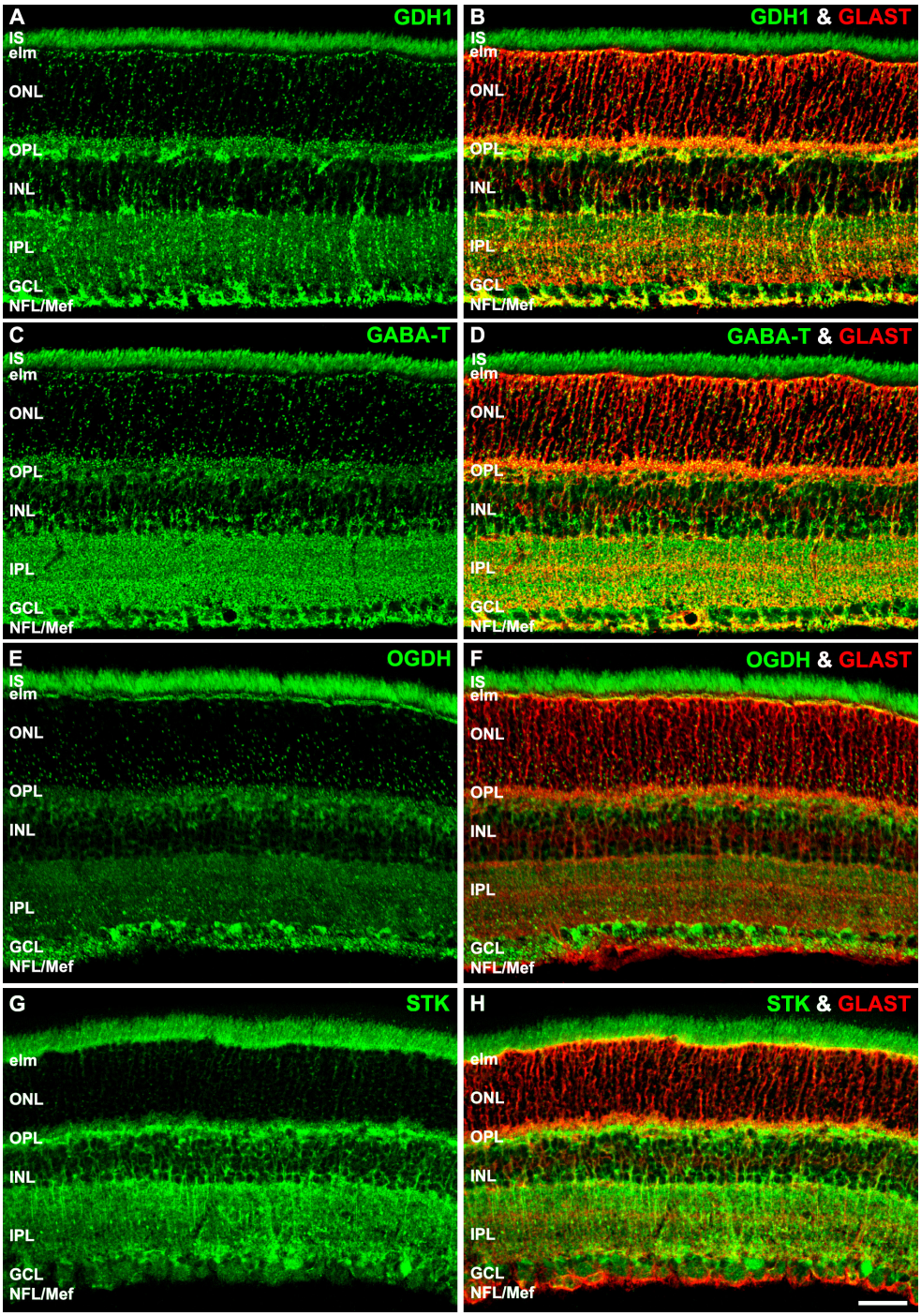

Figure 10. Confocal images reveal a unique metabolic signature of Müller cell mitochondria. **A**: Retinas immunolabeled for glutamate dehydrogenase 1 (GDH1) reveal intense expression in rod and cone ISs and synaptic terminals, and a strong to intense in the ELM, IPL, GCL, and MGC end-feet. The expression in the ONL is punctate and strong to intense. **B**: Strong to intense colocalization of GDH1-IR and glial high-affinity glutamate-aspartate transporter (GLAST-IR) is seen throughout the MGCs. **C**: Retinas immunolabeled for GABA-transaminase (GABA-T) reveal an intense expression in rod and cone ISs and synaptic terminals, and a strong to intense in the ELM, IPL, GCL, and MGC end-feet. The expression in the ONL is punctate and strong to intense. **D**: Strong to intense colocalization of GABA-T-IR and GLAST-IR is seen throughout the MGCs. **E**: Retinas immunolabeled for the lipoamide subunit of the 2-oxoglutarate (α-ketoglutarate) dehydrogenase complex (OGDH) reveal intense expression in the rod and cone IS and synaptic terminals and a strong to intense in the ELM, IPL, GCL, and MGC end-feet. The expression in the ONL is punctate and strong to intense. **F**: OGDH-IR and GLAST colocalization is strong in the ELM and end-feet, and moderate distal and proximal processes, OPL, and somas. **G**: Retinas immunolabeled for succinate thiokinase (STK) reveal intense expression in the rod and cone ISs and synaptic terminals and strong to intense expression in the ELM, IPL, GCL, and MGC end-feet. The expression in the ONL is moderate and more like that of COX IV-IR (Figure 4, Figure 5, and Figure 7). **H**: STKH-IR and GLAST colocalization is strong in the ELM, proximal processes, and end-feet and moderate in the distal processes, OPL, and somas. COX IV-IR = cytochrome oxidase IV immunoreactivity, ELM = external limiting membrane, GCL = ganglion cell layer, INL = inner nuclear layer, IPL = inner plexiform layer, ISs = inner segments, MGC = Müller glial cell, NFL = nerve fiber layer, ONL = outer nuclear layer. A–H, scale bars = 40 µm.

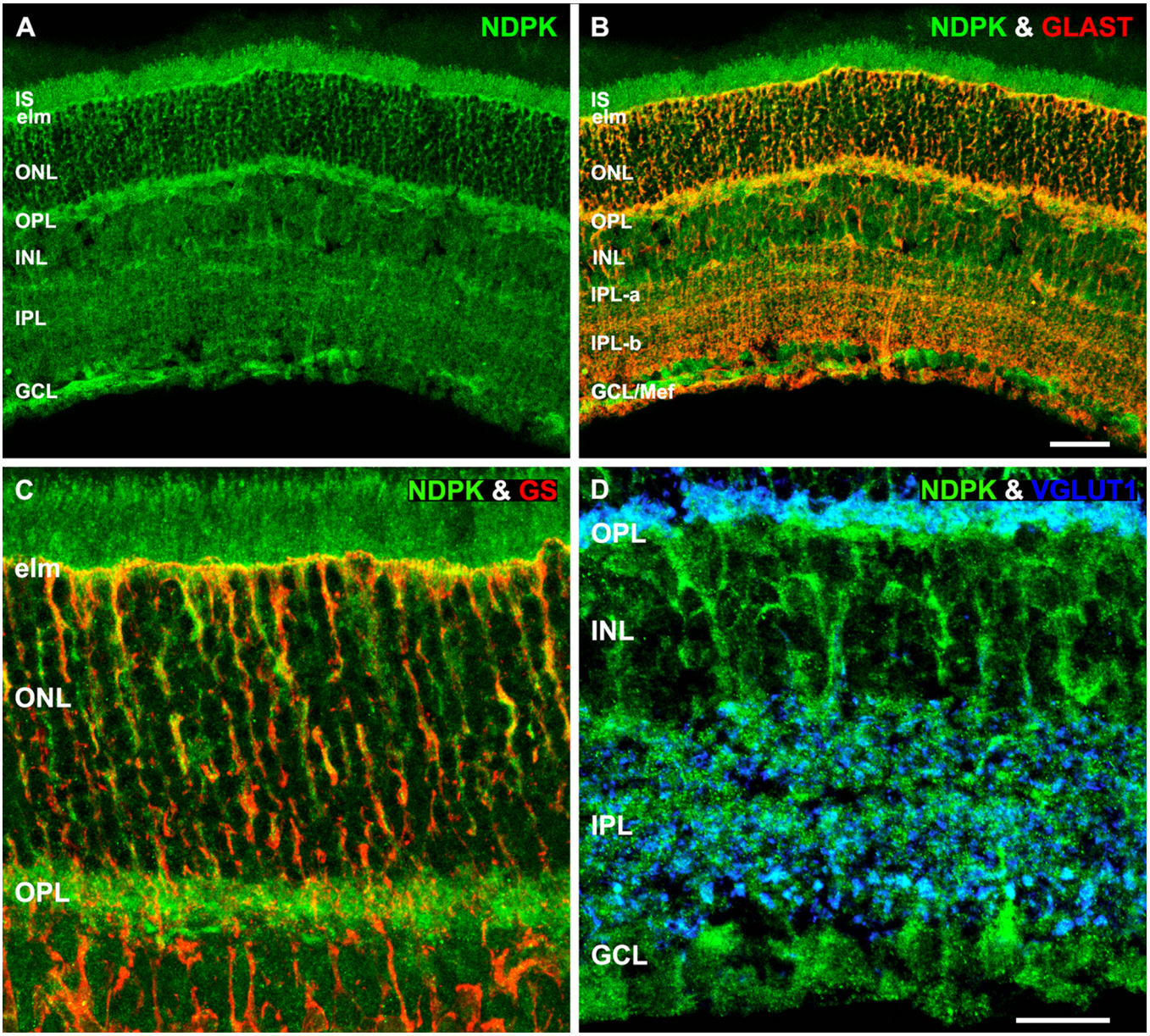

Figure 11. Confocal images show that NDPK is widely expressed throughout the retina. **A**: Retina immunolabeled for nucleoside diphosphate kinase isoform A (NDPK). **B**: Retinas double-labeled for NDPK and the glial high-affinity glutamate-aspartate transporter (GLAST) show colocalization in all MGC regions: the ELM, distal and proximal processes, soma, and end-feet (yellow-orange pixels). **C**: A higher-magnification image shows colocalization of NDPK and GS in the distal and proximal MGC processes (yellow-orange pixels). **D**: A high-magnification image of a retina double-labeled for NDPK and VGLUT1 reveals greater colocalization in the OPL than in the IPL (aquamarine pixels). COX IV-IR = cytochrome oxidase IV immunoreactivity, ELM = external limiting membrane, GCL = ganglion cell layer, GS = glutamine synthetase, INL = inner nuclear layer, IPL = inner plexiform layer, IPL-a = IPL sublamina-a, IPL-b = IPL sublamina-b, ISs = inner segments, MGC = Müller glial cell, ONL = outer nuclear layer, OPL = outer plexiform layer, VGLUT1 = vesicular glutamate transporter 1. A and B, scale bar = 40 µm. C and D, scale bar = 20 µm.

was highest among the NDPK isoforms (Figure 1B). We determined the retinal distribution and relative intensity of NDPK-A-IR (Figure 11; Appendix 1). Most, but not all, retinal compartments expressed NDPK. The exceptions were the BC dendrites, HC somas, and HC processes (detailed data not shown). We observed weak NDPK-A-IR in the OSs. Consistent with this finding, the lowest NDPK activity in the monkey and rabbit retina was in the OSs [70]. Double-labeling with NDPK-A and GLAST (Figure 11B) or GS (Figure 11C) showed strong to intense NDPK-A-IR in the distal and proximal MGC processes, somas, and end-feet. Double-labeling with NDPK-A and VGLUT1 showed strong to intense expression in the spherules and pedicles and strong intensity in the IPL (Figure 11D).

AK1 and AK2 have differential compartmental and laminar expression: The adult retina expresses five isozymes of *Ak* mRNA (Figure 1B). We determined the cellular and compartmental distribution of AK1 and AK2 in the retinas (Figure 12; Appendix 1). The immunolabeling revealed that there was no AK1 expression in the outer retina and strong to intense AK1-IR in the inner retina, except in the BC somas in the distal INL somas and the rod BC somas (Figure 11A; Appendix 1). Double-labeling with AK1 and GLAST revealed limited and weak expression of AK1 only in the MGC distal processes and end-feet/nerve fiber layer (NFL) (Figure 12B). The triple-labeling experiments with AK1, CHX10, and VGLUT1 (Figure 12C) revealed an absence of AK1 in the photoreceptor terminals. Strong to intense AK1-IR was seen in the HC somas and processes, proximal INL, and IPL. Double-labeling with AK1 and GABA showed strong AK1-IR in the GABAergic AC somas in the INL and displaced GABAergic AC somas in the GCL (Figure 12D: arrows). Double-labeling with AK1 and ChAT or DAB1 revealed that AK1 was not present in the CHAT-IR ACs (Figure 12E), but the glycinergic (DAB-IR) ACs had weak to moderate AK1-IR (Figure 12F: white arrows), respectively. Large diameter somas in the GCL showed moderate AK1-IR (Figure 12F). AK2-IR was moderate to intense in most layers and cells of the neuronal retina, except in the BC somas in the distal INL somas and the rod BC somas (Figure 12G; Appendix 1). Double-labeling with AK2 and VGLUT1 indicated higher AK2 expression in the presynaptic OPL compared to the postsynaptic OPL and IPL (Figure 12H). Double-labeling with AK2 and GLAST showed moderate to strong expression in all MGC compartments, except the end-feet/NFL (Figure 12I).

CK-B, mi-CK, and CK-M show differential cellular and compartment expression: Our Affymetrix data showed that four isoforms of CK were expressed in the adult mouse retina: *Ckb, Ckm, Ck-mt1*, and *Ck-mt2* (Figure 1B). All were significantly expressed, although *Ckb* and *Ck-mt1* were more highly expressed than *Ckm* and *Ck-mt2*. Therefore, the cellular and compartment distributions of CK-B-IR, CK-M-IR, and mi-CK-IR were determined (Figure 13, Figure 14, and Figure 15; Appendix 1). We observed differential cellular- and compartment-selective CK-B-IR throughout the mouse retina, including the MGC ELM and end-feet (Figure 13), as described [83]. Detailed cellular and compartmental characterization of CK-B-IR in the photoreceptors was conducted using *Nrl*-GFP retinas immunolabeled with CK-B. Weak CK-B-IR was seen throughout the rods in the ROSs, RISs, rod somas, and spherules (Figure 13B,C). In contrast, moderate to intense CK-B-IR was seen in the cones. The COSs and the pedicles had moderate CK-B-IR (Figure 13C,D), while the CISs (Figure 13C: arrows) and cone somas (Figure 13A: arrowheads) had intense CK-B-IR (also see higher magnification of the CK-B-IR insert in Figure 13C). The double-labeling experiments with CK-B and calbindin indicated strong and weak expression in the HC processes and somas, respectively (Figure 13E,F). The double- and triple-labeling experiments with CK-B, PKCα, and/or VGLUT1 revealed moderate to strong CK-B-IR in the rod BC dendrites, somas, and axon terminals in the IPL-b (Figure 13G,H). Double-labeling of CK-B with GLAST (Figure 13I) and CK-B with GS (Figure 13J) revealed differential labeling throughout the MGCs. Intense CK-B-IR was seen in the MGC ELM and end-feet, but weak to moderate in the MGC processes and somas.

Figure 14 shows that the overall pattern of mi-CK-IR is quite different from that of CK-B (Figure 13), except in the photoreceptor ISs and somas. The photoreceptor OSs, BCs (dendrites, somas, and processes), HCs (processes and somas), and ACs in the proximal INL exhibited no mi-CK-IR (Appendix 1). In addition, double-labeling of mi-CK with GS revealed that the MGCs lacked mi-CK-IR, except in the end-feet (Figure 14B; Appendix 1). Double-labeling of mi-CK with COX-IV confirmed the intense mi-CK-IR in the pedicles and perinuclear cone mitochondria in the ONL (Figure 14C).

CK-M-IR was detected in the skeletal muscle (Figure 15A,B), cerebral cortex (Figure 15C,D), and retina (Figure 15E–J). DRAQ5 dye labeled the nuclei (Table 1). CK-M-IR was localized near the nuclei of myocytes and cortical neurons (Figure 15B,D). In the neural retina, the overall cellular and compartmental pattern of CK-M (Figure 15E) shares similarities with CK-B (Figure 13A) and CK-mi (Figure 14A); see Appendix 1 for detailed compartmental comparisons. That is, CK-M is not expressed in the photoreceptor OSs or in the HC processes and somas. CK-M exhibits strong to intense expression in the photoreceptors (ISs, somas, and synaptic

terminals) and the GCL and moderate to strong expression in the BCs (dendrites, somas, and synaptic terminals) as seen in Figure 15E–J. Interestingly, the pattern of CK-M-IR observed in the ISs, ONL, and OPL (Figure 15F,G) resembled the expression pattern of SERCA 3 that we have previously characterized [9]. The punctate expression pattern is similar to and coincides with the COX IV-IR in the ellipsoids (Figure 15H), cone somas, and photoreceptor synaptic terminals (Figure 15I). The INL showed a diffuse CK-M-IR pattern in the rod BCs and the GCL. The double-labeling experiments with CK-M and PKCα (Figure 15J) showed, at higher resolution, moderate to strong CK-M-IR in the BC compartments. The MGCs had no to weak expression in all compartments, except the end-feet that had strong CK-M-IR (Figure 15E,J).

Figure 16 presents an integrated summary of relative antibody intensity levels obtained from the immunoreactivity of bioenergetic regulating and buffering enzymes in the neuronal and glial compartments of the adult light-adapted C57BL/6N mouse retina. It is discussed in detail in the figure legend and discussion.

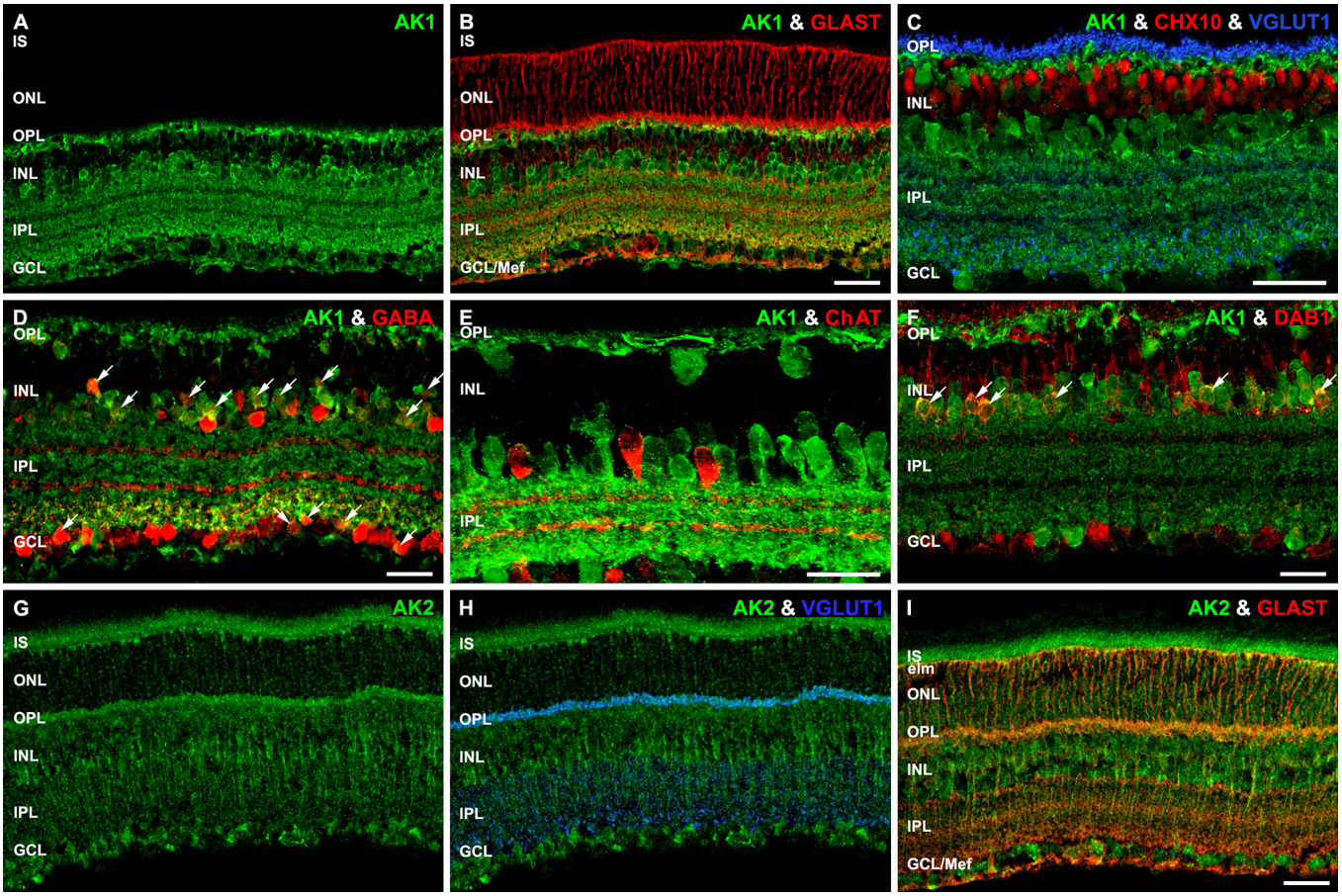

Figure 12. Confocal images show that two functionally distinct isozymes of adenylate kinase (AK1 and AK2) are differentially expressed throughout the retina. **A**: AK1 is selectively expressed in the inner retina. **B**: Retinas double-labeled for AK1 and GLAST show no colocalization. **C**: A high-magnification image of the retina reveals that AK1 does not colocalize with either CHX10 or VGLUT1. **D**–**F**: High magnification images of the inner retina double-labeled for AK1 and three antibodies for different types of amacrine cells. **D**: AK1 and GABA colocalize in weakly GABAergic-IR cells in the INL and the GCL (white arrows). **E**: AK1 and ChAT do not colocalize in cholinergic amacrine cells or the two cholinergic strata in the IPL. **F**: AK1 and disabled 1 (DAB1) colocalize in distal amacrine cells (white arrows). **G**: Retina immunolabeled for AK2. **H**: Retinas double-labeled for AK2 and VGLUT1 show colocalization in the OPL and the IPL (aquamarine pixels). **I**: Retinas double-labeled for AK2 and GLAST show extensive colocalization (yellow-orange pixels). ChAT = choline acetyltransferase, GCL = ganglion cell layer, GLAST = glutamate-aspartate transporter, INL = inner nuclear layer, IPL = inner plexiform layer, ISs = inner segments, ONL = outer nuclear layer, OPL = outer plexiform layer, VGLUT1 = vesicular glutamate transporter 1. A, B, D, and F–I, scale bar = 40 µm. C, scale bar = 20 µm. E, scale bar = 20 µm.

DISCUSSION

Our combined results indicate the following: 1) Outer retinal glycolytic metabolism is significantly different from inner retinal glycolytic metabolism. 2) Photoreceptors and their synapses exhibit the highest capacity for glycolysis, aerobic glycolysis, and OXPHOS, and regulate glucose metabolism by the compartment-selective expression of HK-1, HK-2, PFK-L, PK-M1, and PK-M2. 3) Cones, but not rods, coexpress cytosolic CK-B and mi-CK to maintain ATP homeostasis. 4) HC somas, HC processes, BC dendrites, and MGCs have a limited capacity for glycolysis and aerobic glycolysis. 5) HC somas, HC processes, and BC dendrites express high levels of GDH, OGDH, STK, and GABA-T (TCA cycle enzymes) and thus likely utilize glutamine and non-glucose derived monocarboxylates to support mitochondrial GTP and ATP production. 6) Expression of cytosolic NDPK, mitochondria-associated AK2, and mitochondria-associated CK-M is higher in the outer retina than in the inner retina, whereas expression of cytosolic AK1 and cytosolic CK-B is highest in HCs and ACs. 7) MGCs have the lowest overall expression level of glycolytic isozymes and COX IV as well as LDH and COX activity. In contrast, MGCs exhibit high expression levels of GDH, OGDH, STK, and GABA-T indicating that the TCA cycle anaplerotic and cataplerotic reactions are significant in MGCs and likely support the MGC energy requirements by generating GTP. 8) In MGCs, NDPK, AK2, and CK-B participate in regulating ATP synthesis and homeostasis. Overall, our findings indicate differential cellular and compartmental metabolism of glucose, amino acids, lactate, and creatine as well as ATP-buffering strategies that result in corresponding spatial differences in retinal glycolysis, aerobic glycolysis, TCA cycle metabolism,

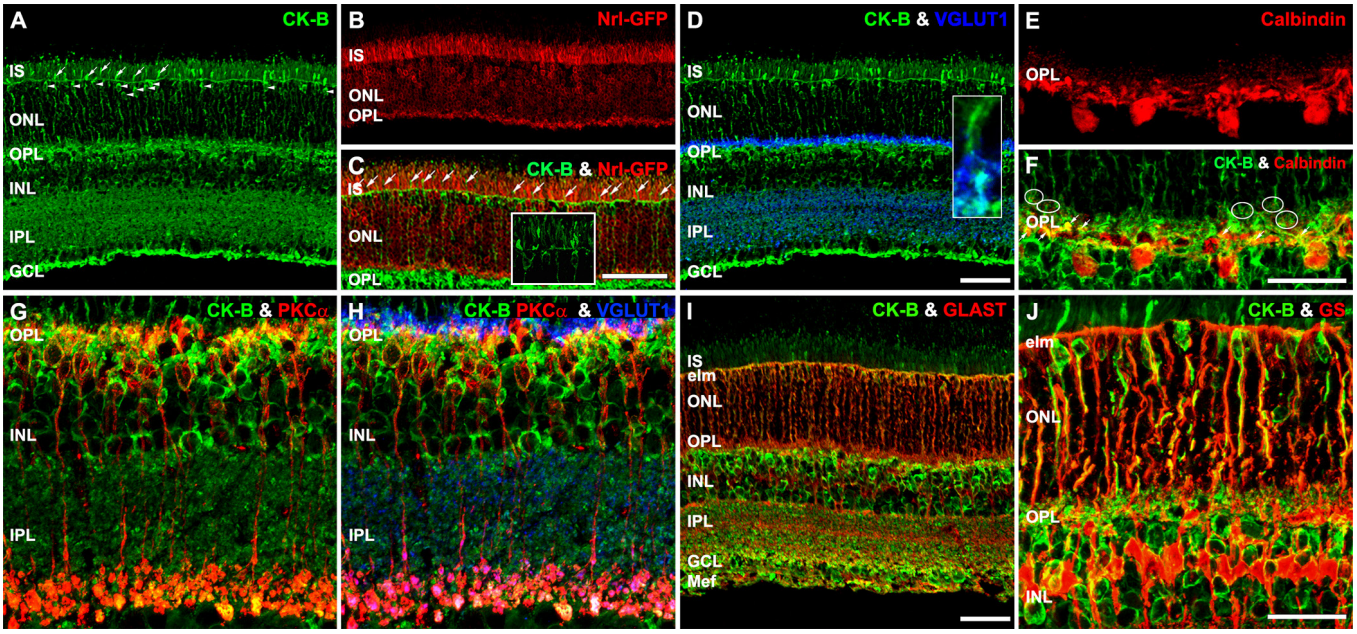

Figure 13. Confocal images reveal that the brain-type CK-B is differentially expressed throughout the retina. **A**: Retinas immunolabeled for creatine kinase isozyme (CK-B) show that the cone ISs (white arrows) and cytoplasm of the cone somas in the distal ONL (white arrowheads) are intensely labeled. **B** and **C**: Retinas of *neural retina leucine zipper*-green fluorescent protein (*Nrl*-GFP) transgenic mice pseudocolored in red (**B**) that were (**C**) double-labeled for CK-B show that rods minimally express CK-B, while the CK-B-IR cone ISs are visible (white arrows). Insert: Higher-magnification image of CK-B-IR. **D**: Retinas double-labeled for CK-B and VGLUT1 reveal colocalization in the OPL (aquamarine pixels). The high-magnification inset shows colocalization in the presynaptic terminal of a cone pedicle. **E** and **F**: High-magnification images of the OPL (**E**) single-labeled for calbindin, which selectively labels horizontal cells and their processes, and (**F**) double-labeled for CK-B and calbindin, which colocalized in the horizontal cell dendrites of cone pedicles (white arrows: yellow-orange pixels) and horizontal cell axon terminals in the rod spherules (inside white stroked circles: pairs of yellow-orange pixels). **G** and **H**: Retinas double-labeled for CK-B and PKCα and/or triple-labeled with VGLUT1 reveal colocalization of CK-B in rod spherules located in the distal OPL (yellow-orange pixels). **I** and **J**: Retinas double-labeled for CK-B either (**I**) GLAST or (**J**) GS show colocalization in the ELM, in close apposition to cone axons in the ONL and MGC end-feet. ELM = external limiting membrane, GCL = ganglion cell layer, GLAST = glutamate-aspartate transporter, GS = glutamine synthetase, INL = inner nuclear layer, IPL = inner plexiform layer, ISs = inner segments, MGC = Müller glial cell, ONL = outer nuclear layer, OPL = outer plexiform layer, PKCα = protein kinase C α, VGLUT1 = vesicular glutamate transporter 1. A, B, D, and I, scale bar = 40 µm. C, scale bar = 30 µm. E–H and J, scale bar = 20 µm.

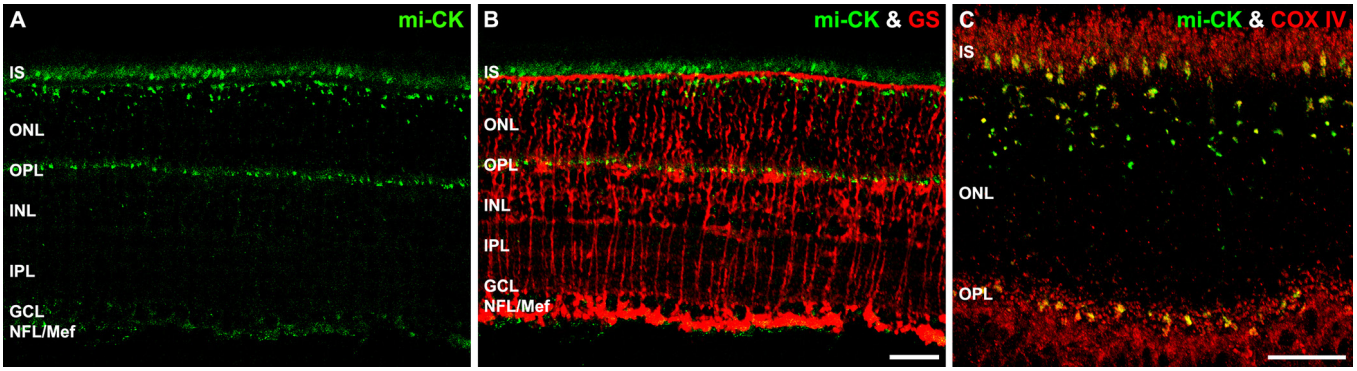

Figure 14. Confocal images show selective expression of the ubiquitous mi-CK in mouse retina. **A**: Retinas immunolabeled for mitochondrial creatine kinase (mi-CK) show that the ISs, distal ONL, OPL, GCL, and NFL/MGC end-feet are labeled. **B**: Retinas double-label with mi-CK and GS show moderate mi-CK-IR in the MGC end-feet. **C**: Retinas double-labeled with mi-CK and COX IV show that the cone ISs and the perinuclear mitochondria of cone somas in the distal ONL are intensely labeled while rod inner segments (RISs) and spherules show weak to moderate mi-CK-IR. COX IV = cytochrome c oxidase subunit IV, GCL = ganglion cell layer, GS = glutamine synthetase, IPL = inner plexiform layer, ISs = inner segments, MGC = Müller glial cell, NFL = nerve fiber layer, ONL = outer nuclear layer, OPL = outer plexiform layer. A and B, scale bar = 40 µm. C, scale bar = 20 µm.

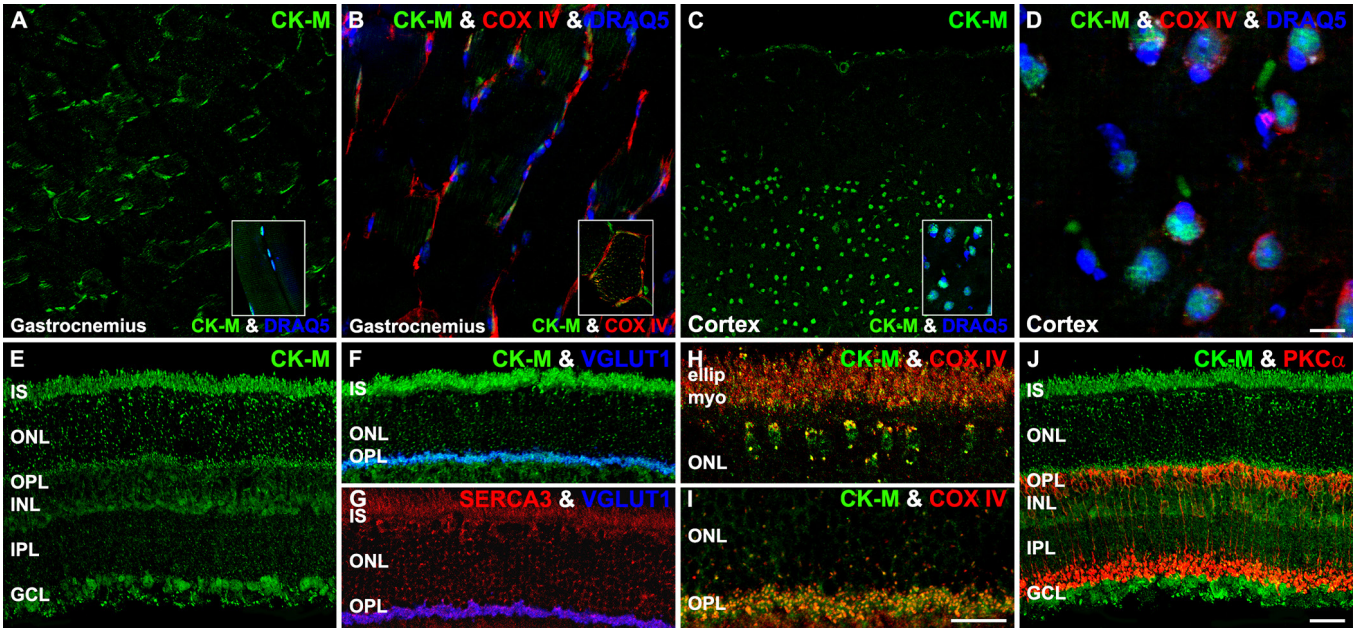

Figure 15. Confocal images illustrate that the creatine kinase isozyme found in muscle and the brain (CK-M) is distributed in cellular regions of the retina where endoplasmic reticulum proteins are located. **A**: A transverse section of mouse gastrocnemius immunolabeled for CK-M. The inset shows a longitudinal section of the gastrocnemius immunolabeled for CK-M and stained with the nuclear dye DRAQ5. **B**: A longitudinal section of gastrocnemius triple-labeled for CK-M, COX IV, and DRAQ5. The inset shows a high-magnification image of a transverse section of the gastrocnemius double-labeled for CK-M and COX IV. **C**: A sagittal section of the mouse frontal cortex immunolabeled for CK-M. The inset shows a high magnification image of cortical cells labeled for CK-M and stained with DRAQ5. **D**: A higher magnification image of frontal cortex triple-labeled for CK-M, COX IV, and DRAQ5. **E**: Retina immunolabeled for CK-M. **F**: Outer retina double-labeled for CK-M and VGLUT1. **G**: Outer retina double-labeled for SERCA3 and VGLUT1. **H** and **I**: High-magnification images of the outer retina double-labeled for CK-M and COX IV. **J:** Retina double-labeled for CK-M and PKCα. COX IV = cytochrome c oxidase subunit IV, GCL = ganglion cell layer, INL = inner nuclear layer, IPL = inner plexiform layer, ISs = inner segments, ONL = outer nuclear layer, OPL = outer plexiform layer, PKCα = protein kinase C α, VGLUT1 = vesicular glutamate transporter 1. A–C, E–G and J, scale bar = 40 µm. D, scale bar = 10 µm. H and I, scale bar = 20 µm.

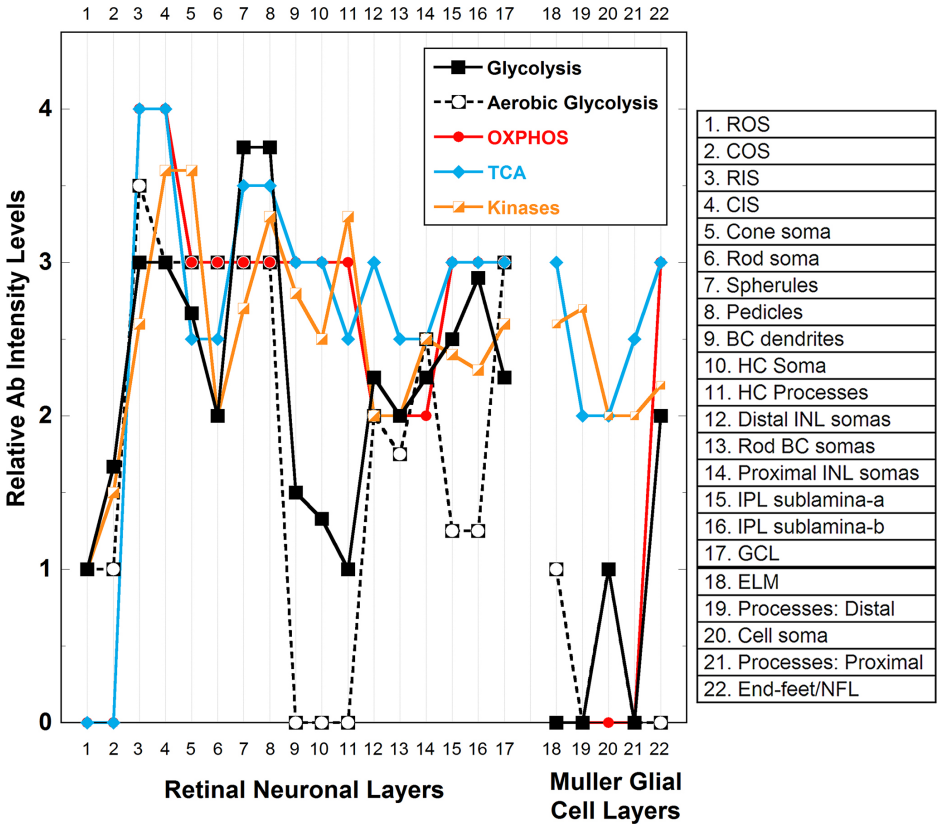

Figure 16. Integrated summary of relative Ab intensity levels obtained from the immunoreactivity of bioenergetic regulating and buffering enzymes in the neuronal and glial compartments of the adult light-adapted C57BL/6N mouse retina. The numbers on the x-axis (from 1 to 22) indicate the specific retinal compartments (see key). The values on the y-axis represent the integrated mean relative intensity values of immunoreactivity levels for enzymes that regulate glycolysis (HK-1, HK-2, PFK-L1, PK-M1, and PK-M2), aerobic glycolysis (pan-LDH and LDH-5), the tricarboxylic acid (TCA) cycle (OGDH and STK), oxidative phosphorylation (OXPHOS; cytochrome c oxidase subunit IV, COX IV), and the ~P transferring kinases (NDPK, AK1, AK2, CK-B, CK-M, and mi-CK) obtained from Appendix 1. Overall, the findings reveal highly compartmentalized and graded expression levels of the different enzymes in the outer compared to the inner retina as well as in the Müller glial cells (MGCs) compared to the neurons. Glycolytic enzymes (solid black squares and line) are higher in the outer retina than in the inner retina, except in the rod and cone outer segments (ROSs; COSs). Specifically, the highest levels (i.e., ≥3 on intensity scale) are in the rod and cone inner segments (RISs; CISs), rod spherules, and cone pedicles where most of the retinal mitochondria are located [7,9]. Enzyme levels are slightly lower (i.e., 2.5–3.0) in the cone somas, the inner plexiform layer (IPL), the IPL sublamina-a, and sublamina-b (IPL-a; IPL-b) and still lower (i.e., 2.0–2.5) in the rod somas, inner nuclear layer (INL) somas, ganglion cell layer (GCL), and MGC end-feet/nerve fiber layer (NFL), and lowest (i.e., 1.0–1.75) in the ROS and COS, bipolar cell (BC) dendrites, horizontal cell (HC) somas and processes, and MGC somas. No glycolytic enzyme immunoreactivity was detected in the MGC external limiting membrane (ELM) or processes. Similar to glycolysis, aerobic glycolysis is higher in the outer retina than in the inner retina, except again for the ROSs and COSs. Compared to the RIS, aerobic glycolysis is just slightly lower in the CISs, rod and cone somas, and spherules and pedicles, as seen with the lactate dehydrogenase (LDH) activity (Figure 8). The BC dendrites, HC somas, and HC process have no apparent aerobic glycolytic capacity. Except amacrine cells in the proximal INL and the GCL, aerobic glycolysis is low (i.e., 1.0–2.0) in the inner retina. Aerobic glycolysis is absent to low (i.e., ≤1.0) throughout the MGCs. OXPHOS capacity is present and relatively high in all outer and inner retinal compartments, except in the ROS and COS (no COX IV or COX activity detected) and the INL somas (i.e., ≤2.0). As the IS showed high expression of GDH1 (Figure 10) and the inner retinal neurons had the highest GLS expression levels (Figure 4), the high OXPHOS capacity in these compartments may be supported by non-glucose derivatives. Except the MGC end-feet/NFL, OXPHOS capacity was not detected in any MGC compartments, consistent with the COX activity (Figure 9) and [9]. In the outer retina, the TCA cycle expression profile essentially mirrors that of OXPHOS. In the inner retina, except in the INL somas, the TCA cycle expression is moderately high (i.e., 2.5 to 3.0) and mirrors that of OXPHOS. The TCA cycle expression profile in MGCs is characterized by moderate to high expression (i.e., 2.5 to 3.0) in the ELM, proximal processes, and end-feet/NFL and lower expression (i.e., 2.0) in the distal process and somas. This is in marked contrast to their expression of enzymes related to glycolysis, aerobic glycolysis, and OXPHOS. MGCs also have a capacity for glutamate and GABA catabolism, as well as GTP production (Figure 10). Together, this suggests that MGCs support their bioenergetics demands using non-glucose derivatives to generate GTP. The ~P transferring kinases were differentially distributed among all compartments of the inner and outer retinal neurons. The ~P transferring kinases were more highly expressed in all cone compartments (CIS, somas, and pedicles, i.e., 3.5) compared to similar rod compartments (i.e., 2.0–2.5). The ~P transferring kinases were also moderately to highly expressed in the BC dendrites, HC somas, and HC processes, compartments that had low glycolytic and/or aerobic glycolytic capacity. In the MGCs, the ~P transferring kinases were moderately expressed in the ELM and distal processes and had lower expression (i.e., ≥2.0) the somas, proximal processes, and end-feet/NFL. As the MGCs lack OXPHOS capacity, except in the end-feet/NFL, the ~P transferring kinases likely convert the GTP produced in the TCA cycle to ATP, as well as buffer the ATP concentration.

OXPHOS, and ~P transferring kinases (see Figure 16 for an integrative spatial and quantitative summary).

Glycolysis, OXPHOS, and ~P transferring kinases in the OSs: The phototransduction cascade requires kinetically efficient mechanisms to maintain compartmental ATP and GTP and a large membrane surface area to maintain high photon-sensitivity and ion exchange [70,120]. The OSs maintain high intracellular ATP and GTP, and the [ATP] is larger than the [GTP] in the light-adapted OSs of the monkey retina [70]. The OSs likely rely on cytosolic ATP synthesis and ~P transferring kinases as these compartments are devoid of mitochondria or COX activity. Isolated homogenized OSs from the bovine retina possess significant activity of all glycolytic enzymes, LDH, and express glucose transporter-1 (GLUT1) [121,122]. However, the ATP required by light-adapted bovine OSs is only partially maintained by glycolysis [123]. Studies of serial tangential sections in the monkey and rabbit retina showed that the OSs have the lowest specific activity of HK, PFK, and LDH [12,13]. Accordingly, the OSs of the rat retina show low expression levels of all glycolytic enzymes [16]. In addition, the OSs of rat retina do not express GLUT1 [124] or GLUT4 [125]. Furthermore, our results show that mouse OSs do not express GLUT1 or GLUT3 (Appendix 4) and have the lowest expression of HK, PFK, PK, and LDH (Figure 3, Figure 4, Figure 5, Figure 6, and Figure 7) and LDH histochemical activity (Figure 8) among the photoreceptor compartments. The small cytoplasmic space within the mouse OSs (approximately 10^{-10} cm^3) [126] may limit the number of cytosolic proteins that can be present, but are necessary to support metabolic pathways, especially the protein components of phototransduction [127]. Together, these studies suggest that although there are species differences, the glycolytic synthesis of ATP is limited in mammalian OSs.

We observed low, but detectable, NDPK-IR and CK-B-IR in the OSs of the mouse retina (Figure 10 and Figure 12) indicating that the [~P] in light-adapted mouse OSs is supported by the ~P transferring kinase systems. In addition, the COSs contain higher cytoplasmic CK-B-IR compared to the ROSs (Figure 13). This is consistent with studies of the cone-rich chicken retina, which showed significant expression of CK-B in the OSs [121,128]. Similarly, the COSs in the frog retina compared to the ROSs contain larger amounts of ATP [129]. Our combined results for the OSs indicate the following: 1) The rate of glycolysis is regulated by HK-1, PFK-L1, and PK-M1 with HK showing the lowest expression. 2) NDPK and CK-B support the maintenance of ATP in light. 3) The higher demand of ATP in cones, compared to rods [7,130], is likely supported by CK-B. 4) The OSs do not express COX IV or have COX activity (Figure 2 and Figure 9) [9,131], despite the suggestion that the OSs express COX IV and have COX activity [132].

Glycolysis, OXPHOS, and TCA metabolism in the ISs: The ellipsoid membrane contains potassium and calcium channels, as well as expresses high levels of Na^+,K^+-ATPase (NAKA), which support the homeostasis of ionic concentration gradients that maintain the dark current [133]. Our integrative analysis showed that the ISs maintain the highest capacity for glycolysis, OXPHOS, TCA metabolism, and ATP buffering (Figure 16). The ISs contain the largest number of mitochondria compared to other photoreceptor compartments [10,134], consume 75% of the oxygen in the outer retina [4,7], exhibit the highest HK-specific activity [12], express HK-2 and HK-1 (Figure 3 and Figure 4) [16], express PFK-L1 (Figure 5), and express the constitutively active PK-M1 isoform of PK (Figure 6) [30]. The expression of HK-2 and PK-M1, as well as LDH activity in the ISs, suggests a high glycolytic capacity in these compartments. Moreover, in the light-adapted monkey [8] and mouse (Figure 9) retinas, the highest COX activity is localized to the ISs.

HK controls the glycolytic flux in the mouse brain [135] and has lower specific activity compared to PK in the retina [30]. In bovine and rat brain homogenates [136-138], HK activity is mostly present in the particulate fraction and is associated with mitochondrial membranes. In rat retinal homogenates, the highest HK activity occurs within the mitochondrial fraction [139]. The binding of high-affinity HK isoforms to the outer mitochondrial membrane is dynamic and is important for HK regulation and function as mitochondria-bound HK preferentially supports complete glucose oxidation [41]. The restricted expression of HK-2 in the ISs and synaptic terminals as well as its colocalization with COX IV (Figure 4) suggests binding of HK-2 with the outer mitochondrial membrane, which can enhance glycolysis and the dependence of the ISs on blood glucose [41,140].

The binding of HK-2 to cone mitochondria may support a higher capacity for glucose oxidation as human and mouse CISs contain ten- and twofold more mitochondria than the RISs, respectively, and CIS mitochondria have higher COX activity than RIS mitochondria [10,134]. In addition, COX activity, COX IV expression, and HK-2 expression are detected in the cone perinuclear mitochondria (see Figure 3I,K, Figure 4, Figure 9 and [9]), consistent with the idea that cones have higher metabolic requirements than rods.

The ISs also support the energetic and synthetic requirements of OS renewal [141]. HK provides G6P for glycolysis and the pentose phosphate pathway. G6P is used in the pentose phosphate pathway to regenerate the NADPH

needed for membrane biosynthesis for the newly formed OSs. NADPH is also used for glutathione synthesis to support the enzymatic mechanisms that reduce reactive oxygen species in photoreceptors [123]. Evidence suggests that HK-2 promotes anabolic pathways in the liver [142]. The enzymatic activity of glucose-6-phosphate dehydrogenase (G6PDH), the rate-limiting step of the pentose phosphate pathway, is highest in the ISs and synaptic terminals of photoreceptors, and the ratio of G6PDH enzyme activity to HK is greater than four in the ellipsoids [12]. Consistent with these findings, we observed intense G6PDH-IR in the ISs (Appendix 5). Although some evidence suggests that primate cones can utilize endogenous glycogen [143], the coordinated activity of HK and G6PDH is essential for glucose consumption in the mouse cone and rod photoreceptors, as glycogen is not a significant source of glucose in mouse retinas [144] and was not seen in the light-adapted rat retinas [145]. Our studies indicate that HK-2 in the ISs supports the high HK activity required to maintain ATP for catabolic as well as metabolites for anabolic pathways. Moreover, the TCA cycle enzymes necessary to generate GTP are highly expressed in rod and cone ISs (Figure 10), which likely accounts for the high concentration of GTP found in this layer [70]. This local source of GTP could also be used to support the GTP requirement during phototransduction [120].

~P transferring kinases in the ISs: The mouse CISs express high levels of NDPK, AK2 and CK-B, mi-CK, and CK-M, whereas the RISs express lower levels of these enzymes (Figure 11, Figure 12, Figure 13, Figure 14, and Figure 15; Appendix 1). The high expression level of the mitochondrial-associated AK (AK2), but not the cytosolic isoform (AK1), indicates partial support of an AK shuttle in the photoreceptors. Our Affymetrix microarray data (Figure 1) showed high mRNA levels of the isozymes *Ak3* and *Ak5*. It is possible that photoreceptors utilize other isoforms of AK and NDPK to shuttle ATP and GTP between ISs and OSs. Mouse CISs express the cytosolic CK-B [83] and mi-CK (Figure 13, Figure 14, and Figure 15). The RISs express CK-M and low levels of CK-B (Figure 12 and Figure 13). This suggests that the COSs and the CISs, compared to the ROSs and the RISs, rely more on a CK shuttle, consistent with findings in the cone-rich chicken retina [121,128]. These data suggest a fundamental difference in the strategies that rods and cones utilize to maintain high ATP. Unlike rods, cones do not saturate during light adaptation, and the mechanism to maintain this graded process continuously consumes ~P that most efficiently can be supported by ~P transferring kinases. The higher expression of CKs in cones, compared to rods, also suggests that cones buffer and sustain the ATP more efficiently than rods under varying metabolic conditions. Consistent with this idea, in the perfused cat retina, the cone-driven light-evoked responses are less sensitive than rod-driven responses to extreme (high or low) changes in glucose concentrations [20]. Rods may not be kinetically capable of overcoming rapid changes in glucose concentrations as our results indicate that rods are more dependent on glycolytic ATP production and less dependent on ATP buffering than cones.

Presynaptic glycolytic, OXPHOS, and TCA metabolism in the OPL: The regulation of calcium dynamics in photoreceptors is coupled to mitochondrial ATP synthesis and is differentially regulated in rods and cones [9]. Our integrative analysis showed that the photoreceptor synaptic terminals also exhibit a high dependence on glycolysis (Figure 16). Compared to the ISs, the photoreceptor synaptic terminals operate under lower oxygen tension and consume less oxygen during light- or dark-adaptation [4,7] and have relatively lower COX activity compared to the ISs (Figure 9). LDH activity is high in the OPL of the monkey retina [146]. Similarly, we observed intense PFK-L (Figure 5), LDH-IR (Figure 7), and high LDH activity (Figure 8) in the OPL that was confined to the presynaptic region. Although LDH catalyzes a reversible reaction, the significant expression and activity of HK, PFK, and PK [12,30] and this study (Figure 3, Figure 4, Figure 5, and Figure 6) indicate a high capacity for aerobic glycolysis in the photoreceptor synaptic terminals. Recent data showed tight coupling of glycolysis and NAKA activity [147]. Glycolysis is coupled to neurotransmission in hippocampal slices, as substitution of D-glucose for lactate, pyruvate, or citrate did not maintain the ATP levels necessary for excitation [148]. In addition, glycolytic ATP supported by a PK bound to synaptic vesicles supports neurotransmitter uptake in isolated synaptic vesicles [149]. Whether glycolysis is a significant source of ATP for neurotransmission in the photoreceptor terminals is still unknown, although our results combined with those of others suggest that this is possible. Furthermore, the TCA cycle enzymes necessary to generate GTP are located in the OPL (Figure 10), which likely accounts for the high concentration of GTP found in this layer [70].

The coexpression of PK-M1 and PK-M2 (Figure 6) [30] in the photoreceptor terminals indicates that the rate of aerobic glycolysis in these compartments is highly modulated. Although there is no direct evidence of PK-M2 related to biosynthesis in the synaptic terminals, it is possible that PK-M2 is related to biosynthesis as tonic synapses undergo large vesicle-membrane turnover [150]. Therefore, we postulate that the glycolytic flux that produces pyruvate and promotes OXPHOS in the photoreceptor synaptic terminals is supported by PK-M1, whereas PK-M2 reduces pyruvate production when glycolytic intermediates are needed for biosynthesis or when extracellular lactate, pyruvate, or

glutamate is abundant to support OXPHOS. This is supported by the observations that MCT1, MCT2, and MCT4 are highly expressed in the photoreceptor terminals (Appendix 3) and the capacity of MCT2 to transport pyruvate [64] from the blood. Pyruvate uptake is possible as the blood pyruvate concentrations are higher than the Michaelis constant of MCT2 for pyruvate [151].

Glutamate is not only the major neurotransmitter in the brain, but also a component of intermediary metabolism [152]. In neurons with tonic responses, glutamate must be constantly synthesized and recycled. In the mouse retina, rod terminal EAATs, but not EAATs in MGCs or postsynaptic neurons, play a predominant role in removing glutamate from the synaptic cleft [153,154]. Deamination of glutamate by mitochondrial GDH supports glutamate recycling, which results in the production of α-ketoglutarate, a TCA cycle intermediate that can contribute to cataplerosis to support OXPHOS. The presence of GDH in the OPL (Figure 10) indicates that the photoreceptor synaptic terminals can oxidatively deaminate glutamate to produce α-ketoglutarate. In homogenized light-adapted mouse retinas, the malate-aspartate shuttle contributes to the recycling of glutamate [29]. However, an increase in intracellular [glutamate] may be also be balanced by catabolism of glutamate in the TCA cycle. Evidence of this has been shown in cultured neurons where high levels of glutamate induce a decrease in glucose utilization [155]. Therefore, photoreceptors may rely on intermediary metabolism and aerobic glycolysis to compensate for the change in glutamate recycling and catabolism.

Similar to the regeneration of NAD^+ in the cytosol by LDH activity, in the malate-aspartate shuttle the NADH/NAD^+ can be reestablished by oxidatively deaminating aspartate in the cytosol and oxidizing malate in the mitochondria through malate dehydrogenase. One testable hypothesis is that when high rates of aerobic glycolysis occur, LDH produces NAD^+ in the cytosol affecting the contribution of the malate-aspartate shuttle to transfer reducing equivalents between cytoplasm and mitochondria. In the OPL of the monkey retina, the activity of LDH is higher than the malate dehydrogenase activity, while the activity of GDH is highest in the OPL compared to other retinal layers [11]. We observed LDH-5 expression (Figure 7), LDH activity (Figure 8), and GDH expression (Figure 10) in the presynaptic OPL suggesting reduction of pyruvate to lactate and oxidation of glutamate. The presence of PK-M2 (Figure 6) may contribute to balance glutamate recycling by decreasing the production of pyruvate. In addition, the high expression of MCT4 and MCT2 in the photoreceptor terminals (Appendix 3) may support pyruvate and lactate metabolism in these compartments.

~P transferring kinases in the OPL: Rod and cone synaptic terminals differ in several aspects, notably in the number and substructure of the mitochondria and the regulation of calcium homeostasis that is directly dependent on ATP [9]. Mouse rod spherules have a single large mitochondrion near the ribbon synapse, whereas the larger cone pedicles have five to six smaller mitochondria clustered in the distal region of the terminal and a twofold higher total number of cristae membranes, consume more ATP [9], and dock fivefold more vesicles than rod ribbons [156]. These differences between spherules and pedicles suggest the need for distinct bioenergetic profiles between photoreceptors. We observed several differences in the energy metabolism profile of spherules and pedicles. Pedicles, but not spherules, coexpressed cytosolic and mitochondrial associated CKs (Figure 13, Figure 14, and Figure 15). This suggests that a CK shuttle is used by the larger cone pedicles to support the rapid transfer of ~P needed to maintain neurotransmission and calcium homeostasis. The CK buffer system may be preferentially located in cone pedicles as they must rapidly regenerate their ATP to maintain high NAKA activity in coordination with the rapid removal of intracellular calcium by the sodium-calcium exchanger (NCX) and to provide ATP for the synaptic vesicle V-type ATPase [9].

Glycolytic, OXPHOS, and TCA metabolism in bipolar cells and their dendrites: Dendrites in the central nervous system (CNS) exhibit the highest concentrations of mitochondria and COX activity [8]. Excitatory synapses of the hippocampus and the cerebellar and cerebral cortex have a higher density of subcellular organelles needed to sustain synaptic transmission, and their size is proportional to the presynaptic vesicle content [157]. The high and continuous ATP demand in the dendrites of the excitatory neurons is driven by the constant NAKA activity that reverses the ion movement and tunes the postsynaptic responses [158]. RPs and BCs make up the largest population of excitatory neurons in the retina. Similar to photoreceptors, retinal BCs are non-spiking neurons that constantly utilize ATP to maintain their changes in membrane potential. We used the molecular marker PKCα to examine the rod BC dendrites, which are depolarized in light-adapted retinas. BC dendrites and somas have low expression of GLUT1, do not express GLUT3 (Appendix 4) or GLUT4 [125], and have low HK activity [12]. The absence of LDH-IR and low LDH activity in the BC dendrites suggest low capacity for aerobic glycolysis. BCs express SNT1 and SNT2 [60] and exhibit the highest expression of GLS in the retina (Figure 4; Appendix 1). In addition, BCs express MCT1

and MCT4 (Appendix 3) and have high levels of COX activity (Figure 9). One possible interpretation of these results is that the TCA cycle anaplerotic and cataplerotic reactions—likely supported by lactate, pyruvate, glutamine, or glutamate—support neurotransmission, as well as energy production in BCs. The contrasting metabolism between the photoreceptor synaptic terminals and the BC dendrites demonstrate the diversity of metabolic strategies used by the glutamatergic neurons of the retina.

Glycolytic, OXPHOS, and TCA metabolism in horizontal and amacrine cells: HCs and ACs make up about 44% of the INL [159]. HCs mediate lateral inhibition to the outer retina, modulate the responses of large numbers of photoreceptors under different lighting conditions, and contribute to the formation of the BC receptive field [160]. Recent studies in fish indicate that HCs use a proton-mediated mechanism that involves ATP release and subsequent extracellular ATP hydrolysis to control photoreceptor responses [161]. Most ACs are non-spiking neurons that utilize glycine, GABA, or dopamine to modulate and integrate the visual responses between the outer and inner retina. As inhibitory interneurons, HCs and ACs support tonic responses that are constantly consuming ATP [162]. The low expression of glycolytic enzymes and low LDH activity in HCs and ACs suggest that these interneurons possess a strategy for limiting their glucose consumption. However, HCs exhibit high levels of COX activity (Figure 9) and similar to BCs may utilize amino acids and monocarboxylic acids to maintain the production of neurotransmitters and support mitochondrial ATP production. HCs as well as ACs express high concentrations of different isoforms of AK and CK throughout their cell bodies and processes (Figure 11, Figure 12, and Figure 13). In the OPL, cytosolic AK1 is exclusively expressed in HCs (Figure 12). We observed high expression levels of NDPK, AK2, CK-B, and CK-M in the proximal and distal INL (Figure 10, Figure 11, Figure 12, and Figure 13). The high expression of ~P transferring kinases in BCs and ACs may be required to support the tonic photoreceptor and BC responses under different lighting conditions.

Glycolytic and OXPHOS metabolism in the IPL and the GCL: Light adaptation in the inner retina requires sustained vesicular glutamate uptake [163,164] and the coordinated responses of HCs, BCs, and ACs. In contrast to the outer retina, the inner retina contains a larger number of presynaptic and postsynaptic processes and undergoes sustained (BCs, HCs, and ACs), as well as transient retinal ganglion cell physiologic responses that require a high pool of ATP for fluctuating neurotransmission. Moreover, the intermittent physiologic activity of the ON and OFF pathways and glutamate utilization in the inner retina suggest a corresponding intermittent demand for ATP. In contrast to the outer retina, the inner retina does not show significant light-induced changes in oxygen consumption [6], oxygen tension [4], or COX activity (dark-adaptation data not shown) indicating that the inner retina maintains a relatively constant steady-state of OXPHOS. In the monkey and the rabbit, the ATP in the light-adapted inner retina is several-fold higher than in the outer retina [70]. The IPL and the GCL show layer-selective activity of HK and PFK [12] and layer-selective expression of GLUT3 (Appendix 4), HK-1, HK-2, PFK-L, and PK-M1 (Figure 3, Figure 4, Figure 5, and Figure 6). The IPL-a and IPL-b and the GCL exhibit significant COX activity, but not LDH activity (Figure 8 and Figure 9). The combined evidence suggests that the production of ATP in the BC synaptic terminals, AC processes, and GC dendrites is supported by complete glucose oxidation and that these compartments do not exhibit a capacity for the Pasteur effect. Moreover, the IPL has low GLS activity compared to the OPL or the INL [165], and similarly, we did not observe significant GLS-IR (data not shown). This indicates that glutamate synthesized in the synaptic terminals is likely derived from glucose instead of from glutamine. These combined results are in accordance with the higher sensitivity of inner retinal neurons to large changes in the glucose concentration [24] and amino acid availability [61] and likely explains why under anoxic conditions the b-wave/PII ERG responses of the BCs are decreased before the a-wave/PIII responses of the photoreceptors [23].

Aerobic glycolysis in MGCs: Cell culture studies suggest that lactate, produced by glial cells in the brain and MGCs in the retina, is a substrate for neuronal mitochondrial energy production [32,56,166]. Human and rat cultured MGCs produce lactate at a higher rate compared to neurons [31,139]. However, MGCs cultured from young mice do not produce significant amounts of lactate; instead, the uptake of lactate is likely used to synthesize glutamine [30]. Our results indicate that glucose oxidation in adult MGCs is limited and possibly compartmentalized to the ELM. In our studies, the MGCs expressed low levels of high-affinity HKs (HK-1 or HK-2) as well as PK-M1 or PK-M2 throughout their length (Figure 3 and Figure 6). Except in the ELM, pan-LDH-IR or LDH-5-IR was not detected in MGCs (Figure 7), and only low LDH activity was seen in the MGC somas and processes at saturating concentrations of lactate (25 mM: data not shown). Moreover, MGCs express MCT1 throughout their entire length and selectively express MCT2 in the proximal processes and MGC end-feet (Appendix 3). Thus, we conclude that although lactate can be metabolized in the ELM, lactate is not a major substrate for MGC metabolism. Moreover, the expression of MCT1 throughout the MGC somas and processes, as well as the compartmentalized expression of

MCT2 in the MGC end-feet, suggests that MGCs are able to uptake lactate. However, the absence of LDH expression and LDH activity suggests that MGCs do not further metabolize lactate.

Glycolytic, OXPHOS, and TCA metabolism and ~P production in MGCs: MGC cultures show significant metabolism of amino acids and recycling of metabolic intermediates [30,167]. In addition, the production of glutamine in MGCs supports glutamate recycling [167], thus coupling energy metabolism and neuronal function. It is possible that MGCs compartmentalize the production of pyruvate from exogenous amino acids or monocarboxylic acids. Consistent with this idea, MGC ELM, end-feet, and proximal and distal MGC processes contain mitochondria [118]. However, most of these mitochondria are weakly COX IV-IR [9] and have a minimal amount of COX activity (Figure 9). In the absence of a significant OXPHOS flux in MGCs, the anaplerotic reactions of the TCA cycle are expected to be coupled to cataplerotic reactions to balance the NADH/NAD^+ ratio and support the recycling and conservation of intermediate metabolites, such as α-ketoglutarate, aspartate, and glutamine. Such intermediate substrates can be used by the MGCs to shuttle metabolites between the MGCs and retinal neurons or for the production of MGC GTP (vide infra). In contrast, the mitochondria of the MGC processes and somas express high levels of GDH and GABA-T (Figure 10), mitochondrial enzymes involved in glutamate and GABA metabolism, respectively. Catabolism of glutamate occurs at a higher rate than glucose, glutamine, and lactate oxidation in astrocytes [110]. The coexpression of GDH and GABA-T in MGCs indicates that, similar to astrocytes, MGC mitochondria catabolize as well as recycle GABA and glutamate.

MGCs express high levels of GLAST (Figure 10E,F), and MGC mitochondria express high levels of OGDH (Figure 10), STK (Figure 10G,H), NDPK (Figure 11A,B), AK2 (Figure 12G,I), and succinate dehydrogenase (data not shown). The TCA enzyme STK produces GTP during the conversion of succinyl CoA to succinate. In addition, previously unpublished findings reveal that adult mouse retinas express the mitochondrial glutamate-aspartate transporter genes *slc25a12* and *slc25a13* (Rueda et al., manuscript in preparation). Together, these results suggest that MGC mitochondria uptake cytosolic glutamate; use GDH, OGDH, and STK to produce GTP; and use SDH, malate dehydrogenase, and aspartate aminotransferase [168,169] and then export aspartate. The ~P of GTP produced by STK can be transferred to ADP by NDPK to produce ATP and be interconverted with AK2. Our integrative analysis (Figure 16) showed that MGCs highly compartmentalize their energy metabolism, likely relying on amino acid metabolism and the TCA cycle for GTP synthesis and the ~P kinases for maintaining their cellular and compartmental ATP.

Cell-selective capacity for amino, keto, and monocarboxylic acid metabolism in retina: The expression levels of genes that encode for selective isoforms of MCTs, SNTs, GLS, GDH, aspartate aminotransferase, alanine aminotransferase, and GABA-T (Rueda et al., manuscript in preparation) are similar to the gene expression levels of the genes that encode for enzymes involved in glucose metabolism (Figure 1A). This supports the idea that the retina has a high cytosolic and mitochondrial capacity to transport and metabolize lactate, glutamine, aspartate, alanine, glutamate, and GABA. This is supported by the retinal GLS [165], GDH [11], aspartate aminotransferase, and malate dehydrogenase activity [168]. Our IHC experiments demonstrated that the capacity to metabolize monocarboxylic acids, amino acids, and keto-acids is cell-specific and compartment-specific. That is, photoreceptors have a high capacity to metabolize lactate, BC dendrites have a high capacity to metabolize glutamine, and MGCs, which do not have significant glycolytic or OXPHOS capacity, likely rely on amino acid and ketoacid metabolism to support ATP synthesis. In addition, the layer-selective LDH activity in monkey [11], and the LDH protein expression (Figure 7) and LDH activity (Figure 8) in mouse retina suggest that the homeostasis of the NAD+/NADH ratio is maintained differently in the inner and outer retina.

Advantages of compartment- and cell-specific IHC and histochemistry for enzyme profiling: Proteomic approaches are useful tools for identifying molecular targets that mediate organelle and cellular dysfunction or biomarkers that can be used to target neuroprotection. For example, proteomics yield information about the molecular alterations associated with retinal conditions, including age-related macular degeneration [170], diabetic retinopathy [171], and glaucoma [172]. In addition, proteomic studies identified molecular targets that mediate metabolic failure in retinal degeneration [173,174]. However, these proteomics studies used homogenized retinas or layers of sliced retina [16], which do not provide information about specific types of retinal cells or their compartments. In addition, studies that attempted to profile specific types of neurons have used cultured cells exposed to non-physiologic conditions such as high concentrations of glucose (20 mM) or oxygen (95%). This can result in condition-dependent artifacts. For example, Dittmann et al. compared the rate of oxygen uptake, ATP content, and lactate production in fresh neuronal cells and cultured neuronal cells and found that they later adapted their energy metabolism to the culture conditions [175]. Thus, we

used cell- and compartment-specific IHC techniques and enzyme histochemistry to explore, characterize, and integrate uncharacterized aspects of retinal bioenergetics. The results of this thorough and comprehensive study will significantly contribute to an increased understanding of the spatiotemporal interrelation of energy metabolism and neuronal function in the adult mammalian retina.

Implications of compartmental energy metabolism in retinal health: The cell- and compartment-specific vulnerability in several neurologic diseases highlights the importance of identifying the factors that contribute to neural degeneration and regeneration in the CNS. As part of the CNS, the retina exhibits cell-selective loss in retinopathies. Rods and their mitochondria, compared to cones, are more susceptible to age-related degeneration [176] and lead-induced neurotoxicity [7,177,178]. Retinal ganglion cell death is prevalent in retinal ischemic insults and common degenerative eye diseases such as glaucoma and Leber's hereditary optic neuropathy [179,180]. Moreover, studies of mitochondrial structure and function revealed that synaptic mitochondria are more vulnerable than non-synaptic mitochondria to Ca^{2+} and Pb^{2+} overload [7,181,182]. Given the relationship between ATP utilization, mitochondrial ATP synthesis, and neuronal activity, mitochondrial energy metabolism is a target for neuroprotection and rescue [183]. However, restoring neuronal function and increasing cell viability is still limited. Lactate and creatine supplementation have neuroprotective effects against anoxia and ischemia [184-186]. Similar to the retina, the brain exhibits a cell-selective capacity for creatine metabolism such that inhibitory neurons contain higher expression of CK compared to excitatory neurons [187-189]. In addition, the cell-selective metabolism of lactate in the brain is still controversial [56].

There is a paucity of information about the contribution of glycolysis, OXPHOS, and the ~P transferring kinases to each retinal cell type and their compartments. The current retinal study indicates that glucose, glutamine, lactate, and creatine metabolism is cellular- and compartment-specific. The data emphasize the need for further investigation of the profile and role of MCTs, CK, AK, and NDPK in specific regions of the CNS and the retina to identify specific proteins and molecular targets for potential contribution to cellular- and compartment-specific neuroprotection as well as advance the development of therapeutic strategies for diseases of the eye.

APPENDIX 1. CELLULAR AND COMPARTMENTAL ANALYSIS OF RELATIVE ANTIBODY EXPRESSION LEVELS IN MOUSE RETINA.

To access the data, click or select the words "Appendix 1."

APPENDIX 2. EXPRESSION OF PK-M2 IS PREDOMINANT IN PRS. MOUSE RETINA IMMUNOLABELED FOR PK-M2.

To access the data, click or select the words "Appendix 2." **A**: PK-M2 IR is intense in ISs and PRs synaptic terminals; moderate in the ONL and IPL-b; and weak in the OSs and distal INL. **B**: Retinas double labeled for PK-M2 and GS showed no colocalization, except in the elm. Scale bar = 40 µm.

APPENDIX 3. EXPRESSION OF MONOCARBOXYLATE TRANSPORTERS (MCTS) ISOFORMS 1, 2 AND 4 IN ADULT MOUSE RETINA.

To access the data, click or select the words "Appendix 3." **A:** Retinas immunolabeled for MCT1. MCT1-IR is intense in the elm, OPL, and some GCs. MCT1-IR is moderate to strong in the ISs, ONL, INL, and IPL. **B**: Retinas double labeled for MCT1 and GLAST show colocalization from the elm to the Mef. **C**: Retinas immunolabeled for MCT2. MCT2-IR is intense in OPL and IPL **D**: Retinas double labeled for MCT2 and GS show expression of MCT2 in Mef. **E**: Retinas immunolabeled for MCT4. MCT4-IR is intense in the OPL and IPL. Strong MCT4-IR is observed in the ISs, ONL, OPL and distal INL **F**: Retinas double labeled for MCT4 and GLAST reveal the absence of MCT4-IR in Mef. Scale bar = 40 µm.

APPENDIX 4. EXPRESSION OF GLUCOSE TRANSPORTERS (GLUTS) ISOFORMS 1 AND 3 IN ADULT MOUSE RETINA.

To access the data, click or select the words "Appendix 4." **A**: Retina immunolabeled for GLUT1. GLUT1-IR is strong in the elm, ONL, OPL, INL, IPL and some GCL. GLUT1-IR is weak to moderate in ISs. **B**: Retinas double labeled for GLUT1 and GS show colocalization in the elm and Mef/NFL. **C**: High magnification confocal image of a retina immunolabeled for GLUT1. **D**: Retina double labeled for GLUT1 and VGLUT1 show colocalization in the OPL and IPL. **E**: Retina immunolabeled for GLUT3. GLUT3-IR is strong to intense in the OPL and IPL. **F**: Retinas double labeled for GLUT3 and VGLUT1 show strong GLUT3-IR in glutamatergic synapses. For A-B and E, scale bar = 40 µm. For C-D and F, scale bar = 20 µm.

APPENDIX 5. EXPRESSION OF GLUCOSE-6-PHOSPHATE DEHYDROGENASE (G6PDH) IN ADULT MOUSE RETINA.

To access the data, click or select the words "Appendix 5." **A**: Retinas immunolabeled for G6PDH. G6PDH-IR is intense in the ISs; strong in OPL, distal and proximal INL and GCL; and weak in the ONL, middle INL and IPL. **B**: Retinas double labeled for G6PDH and GS. MGCs are not G6PDH-IR. **C**: Retinas double labeled for G6PDH and VGLUT1 show colocalization in the OPL and IPL. Scale bar = 40 µm.

ACKNOWLEDGMENTS

We thank Dr. Weimin Xiao for technical assistance, Dr. Cheryl Craft for the M-Car antibody, Dr. Jang-Yen Wu for the GABA-T antibody, and Dr. David R. Beers for the mouse muscle tissue. In addition, we thank Dr. Laura J. Frishman and Dr. Ross A. Poché for valuable discussions. This work was partially supported by NIH Grants RO1ES012482 to DAF, P30EY07551, T32EY07024 for SYC, T35EY07024 for IS, UHCO Student Vision Research Support Grants to EMR, and a UHD ORC Grant 206400004B0303 to JEJ. Part of this data was presented by EMR on a poster at the FASEB Retinal Neurobiology & Visual Processing 2014 annual meeting.

REFERENCES

1. Craig FN, Beecher HK. The effect of low oxygen tension on tissue metabolism (Retina). J Gen Physiol 1943; 26:467-72. [PMID: 19873358].
2. Noell WK. Electrophysiologic study of the retina during metabolic impairment. Am J Ophthalmol 1952; 35:126-33. [PMID: 14923766].
3. Winkler BS. Glycolytic and oxidative metabolism in relation to retinal function. J Gen Physiol 1981; 77:667-92. [PMID: 6267165].
4. Lau JC, Linsenmeier RA. Oxygen consumption and distribution in the Long-Evans rat retina. Exp Eye Res 2012; 102:50-8. [PMID: 22828049].
5. Yu DY, Cringle SJ. Oxygen distribution in the mouse retina. Invest Ophthalmol Vis Sci 2006; 47:1109-12. [PMID: 16505048].
6. Medrano CJ, Fox DA. Oxygen consumption in the rat outer and inner retina: light- and pharmacologically-induced inhibition. Exp Eye Res 1995; 61:273-84. [PMID: 7556491].
7. Perkins GA, Scott R, Perez A, Ellisman MH, Johnson JE, Fox DA. Bcl-xL-mediated remodeling of rod and cone synaptic mitochondria after postnatal lead exposure: electron microscopy, tomography and oxygen consumption. Mol Vis 2012; 18:3029-48. [PMID: 23288995].
8. Wong-Riley M, Anderson B, Liebl W, Huang Z. Neurochemical organization of the macaque striate cortex: correlation of cytochrome oxidase with Na^+K^+ATPase, NADPH-diaphorase, nitric oxide synthase, and N-methyl-D-aspartate receptor subunit 1. Neuroscience 1998; 83:1025-45. [PMID: 9502244].
9. Johnson JE Jr, Perkins GA, Giddabasappa A, Chaney S, Xiao W, White AD, Brown JM, Waggoner J, Ellisman MH, Fox DA. Spatiotemporal regulation of ATP and Ca^{2+} dynamics in vertebrate rod and cone ribbon synapses. Mol Vis 2007; 13:887-919. [PMID: 17653034].
10. Perkins GA, Ellisman MH, Fox DA. Three-dimensional analysis of mouse rod and cone mitochondrial cristae architecture: bioenergetic and functional implications. Mol Vis 2003; 9:60-73. [PMID: 12632036].
11. Lowry OH, Roberts NR, Lewis C. The quantitative histochemistry of the retina. J Biol Chem 1956; 220:879-92. [PMID: 13331946].
12. Lowry OH, Roberts NR, Schulz DW, Clow JE, Clark JR. Quantitative histochemistry of retina. II. Enzymes of glucose metabolism. J Biol Chem 1961; 236:2813-20. [PMID: 14466982].
13. Matschinsky FM. Energy metabolism of the microscopic structures of the cochlea, the retina, and the cerebellum. Adv Biochem Psychopharmacol 1970; 2:217-43. [PMID: 4256754].
14. Niemi M, Merenmies E. Cytochemical localization of the oxidative enzyme systems in the retina. II. Cytochrome oxidase. J Neurochem 1961; 6:206-9. [PMID: 13728975].
15. Niemi M, Merenmies E. Cytochemical localization of the oxidative enzyme systems in the retina. I. Diaphorases and dehydrogenases. J Neurochem 1961; 6:200-5. [PMID: 13728974].
16. Reidel B, Thompson JW, Farsiu S, Moseley MA, Skiba NP, Arshavsky VY. Proteomic profiling of a layered tissue reveals unique glycolytic specializations of photoreceptor cells. Mol Cell Proteomics 2011; 10:M110-[PMID: 21173383].
17. Lasansky A, De Robertis E. Submicroscopic changes in visual cells of the rabbit induced by iodoacetate. J Biophys Biochem Cytol 1959; 5:245-50. [PMID: 13654444].
18. Wang W, Fernandez de Castro J, Vukmanic E, Zhou L, Emery D, Demarco PJ, Kaplan HJ, Dean DC. Selective rod degeneration and partial cone inactivation characterize an iodoacetic acid model of Swine retinal degeneration. Invest Ophthalmol Vis Sci 2011; 52:7917-23. [PMID: 21896868].
19. Noell WK. The effect of iodoacetate on the vertebrate retina. J Cell Physiol 1951; 37:283-307. [PMID: 14832350].
20. Macaluso C, Onoe S, Niemeyer G. Changes in glucose level affect rod function more than cone function in the isolated, perfused cat eye. Invest Ophthalmol Vis Sci 1992; 33:2798-808. [PMID: 1526729].
21. Kurtenbach A, Mayser HM, Jagle H, Fritsche A, Zrenner E. Hyperoxia, hyperglycemia, and photoreceptor sensitivity in normal and diabetic subjects. Vis Neurosci 2006; 23:651-61. [PMID: 16962009].

22. Dawson WW, Hazariwala K, Karges S. Human photopic response to circulating glucose. Doc Ophthalmol 2000; 101:155-63. [PMID: 11200547].

23. Granit R. The components of the retinal action potential in mammals and their relation to the discharge in the optic nerve. J Physiol 1933; 77:207-39. [PMID: 16994385].

24. Umino Y, Everhart D, Solessio E, Cusato K, Pan JC, Nguyen TH, Brown ET, Hafler R, Frio BA, Knox BE, Engbretson GA, Haeri M, Cui L, Glenn AS, Charron MJ, Barlow RB. Hypoglycemia leads to age-related loss of vision. Proc Natl Acad Sci USA 2006; 103:19541-5. [PMID: 17159157].

25. Kaur C, Foulds WS, Ling EA. Hypoxia-ischemia and retinal ganglion cell damage. Clin Ophthalmol 2008; 2:879-89. [PMID: 19668442].

26. Wygnanski T, Desatnik H, Quigley HA, Glovinsky Y. Comparison of ganglion cell loss and cone loss in experimental glaucoma. Am J Ophthalmol 1995; 120:184-9. [PMID: 7639302].

27. Schmid H, Renner M, Dick HB, Joachim SC. Loss of inner retinal neurons after retinal ischemia in rats. Invest Ophthalmol Vis Sci 2014; 55:2777-87. [PMID: 24699380].

28. Molday RS. Photoreceptor membrane proteins, phototransduction, and retinal degenerative diseases. The Friedenwald Lecture. Invest Ophthalmol Vis Sci 1998; 39:2491-513. [PMID: 9856758].

29. Du J, Cleghorn W, Contreras L, Linton JD, Chan GC, Chertov AO, Saheki T, Govindaraju V, Sadilek M, Satrustegui J, Hurley JB. Cytosolic reducing power preserves glutamate in retina. Proc Natl Acad Sci USA 2013; 110:18501-6. [PMID: 24127593].

30. Lindsay KJ, Du J, Sloat SR, Contreras L, Linton JD, Turner SJ, Sadilek M, Satrustegui J, Hurley JB. Pyruvate kinase and aspartate-glutamate carrier distributions reveal key metabolic links between neurons and glia in retina. Proc Natl Acad Sci USA 2014; 111:15579-84. [PMID: 25313047].

31. Winkler BS, Arnold MJ, Brassell MA, Puro DG. Energy metabolism in human retinal Muller cells. Invest Ophthalmol Vis Sci 2000; 41:3183-90. [PMID: 10967082].

32. Poitry-Yamate CL, Poitry S, Tsacopoulos M. Lactate released by Muller glial cells is metabolized by photoreceptors from mammalian retina. J Neurosci 1995; 15:5179-91. [PMID: 7623144].

33. Plagemann PG, Gregory KF, Wroblewski F. The electrophoretically distinct forms of mammalian lactic dehydrogenase. 1. Distribution of lactic dehydrogenase. 1. Distribution of lactic dehydrogenases in rabbit and human tissue. J Biol Chem 1960; 235:2282-7. [PMID: 14433387].

34. Quistorff B, Grunnet N. The isoenzyme pattern of LDH does not play a physiological role; except perhaps during fast transitions in energy metabolism. Aging (Albany, NY Online) 2011; 3:457-60. [PMID: 21566263].

35. Vesell ES. Lactate dehydrogenase Isozymes: substrate inhibition in various human tissues. Science 1965; 150:1590-3. [PMID: 5866654].

36. Markert CL, Shaklee JB, Whitt GS. Evolution of a gene. Multiple genes for LDH isozymes provide a model of the evolution of gene structure, function and regulation. Science 1975; 189:102-14. [PMID: 1138367].

37. Borowsky IW, Collins RC. Metabolic anatomy of brain: a comparison of regional capillary density, glucose metabolism, and enzyme activities. J Comp Neurol 1989; 288:401-13. [PMID: 2551935].

38. Wong-Riley M. Changes in the visual system of monocularly sutured or enucleated cats demonstrable with cytochrome oxidase histochemistry. Brain Res 1979; 171:11-28. [PMID: 223730].

39. Katzen HM, Schimke RT. Multiple forms of hexokinase in the rat: tissue distribution, age dependency, and properties. Proc Natl Acad Sci USA 1965; 54:1218-25. [PMID: 5219826].

40. Sebastian S, Hoebee B, Hande MP, Kenkare UW, Natarajan AT. Assignment of hexokinase types 1,2,3 (Hk1,2,3) and glucokinase (Gck) to rat chromosome band 20q11, 4q34, 17q12 and 14q21 respectively, by in situ hybridization. Cytogenet Cell Genet 1997; 77:266-7. [PMID: 9284933].

41. Wilson JE. Isozymes of mammalian hexokinase: structure, subcellular localization and metabolic function. J Exp Biol 2003; 206:2049-57. [PMID: 12756287].

42. Chylack LT Jr. The characterization of the hexokinases in several tissues of the calf eye. Invest Ophthalmol 1975; 14:854-62. [PMID: 1184318].

43. Kahn A, Meienhofer MC, Cottreau D, Lagrange JL, Dreyfus JC. Phosphofructokinase (PFK) isozymes in man. I. Studies of adult human tissues. Hum Genet 1979; 48:93-108. [PMID: 156693].

44. Vora S, Oskam R, Staal GE. Isoenzymes of phosphofructokinase in the rat. Demonstration of the three non-identical subunits by biochemical, immunochemical and kinetic studies. Biochem J 1985; 229:333-41. [PMID: 2931076].

45. Dunaway GA, Kasten TP, Sebo T, Trapp R. Analysis of the phosphofructokinase subunits and isoenzymes in human tissues. Biochem J 1988; 251:677-83. [PMID: 2970843].

46. Levanon D, Danciger E, Dafni N, Bernstein Y, Elson A, Moens W, Brandeis M, Groner Y. The primary structure of human liver type phosphofructokinase and its comparison with other types of PFK. DNA 1989; 8:733-43. [PMID: 2533063].

47. Aragon JJ, Sols A. Regulation of enzyme activity in the cell: effect of enzyme concentration. FASEB J 1991; 5:2945-50. [PMID: 1752361].

48. Ogush S, Lawson JW, Dobson GP, Veech RL, Uyeda K. A new transient activator of phosphofructokinase during initiation of rapid glycolysis in brain. J Biol Chem 1990; 265:10943-9. [PMID: 2141604].

49. Consler TG, Woodard SH, Lee JC. Effects of primary sequence differences on the global structure and function of an enzyme: A study of pyruvate kinase isozymes. Biochemistry 1989; 28:8756-64. [PMID: 2605219].

50. Hall ER, Cottam GL. Isozymes of pyruvate kinase in vertebrates: their physical, chemical, kinetic and immunological properties. Int J Biochem 1978; 9:785-93. [PMID: 367845].

51. Imamura K, Tanaka T. Multimolecular forms of pyruvate kinase from rat and other mammalian tissues. I. Electrophoretic studies. J Biochem 1972; 71:1043-51. [PMID: 4342282].

52. Kahn A, Marie J, Boivin P. Pyruvate kinase isozymes in man. II. L type and erythrocyte-type isozymes. Electrofocusing and immunologic studies. Hum Genet 1976; 33:35-46. [PMID: 820628].

53. Lunt SY, Muralidhar V, Hosios AM, Israelsen WJ, Gui DY, Newhouse L, Ogrodzinski M, Hecht V, Xu K, Acevedo PN, Hollern DP, Bellinger G, Dayton TL, Christen S, Elia I, Dinh AT, Stephanopoulos G, Manalis SR, Yaffe MB, Andrechek ER, Fendt SM, Vander Heiden MG. Pyruvate kinase isoform expression alters nucleotide synthesis to impact cell proliferation. Mol Cell 2015; 57:95-107. [PMID: 25482511].

54. Anastasiou D, Poulogiannis G, Asara JM, Boxer MB, Jiang JK, Shen M, Bellinger G, Sasaki AT, Locasale JW, Auld DS, Thomas CJ, Vander Heiden MG, Cantley LC. Inhibition of pyruvate kinase M2 by reactive oxygen species contributes to cellular antioxidant responses. Science 2011; 334:1278-83. [PMID: 22052977].

55. Casson RJ, Wood JP, Han G, Kittipassorn T, Peet DJ, Chidlow G. M-Type Pyruvate Kinase Isoforms and Lactate Dehydrogenase A in the Mammalian Retina: Metabolic Implications. Invest Ophthalmol Vis Sci 2016; 57:66-80. .

56. Hertz L. The astrocyte-neuron lactate shuttle: a challenge of a challenge. J Cereb Blood Flow Metab 2004; 24:1241-8. [PMID: 15545919].

57. Schousboe A, Bak LK, Waagepetersen HS. Astrocytic Control of Biosynthesis and Turnover of the Neurotransmitters Glutamate and GABA. Front Endocrinol (Lausanne) 2013; 4:102-[PMID: 23966981].

58. Pellerin L, Magistretti PJ. Sweet sixteen for ANLS. J Cereb Blood Flow Metab 2012; 32:1152-66. [PMID: 22027938].

59. Walls AB, Waagepetersen HS, Bak LK, Schousboe A, Sonnewald U. The glutamine-glutamate/GABA cycle: function, regional differences in glutamate and GABA production and effects of interference with GABA metabolism. Neurochem Res 2015; 40:402-9. [PMID: 25380696].

60. Umapathy NS, Dun Y, Martin PM, Duplantier JN, Roon P, Prasad P, Smith SB, Ganapathy V. Expression and function of system N glutamine transporters (SN1/SN2 or SNAT3/SNAT5) in retinal ganglion cells. Invest Ophthalmol Vis Sci 2008; 49:5151-60. [PMID: 18689705].

61. Bui BV, Hu RG, Acosta ML, Donaldson P, Vingrys AJ, Kalloniatis M. Glutamate metabolic pathways and retinal function. J Neurochem 2009; 111:589-99. [PMID: 19702659].

62. Bergersen L, Johannsson E, Veruki ML, Nagelhus EA, Halestrap A, Sejersted OM, Ottersen OP. Cellular and subcellular expression of monocarboxylate transporters in the pigment epithelium and retina of the rat. Neuroscience 1999; 90:319-31. [PMID: 10188957].

63. Gerhart DZ, Leino RL, Drewes LR. Distribution of monocarboxylate transporters MCT1 and MCT2 in rat retina. Neuroscience 1999; 92:367-75. [PMID: 10392858].

64. Halestrap AP. The SLC16 gene family - structure, role and regulation in health and disease. Mol Aspects Med 2013; 34:337-49. [PMID: 23506875].

65. Dzeja PP, Terzic A. Phosphotransfer networks and cellular energetics. J Exp Biol 2003; 206:2039-47. [PMID: 12756286].

66. Boissan M, Dabernat S, Peuchant E, Schlattner U, Lascu I, Lacombe ML. The mammalian Nm23/NDPK family: from metastasis control to cilia movement. Mol Cell Biochem 2009; 329:51-62. [PMID: 19387795].

67. Lacombe ML, Tokarska-Schlattner M, Epand RF, Boissan M, Epand RM, Schlattner U. Interaction of NDPK-D with cardiolipin-containing membranes: Structural basis and implications for mitochondrial physiology. Biochimie 2009; 91:779-83. [PMID: 19254751].

68. Panayiotou C, Solaroli N, Karlsson A. The many isoforms of human adenylate kinases. Int J Biochem Cell Biol 2014; 49:75-83. [PMID: 24495878].

69. Dzeja P, Terzic A. Adenylate kinase and AMP signaling networks: metabolic monitoring, signal communication and body energy sensing. Int J Mol Sci 2009; 10:1729-72. [PMID: 19468337].

70. Berger SJ, DeVries GW, Carter JG, Schulz DW, Passonneau PN, Lowry OH, Ferrendelli JA. The distribution of the components of the cyclic GMP cycle in retina. J Biol Chem 1980; 255:3128-33. [PMID: 6102093].

71. Abdulaev NG, Karaschuk GN, Ladner JE, Kakuev DL, Yakhyaev AV, Tordova M, Gaidarov IO, Popov VI, Fujiwara JH, Chinchilla D, Eisenstein E, Gilliland GL, Ridge KD. Nucleoside diphosphate kinase from bovine retina: purification, subcellular localization, molecular cloning, and three-dimensional structure. Biochemistry 1998; 37:13958-67. [PMID: 9760230].

72. Hall SW, Kuhn H. Purification and properties of guanylate kinase from bovine retinas and rod outer segments. Eur J Biochem 1986; 161:551-6. [PMID: 3024975].

73. Kowluru A, Kowluru RA. Subcellular localization and characterization of nucleoside diphosphate kinase in rat retina: effect of diabetes. Biosci Rep 1998; 18:187-98. [PMID: 9877232].

74. Ravera S, Musante L, Calzia D, Panfoli I, Bruschi M, Candiano G, Pepe IM, Morelli A. Expression of adenylate kinase 1 in bovine retinal cytosol. Curr Eye Res 2007; 32:249-57. [PMID: 17453945].

75. Ingwall JS, Kramer MF, Fifer MA, Lorell BH, Shemin R, Grossman W, Allen PD. The creatine kinase system in normal and diseased human myocardium. N Engl J Med 1985; 313:1050-4. [PMID: 2931604].

76. Saks VA, Khuchua ZA, Vasilyeva EV, Belikova O, Kuznetsov AV. Metabolic compartmentation and substrate channelling in muscle cells. Role of coupled creatine kinases in in vivo

regulation of cellular respiration–a synthesis. Mol Cell Biochem 1994; 133–134:155-92. [PMID: 7808453].

77. Wallimann T, Hemmer W. Creatine kinase in non-muscle tissues and cells. Mol Cell Biochem 1994; 133–134:193-220. [PMID: 7808454].

78. Goldberg ND, Passonneau JV, Lowry OH. Effects of changes in brain metabolism on the levels of citric acid cycle intermediates. J Biol Chem 1966; 241:3997-4003. [PMID: 5922095].

79. Jacobs H, Heldt HW, Klingenberg M. High activity of creatine kinase in mitochondria from muscle and brain and evidence for a separate mitochondrial isoenzyme of creatine kinase. Biochem Biophys Res Commun 1964; 16:516-21. [PMID: 5871842].

80. Payne RM, Strauss AW. Expression of the mitochondrial creatine kinase genes. Mol Cell Biochem 1994; 133–134:235-43. [PMID: 7808456].

81. Wallimann T, Wyss M, Brdiczka D, Nicolay K, Eppenberger HM. Intracellular compartmentation, structure and function of creatine kinase isoenzymes in tissues with high and fluctuating energy demands: the 'phosphocreatine circuit' for cellular energy homeostasis. Biochem J 1992; 281:21-40. [PMID: 1731757].

82. Hemmer W, Riesinger I, Wallimann T, Eppenberger HM, Quest AF. Brain-type creatine kinase in photoreceptor cell outer segments: role of a phosphocreatine circuit in outer segment energy metabolism and phototransduction. J Cell Sci 1993; 106:671-83. [PMID: 8282772].

83. Linton JD, Holzhausen LC, Babai N, Song H, Miyagishima KJ, Stearns GW, Lindsay K, Wei J, Chertov AO, Peters TA, Caffe R, Pluk H, Seeliger MW, Tanimoto N, Fong K, Bolton L, Kuok DL, Sweet IR, Bartoletti TM, Radu RA, Travis GH, Zagotta WN, Townes-Anderson E, Parker E, Van der Zee CE, Sampath AP, Sokolov M, Thoreson WB, Hurley JB. Flow of energy in the outer retina in darkness and in light. Proc Natl Acad Sci USA 2010; 107:8599-604. [PMID: 20445106].

84. Sistermans EA, de Kok YJ, Peters W, Ginsel LA, Jap PH, Wieringa B. Tissue- and cell-specific distribution of creatine kinase B: a new and highly specific monoclonal antibody for use in immunohistochemistry. Cell Tissue Res 1995; 280:435-46. [PMID: 7781040].

85. Akimoto M, Cheng H, Zhu D, Brzezinski JA, Khanna R, Filippova E, Oh EC, Jing Y, Linares JL, Brooks M, Zareparsi S, Mears AJ, Hero A, Glaser T, Swaroop A. Targeting of GFP to newborn rods by Nrl promoter and temporal expression profiling of flow-sorted photoreceptors. Proc Natl Acad Sci USA 2006; 103:3890-5. [PMID: 16505381].

86. Mekada K, Abe K, Murakami A, Nakamura S, Nakata H, Moriwaki K, Obata Y, Yoshiki A. Genetic differences among C57BL/6 substrains. Exp Anim 2009; 58:141-9. [PMID: 19448337].

87. Zacks DN, Han Y, Zeng Y, Swaroop A. Activation of signaling pathways and stress-response genes in an experimental model of retinal detachment. Invest Ophthalmol Vis Sci 2006; 47:1691-5. [PMID: 16565410].

88. Shackelford DB, Vasquez DS, Corbeil J, Wu S, Leblanc M, Wu CL, Vera DR, Shaw RJ. mTOR and HIF-1alpha-mediated tumor metabolism in an LKB1 mouse model of Peutz-Jeghers syndrome. Proc Natl Acad Sci USA 2009; 106:11137-42. [PMID: 19541609].

89. Salani B, Marini C, Rio AD, Ravera S, Massollo M, Orengo AM, Amaro A, Passalacqua M, Maffioli S, Pfeffer U, Cordera R, Maggi D, Sambuceti G. Metformin impairs glucose consumption and survival in Calu-1 cells by direct inhibition of hexokinase-II. Sci Rep 2013; 3:2070-[PMID: 23797762].

90. Sato-Tadano A, Suzuki T, Amari M, Takagi K, Miki Y, Tamaki K, Watanabe M, Ishida T, Sasano H, Ohuchi N. Hexokinase II in breast carcinoma: a potent prognostic factor associated with hypoxia-inducible factor-1alpha and Ki-67. Cancer Sci 2013; 104:1380-8. [PMID: 23869589].

91. Anastasiou D, Yu Y, Israelsen WJ, Jiang JK, Boxer MB, Hong BS, Tempel W, Dimov S, Shen M, Jha A, Yang H, Mattaini KR, Metallo CM, Fiske BP, Courtney KD, Malstrom S, Khan TM, Kung C, Skoumbourdis AP, Veith H, Southall N, Walsh MJ, Brimacombe KR, Leister W, Lunt SY, Johnson ZR, Yen KE, Kunii K, Davidson SM, Christofk HR, Austin CP, Inglese J, Harris MH, Asara JM, Stephanopoulos G, Salituro FG, Jin S, Dang L, Auld DS, Park HW, Cantley LC, Thomas CJ, Vander Heiden MG. Pyruvate kinase M2 activators promote tetramer formation and suppress tumorigenesis. Nat Chem Biol 2012; 8:839-47. [PMID: 22922757].

92. Israelsen WJ, Dayton TL, Davidson SM, Fiske BP, Hosios AM, Bellinger G, Li J, Yu Y, Sasaki M, Horner JW, Burga LN, Xie J, Jurczak MJ, DePinho RA, Clish CB, Jacks T, Kibbey RG, Wulf GM, Di Vizio D, Mills GB, Cantley LC, Vander Heiden MG. PKM2 isoform-specific deletion reveals a differential requirement for pyruvate kinase in tumor cells. Cell 2013; 155:397-409. [PMID: 24120138].

93. Chambers JW, Maguire TG, Alwine JC. Glutamine metabolism is essential for human cytomegalovirus infection. J Virol 2010; 84:1867-73. [PMID: 19939921].

94. Kung HN, Marks JR, Chi JT. Glutamine synthetase is a genetic determinant of cell type-specific glutamine independence in breast epithelia. PLoS Genet 2011; 7:e1002229-[PMID: 21852960].

95. Nieminen AI, Eskelinen VM, Haikala HM, Tervonen TA, Yan Y, Partanen JI, Klefstrom J. Myc-induced AMPK-phospho p53 pathway activates Bak to sensitize mitochondrial apoptosis. Proc Natl Acad Sci USA 2013; 110:E1839-48. [PMID: 23589839].

96. Wilson CH, Indarto D, Doucet A, Pogson LD, Pitman MR, McNicholas K, Menz RI, Overall CM, Abbott CA. Identifying natural substrates for dipeptidyl peptidases 8 and 9 using terminal amine isotopic labeling of substrates (TAILS) reveals in vivo roles in cellular homeostasis and energy metabolism. J Biol Chem 2013; 288:13936-49. [PMID: 23519473].

97. Szel A, Rohlich P, Caffe AR, van Veen T. Distribution of cone photoreceptors in the mammalian retina. Microsc Res Tech 1996; 35:445-62. [PMID: 9016448].

98. Zhu X, Brown B, Li A, Mears AJ, Swaroop A, Craft CM. GRK1-dependent phosphorylation of S and M opsins and their binding to cone arrestin during cone phototransduction in the mouse retina. J Neurosci 2003; 23:6152-60. [PMID: 12853434].

99. Sherry DM, Wang MM, Bates J, Frishman LJ. Expression of vesicular glutamate transporter 1 in the mouse retina reveals temporal ordering in development of rod vs. cone and ON vs. OFF circuits. J Comp Neurol 2003; 465:480-98. [PMID: 12975811].

100. Haverkamp S, Wassle H. Immunocytochemical analysis of the mouse retina. J Comp Neurol 2000; 424:1-23. [PMID: 10888735].

101. Han Y, Massey SC. Electrical synapses in retinal ON cone bipolar cells: subtype-specific expression of connexins. Proc Natl Acad Sci USA 2005; 102:13313-8. [PMID: 16150718].

102. Kim DS, Matsuda T, Cepko CL. A core paired-type and POU homeodomain-containing transcription factor program drives retinal bipolar cell gene expression. J Neurosci 2008; 28:7748-64. [PMID: 18667607].

103. Giddabasappa A, Hamilton WR, Chaney S, Xiao W, Johnson JE, Mukherjee S, Fox DA. Low-level gestational lead exposure increases retinal progenitor cell proliferation and rod photoreceptor and bipolar cell neurogenesis in mice. Environ Health Perspect 2011; 119:71-7. [PMID: 20840909].

104. Jacobsen NO. The histochemical localization of lactic dehydrogenase isoenzymes in the rat nephron by means of an improved polyvinyl alcohol method. Histochemie 1969; 20:250-65. [PMID: 4190307].

105. Boumezbeur F, Petersen KF, Cline GW, Mason GF, Behar KL, Shulman GI, Rothman DL. The contribution of blood lactate to brain energy metabolism in humans measured by dynamic 13C nuclear magnetic resonance spectroscopy. J Neurosci 2010; 30:13983-91. [PMID: 20962220].

106. Emerson PM, Wilkinson JH. Urea and oxalate inhibition of the serum lactate dehydrogenase. J Clin Pathol 1965; 18:803-7. [PMID: 5844214].

107. Baba N, Sharma HM. Histochemistry of lactic dehydrogenase in heart and pectoralis muscles of rat. J Cell Biol 1971; 51:621-35. [PMID: 5128351].

108. Krizaj D. Compartmentalization of calcium entry pathways in mouse rods. Eur J Neurosci 2005; 22:3292-6. [PMID: 16367794].

109. Krizaj D. Serca isoform expression in the mammalian retina. Exp Eye Res 2005; 81:690-9. [PMID: 15967430].

110. McKenna MC. Glutamate pays its own way in astrocytes. Front Endocrinol (Lausanne) 2013; 4:191-[PMID: 24379804].

111. Underwood AH, Newsholme EA. Properties of phosphofructokinase from rat liver and their relation to the control of glycolysis and gluconeogenesis. Biochem J 1965; 95:868-75. [PMID: 14342527].

112. Acosta ML, Fletcher EL, Azizoglu S, Foster LE, Farber DB, Kalloniatis M. Early markers of retinal degeneration in rd/rd mice. Mol Vis 2005; 11:717-28. [PMID: 16163270].

113. Bonavita V, Ponte F, Amore G. Neurochemical Studies on the Inherited Retinal Degeneration of the Rat. I. Lactate Dehydrogenase in the Developing Retina. Vision Res 1963; 61:271-80. [PMID: 14168294].

114. Cohen LH, Noell WK. Glucose catabolism of rabbit retina before and after development of visual function. J Neurochem 1960; 5:253-76. [PMID: 13810977].

115. Graymore C, Tansley K. Iodoacetate poisoning of the rat retina. II. Glycolysis in the poisoned retina. Br J Ophthalmol 1959; 43:486-93. [PMID: 13829137].

116. Graymore C, Tansley K. Iodoacetate poisoning of the rat retina. I. Production of retinal degeneration. Br J Ophthalmol 1959; 43:177-85. [PMID: 13628963].

117. Tanishima K, Gao SX, Yamamoto R, Yoshida H. Biochemical and enzymological study of lactate dehydrogenase isoenzymes from commercial quality control sera and several animal tissue sources. Eur J Clin Chem Clin Biochem 1995; 33:865-8. [PMID: 8620065].

118. Germer A, Biedermann B, Wolburg H, Schuck J, Grosche J, Kuhrt H, Reichelt W, Schousboe A, Paasche G, Mack AF, Reichenbach A. Distribution of mitochondria within Muller cells–I. Correlation with retinal vascularization in different mammalian species. J Neurocytol 1998; 27:329-45. [PMID: 9923979].

119. Acosta ML, Kalloniatis M. Short- and long-term enzymatic regulation secondary to metabolic insult in the rat retina. J Neurochem 2005; 92:1350-62. [PMID: 15748154].

120. Ames A 3rd, Walseth TF, Heyman RA, Barad M, Graeff RM, Goldberg ND. Light-induced increases in cGMP metabolic flux correspond with electrical responses of photoreceptors. J Biol Chem 1986; 261:13034-42. [PMID: 2875993].

121. Hsu SC, Molday RS. Glycolytic enzymes and a GLUT-1 glucose transporter in the outer segments of rod and cone photoreceptor cells. J Biol Chem 1991; 266:21745-52. [PMID: 1939198].

122. Kwok MC, Holopainen JM, Molday LL, Foster LJ, Molday RS. Proteomics of photoreceptor outer segments identifies a subset of SNARE and Rab proteins implicated in membrane vesicle trafficking and fusion. Mol Cell Proteomics 2008; 7:1053-66. [PMID: 18245078].

123. Hsu SC, Molday RS. Glucose metabolism in photoreceptor outer segments. Its role in phototransduction and in NADPH-requiring reactions. J Biol Chem 1994; 269:17954-9. [PMID: 8027053].

124. Gospe SM 3rd, Baker SA, Arshavsky VY. Facilitative glucose transporter Glut1 is actively excluded from rod outer segments. J Cell Sci 2010; 123:3639-44. [PMID: 20923839].

125. Sanchez-Chavez G, Pena-Rangel MT, Riesgo-Escovar JR, Martinez-Martinez A, Salceda R. Insulin stimulated-glucose transporter Glut 4 is expressed in the retina. PLoS ONE 2012; 7:e52959-[PMID: 23285235].

126. Lolley RN, Lee RH, Chase DG, Racz E. Rod photoreceptor cells dissociated from mature mice retinas. Invest Ophthalmol Vis Sci 1986; 27:285-95. [PMID: 3949460].

127. Najafi M, Haeri M, Knox BE, Schiesser WE, Calvert PD. Impact of signaling microcompartment geometry on GPCR dynamics in live retinal photoreceptors. J Gen Physiol 2012; 140:249-66. [PMID: 22891277].

128. Wallimann T, Wegmann G, Moser H, Huber R, Eppenberger HM. High content of creatine kinase in chicken retina: compartmentalized localization of creatine kinase isoenzymes in photoreceptor cells. Proc Natl Acad Sci USA 1986; 83:3816-9. [PMID: 3520556].

129. Scarpelli DG, Craig EL. The fine localization of nucleoside triphosphatase activity in the retina of the frog. J Cell Biol 1963; 17:279-88. [PMID: 13976534].

130. Perkins GA, Ellisman MH, Fox DA. The structure-function correlates of mammalian rod and cone photoreceptor mitochondria: observations and unanswered questions. Mitochondrion 2004; 4:695-703. [PMID: 16120425].

131. Wong-Riley MT, Trusk TC, Tripathi SC, Hoppe DA. Effect of retinal impulse blockage on cytochrome oxidase-rich zones in the macaque striate cortex: II. Quantitative electron-microscopic (EM) analysis of neuropil. Vis Neurosci 1989; 2:499-514. [PMID: 2562110].

132. Calzia D, Garbarino G, Caicci F, Manni L, Candiani S, Ravera S, Morelli A, Traverso CE, Panfoli I. Functional expression of electron transport chain complexes in mouse rod outer segments. Biochimie 2014; 102:78-82. [PMID: 24565809].

133. Lamb TD, Pugh EN Jr. Phototransduction, dark adaptation, and rhodopsin regeneration the proctor lecture. Invest Ophthalmol Vis Sci 2006; 47:5137-52. [PMID: 17122096].

134. Hoang QV, Linsenmeier RA, Chung CK, Curcio CA. Photoreceptor inner segments in monkey and human retina: mitochondrial density, optics, and regional variation. Vis Neurosci 2002; 19:395-407. [PMID: 12511073].

135. Lowry OH, Passonneau JV, Hasselberger FX, Schulz DW. Effect of Ischemia on Known Substrates and Cofactors of the Glycolytic Pathway in Brain. J Biol Chem 1964; 239:18-30. [PMID: 14114842].

136. Crane RK, Sols A. The association of hexokinase with particulate fractions of brain and other tissue homogenates. J Biol Chem 1953; 203:273-92. [PMID: 13069512].

137. Craven PA, Basford RE. Brain hexokinase: immunohistochemical localization at the light microscopic level. Biochemistry 1969; 8:3520-5. [PMID: 4185969].

138. Johnson MK. The intracellular distribution of glycolytic and other enzymes in rat-brain homogenates and mitochondrial preparations. Biochem J 1960; 77:610-8. [PMID: 13790316].

139. Winkler BS, Pourcho RG, Starnes C, Slocum J, Slocum N. Metabolic mapping in mammalian retina: a biochemical and 3H–2-deoxyglucose autoradiographic study. Exp Eye Res 2003; 77:327-37. [PMID: 12907165].

140. BeltrandelRio H, Wilson JE. Hexokinase of rat brain mitochondria: relative importance of adenylate kinase and oxidative phosphorylation as sources of substrate ATP, and interaction with intramitochondrial compartments of ATP and ADP. Arch Biochem Biophys 1991; 286:183-94. [PMID: 1897945].

141. Papermaster DS. The birth and death of photoreceptors: the Friedenwald Lecture. Invest Ophthalmol Vis Sci 2002; 43:1300-9. [PMID: 11980838].

142. Sebastian S, Horton JD, Wilson JE. Anabolic function of the type II isozyme of hexokinase in hepatic lipid synthesis. Biochem Biophys Res Commun 2000; 270:886-91. [PMID: 10772920].

143. Nihira M, Anderson K, Gorin FA, Burns MS. Primate rod and cone photoreceptors may differ in glucose accessibility. Invest Ophthalmol Vis Sci 1995; 36:1259-70. [PMID: 7775103].

144. Kuwabara T, Cogan D. Retinal glycogen. Trans Am Ophthalmol Soc 1961; 59:106-10. [PMID: 14460991].

145. Fox DA, Chu LW. Rods are selectively altered by lead: II. Ultrastructure and quantitative histology. Exp Eye Res 1988; 46:613-25. [PMID: 2838312].

146. Strominger JL, Lowry OH. The quantitative histochemistry of brain. IV. Lactic, malic, and glutamic dehydrogenases. J Biol Chem 1955; 213:635-46. [PMID: 14367324].

147. Sepp M, Sokolova N, Jugai S, Mandel M, Peterson P, Vendelin M. Tight coupling of Na+/K+-ATPase with glycolysis demonstrated in permeabilized rat cardiomyocytes. PLoS ONE 2014; 9:e99413-[PMID: 24932585].

148. Kanatani T, Mizuno K, Okada Y. Effects of glycolytic metabolites on preservation of high energy phosphate level and synaptic transmission in the granule cells of guinea pig hippocampal slices. Experientia 1995; 51:213-6. [PMID: 7698281].

149. Ishida A, Noda Y, Ueda T. Synaptic vesicle-bound pyruvate kinase can support vesicular glutamate uptake. Neurochem Res 2009; 34:807-18. [PMID: 18751889].

150. Paillart C, Li J, Matthews G, Sterling P. Endocytosis and vesicle recycling at a ribbon synapse. J Neurosci 2003; 23:4092-9. [PMID: 12764096].

151. Coleman RM, Von Brand T. Blood pyruvate levels of rats during hemoprotozoan infections. J Parasitol 1957; 43:263-70. [PMID: 13439462].

152. Erecinska M, Zaleska MM, Nelson D, Nissim I, Yudkoff M. Neuronal glutamine utilization: glutamine/glutamate homeostasis in synaptosomes. J Neurochem 1990; 54:2057-69. [PMID: 1971010].

153. Hasegawa J, Obara T, Tanaka K, Tachibana M. High-density presynaptic transporters are required for glutamate removal from the first visual synapse. Neuron 2006; 50:63-74. [PMID: 16600856].

154. Winkler B, Kapousta-Bruneau N, Arnold MJ, Green DG. Effects of inhibiting glutamine synthetase and blocking glutamate uptake on b-wave generation in isolated rat retina. Vis Neurosci 1999; 16:345-53. [PMID: 10367968].

155. Tescarollo F, Covolan L, Pellerin L. Glutamate reduces glucose utilization while concomitantly enhancing AQP9 and MCT2 expression in cultured rat hippocampal neurons. Front Neurosci 2014; 8:246-[PMID: 25161606].

156. Sterling P, Matthews G. Structure and function of ribbon synapses. Trends Neurosci 2005; 28:20-9. [PMID: 15626493].

157. Harris KM, Weinberg RJ. Ultrastructure of synapses in the mammalian brain. Cold Spring Harb Perspect Biol 2012; •••:4-[PMID: 22357909].

158. Harris JJ, Jolivet R, Attwell D. Synaptic energy use and supply. Neuron 2012; 75:762-77. [PMID: 22958818].

159. Jeon CJ, Strettoi E, Masland RH. The major cell populations of the mouse retina. J Neurosci 1998; 18:8936-46. [PMID: 9786999].

160. Thoreson WB, Mangel SC. Lateral interactions in the outer retina. Prog Retin Eye Res 2012; 31:407-41. [PMID: 22580106].

161. Vroman R, Klaassen LJ, Howlett MH, Cenedese V, Klooster J, Sjoerdsma T, Kamermans M. Extracellular ATP hydrolysis inhibits synaptic transmission by increasing ph buffering in the synaptic cleft. PLoS Biol 2014; 12:e1001864-[PMID: 24844296].

162. Harris JJ, Attwell D. The energetics of CNS white matter. J Neurosci 2012; 32:356-71. [PMID: 22219296].

163. Oesch NW, Kothmann WW, Diamond JS. Illuminating synapses and circuitry in the retina. Curr Opin Neurobiol 2011; 21:238-44. [PMID: 21349699].

164. Shapley R. The neurobiology of vision: parallel processing in the visual system. Science 1984; 223:1403-4. [PMID: 17746049].

165. Ross CD, Bowers M, Godfrey DA. Distribution of glutaminase activity in retinal layers of rat and guinea pig. Brain Res 1987; 401:168-72. [PMID: 3815090].

166. Pellerin L, Pellegri G, Bittar PG, Charnay Y, Bouras C, Martin JL, Stella N, Magistretti PJ. Evidence supporting the existence of an activity-dependent astrocyte-neuron lactate shuttle. Dev Neurosci 1998; 20:291-9. [PMID: 9778565].

167. Bringmann A, Grosche A, Pannicke T, Reichenbach A. GABA and Glutamate uptake and metabolism in retinal glial (Muller) cells. Front Endocrinol (Lausanne) 2013; 4:48-[PMID: 23616782].

168. Ross CD, Godfrey DA. Distributions of aspartate aminotransferase and malate dehydrogenase activities in rat retinal layers. J Histochem Cytochem 1985; 33:624-30. [PMID: 4008916].

169. Inagaki N, Kamisaki Y, Kiyama H, Horio Y, Tohyama M, Wada H. Immunocytochemical localizations of cytosolic and mitochondrial glutamic oxaloacetic transaminase isozymes in rat retina as markers for the glutamate-aspartate neuronal system. Brain Res 1985; 325:336-9. [PMID: 2858252].

170. Ethen CM, Reilly C, Feng X, Olsen TW, Ferrington DA. The proteome of central and peripheral retina with progression of age-related macular degeneration. Invest Ophthalmol Vis Sci 2006; 47:2280-90. [PMID: 16723435].

171. VanGuilder HD, Bixler GV, Kutzler L, Brucklacher RM, Bronson SK, Kimball SR, Freeman WM. Multi-modal proteomic analysis of retinal protein expression alterations in a rat model of diabetic retinopathy. PLoS ONE 2011; 6:e16271-[PMID: 21249158].

172. Tezel G. A proteomics view of the molecular mechanisms and biomarkers of glaucomatous neurodegeneration. Prog Retin Eye Res 2013; 35:18-43. [PMID: 23396249].

173. Griciuc A, Roux MJ, Merl J, Giangrande A, Hauck SM, Aron L, Ueffing M. Proteomic survey reveals altered energetic patterns and metabolic failure prior to retinal degeneration. J Neurosci 2014; 34:2797-812. [PMID: 24553922].

174. Campello L, Esteve-Rudd J, Bru-Martinez R, Herrero MT, Fernandez-Villalba E, Cuenca N, Martin-Nieto J. Alterations in energy metabolism, neuroprotection and visual signal transduction in the retina of Parkinsonian, MPTP-treated monkeys. PLoS ONE 2013; 8:e74439-[PMID: 24040246].

175. Dittmann L, Hertz L, Schousboe A, Fosmark H, Sensenbrenner M, Mandel P. Energy metabolism of nerve cells during differentiation. O2 uptake, lactate production and ATP content of chick embryo brain cells before and after cultivation in the Rose chamber. Exp Cell Res 1973; 80:425-31. [PMID: 4745386].

176. Jackson GR, Owsley C, Curcio CA. Photoreceptor degeneration and dysfunction in aging and age-related maculopathy. Ageing Res Rev 2002; 1:381-96. [PMID: 12067593].

177. Fox DA, Campbell ML, Blocker YS. Functional alterations and apoptotic cell death in the retina following developmental or adult lead exposure. Neurotoxicology 1997; 18:645-64. [PMID: 9339814].

178. He L, Perkins GA, Poblenz AT, Harris JB, Hung M, Ellisman MH, Fox DA. Bcl-xL overexpression blocks bax-mediated mitochondrial contact site formation and apoptosis in rod photoreceptors of lead-exposed mice. Proc Natl Acad Sci USA 2003; 100:1022-7. [PMID: 12540825].

179. Schmidt KG, Pillunat LE, Osborne NN. Ischemia and hypoxia. An attempt to explain the different rates of retinal ganglion cell death in glaucoma. Ophthalmologe 2004; 101:1071-5. [PMID: 15490183].

180. Nucci C, Martucci A, Cesareo M, Garaci F, Morrone LA, Russo R, Corasaniti MT, Bagetta G, Mancino R. Links among glaucoma, neurodegenerative, and vascular diseases of the central nervous system. Prog Brain Res 2015; 221:49-65. [PMID: 26518072].

181. Brown MR, Sullivan PG, Geddes JW. Synaptic mitochondria are more susceptible to Ca^{2+}overload than nonsynaptic mitochondria. J Biol Chem 2006; 281:11658-68. [PMID: 16517608].

182. Naga KK, Sullivan PG, Geddes JW. High cyclophilin D content of synaptic mitochondria results in increased vulnerability to permeability transition. J Neurosci 2007; 27:7469-75. [PMID: 17626207].

183. Christophe M, Nicolas S. Mitochondria: a target for neuroprotective interventions in cerebral ischemia-reperfusion. Curr Pharm Des 2006; 12:739-57. [PMID: 16472163].

184. Perasso L, Spallarossa P, Gandolfo C, Ruggeri P, Balestrino M. Therapeutic use of creatine in brain or heart ischemia: available data and future perspectives. Med Res Rev 2013; 33:336-63. [PMID: 22135003].

185. Shen H, Goldberg MP. Creatine pretreatment protects cortical axons from energy depletion in vitro. Neurobiol Dis 2012; 47:184-93. [PMID: 22521466].

186. Berthet C, Castillo X, Magistretti PJ, Hirt L. New evidence of neuroprotection by lactate after transient focal cerebral ischaemia: extended benefit after intracerebroventricular injection and efficacy of intravenous administration. Cerebrovasc Dis 2012; 34:329-35. [PMID: 23154656].

187. Lowe MT, Kim EH, Faull RL, Christie DL, Waldvogel HJ. Dissociated expression of mitochondrial and cytosolic creatine kinases in the human brain: a new perspective on the role of creatine in brain energy metabolism. J Cereb Blood Flow Metab 2013; 33:1295-306. [PMID: 23715059].

188. Manos P, Bryan GK, Edmond J. Creatine kinase activity in postnatal rat brain development and in cultured neurons, astrocytes, and oligodendrocytes. J Neurochem 1991; 56:2101-7. [PMID: 2027017].

189. Tachikawa M, Fukaya M, Terasaki T, Ohtsuki S, Watanabe M. Distinct cellular expressions of creatine synthetic enzyme GAMT and creatine kinases uCK-Mi and CK-B suggest a novel neuron-glial relationship for brain energy homeostasis. Eur J Neurosci 2004; 20:144-60. [PMID: 15245487].

Articles are provided courtesy of Emory University and the Zhongshan Ophthalmic Center, Sun Yat-sen University, P.R. China. The print version of this article was created on 23 July 2016. This reflects all typographical corrections and errata to the article through that date. Details of any changes may be found in the online version of the article.